EPFL

Thèse n° 7201

The role of medial amygdala inhibitory neurons in regulating social behavior

Présentée le 12 novembre 2021

Faculté des sciences de la vie
Laboratoire de mécanismes synaptiques
Programme doctoral en neurosciences

pour l'obtention du grade de Docteur ès Sciences

par

Aiste BALEISYTE

Acceptée sur proposition du jury

Prof. C. Petersen, président du jury
Prof. R. Schneggenburger, Dr O. Kochubey, directeurs de thèse
Prof. A. Carleton, rapporteur
Prof. S. Golden, rapporteur
Prof. J. Gräff, rapporteur

École polytechnique fédérale de Lausanne

2021

Abstract

Aggression is an evolutionary conserved social behavior that is necessary for an animal´s survival. The neural substrates coordinating aggression are known to exist in the amygdala and the hypothalamus. While the medial amygdala (MeA) and the ventrolateral subdivision of the ventromedial hypothalamus (VMHvl) have separately been implicated in aggression control and are known to be anatomically inter-connected, it has not yet been described at the circuit-level whether an interaction between these nuclei plays a role in aggression control.

Posteriodorsal MeA (MeApd) is a majorly GABAergic nucleus (~70%), however the role of heterogeneous sub-populations of the MeA-GABA neurons in aggression is poorly understood. Since we were interested to identify the inhibitory cell types in the MeApd that control aggression, we first attempted to stimulate all the GABA neurons in the MeApd. Using a fast variant of channelrhodopsin-$2^{E123T,H134R}$ (ChETA) in $VGAT^{Cre}$ mice, we found that optogenetic stimulation of MeA-GABA neurons in the resident males interrupted intruder-directed aggression, contrary to the previous findings by Hong et al., where stimulation of MeApd-GABA neurons using channelrhodopsin-2^{H134R} (ChR2) evoked aggression. An in-depth investigation of this discrepancy, using two AAV serotypes, revealed that optogenetic stimulation with ChETA *suppressed* aggression, whereas optogenetic stimulation with ChR2 *increased* aggression, irrespective of the AAV serotype. Recordings of the membrane potential changes reported larger plateau depolarizations, smaller action potential amplitudes, and larger local inhibition when using ChR2 as compared to ChETA. Thus, in the first part I showed that optogenetic stimulation of the brain areas with heterogenous population of interconnected GABA neurons such as the MeApd, can strongly depend on the properties of optogenetic tools.

In the second part, we further explored how the MeApd-GABA neurons control aggression via long-range projections to their target nuclei in hypothalamus. Anterograde tracing revealed synapses from the MeApd-GABA neurons in the ventral premammillary (PMv) and the lateral ventromedial hypothalamic nuclei (VMHvl); both nuclei were previously identified in positive control of aggression (Lin et al., 2011; Stagkourakis et al., 2018). Ex-vivo optogenetic mapping of synaptic outputs from the MeApd-GABA projecting axons revealed evoked IPSCs in glutamatergic neurons in the VMHvl and the PMv, suggesting likely mechanism for inhibiting aggression. In-vivo optogenetic activation of the MeApd-GABA axonal terminals above the VMHvl or the PMv had no effect on aggression and instead led to an increased mounting, likely

caused by optic fiber implantation in the hypothalamus. To avoid this artifact, we have combined retrograde AAV with Cre ON/Flip ON approach and specifically stimulated the VMHvl projecting MeApd-GABA neurons. This approach revealed that in aggressive mice, stimulation of this pathway tends to reduce aggression. Finally, we performed in-vivo Ca^{2+} imaging of the VMHvl projecting MeApd-GABA neurons during the RI test, which showed that these neurons are largely multimodal and get activated during different sub-types of social behaviours including aggression.

This study shows that direct inhibitory path from the MeApd-GABA neurons to the VMHvl might suppress aggressive behaviour. Altogether, this work provides a step forward in our understanding of the neural substrates underlying aggression.

Keywords: medial amygdala, hypothalamus, territorial aggression, inhibitory connection, optogenetics

Résumé

L'agressivité est un comportement social conservé au cours de l'évolution et nécessaire à la survie. Les régions du cerveau qui contrôlent l'agressivité se trouvent dans l'amygdale et l'hypothalamus. Alors qu'il a été montré que le noyau médian de l'amygdale (MeA) et la partie ventro-latérale du noyau ventromédian de l'hypothalamus (VMHvl) sont chacun impliqués dans le contrôle de l'agressivité et que ces noyaux sont anatomiquement interconnectés, il n'y a pour le moment aucune preuve que l'interaction entre ces noyaux joue un rôle dans le contrôle de l'agressivité.

La partie postério-dorsal du MeA (MeApd) est composée en majorité (70%) de neurones GABAergiques (neurones MeA-GABA), mais le rôle des sous-populations hétérogènes de ces neurones dans l'agressivité reste mal compris. Voulant identifier les types de cellules dans la MeApd qui contrôlent l'agressivité, nous avons tout d'abord tenté de stimuler tous les neurones MeApd-GABA. En utilisant un variant rapide de la channelrhodopsine-$2^{E123T,H134R}$ (ChETA) dans les souris $VGAT^{Cre}$, nous avons trouvé que la stimulation optogénétique des neurones MeA-GABA chez les souris mâles résidentes interrompait les comportements agressifs contre un intrus et empêchait de nouvelles attaques, ce qui était contradictoire aux résultats de Hong et al., où la stimulation des neurones MeApd-GABA en utilisant la channelrhodopsine-2^{H134R} (ChR2) provoquait de l'agressivité. Une étude approfondie de cette différence de résultats en utilisant 2 sérotypes AAV a révélé que la stimulation optogénétique de ChETA réprimait l'agressivité, tandis que la stimulation optogénétique de ChR2 augmentait l'agressivité, quel que soit le sérotype AAV utilisé. Les mesures des changements de potentiel de membrane lors de stimulations optogénétiques a révélé un plateau de dépolarisation plus grand, des potentiels d'action de plus petites amplitudes et une inhibition locale plus importante *des neurones MeApd-GABA voisins plus importante* avec l'utilisation de ChR2 plutôt que ChETA. Ainsi, dans la première partie, j'ai montré que les expériences avec des stimulations optogénétiques dans des régions du cerveau composées de populations de neurones GABA hétérogènes interconnectés, telles que la MeApd, peut grandement dépendre des propriétés des outils optogénétiques utilisés.

Dans la seconde partie, nous avons voulu étudier en plus de détail comment les neurones MeApd-GABA contrôlent l'agressivité par la modulation des noyaux éloignés de l'hypothalamus. Le traçage antérograde a révélé qu'il existait de potentielles synapses de

neurones MeApd-GABA dans la partie prémamillaire ventrale (PMv) et la partie VMHvl de l'hypothalamus; ces 2 noyaux ont été précédemment identifiés comme des régions de contrôles amplificateurs de l'agressivité (Lin et al., 2011 ; Stagkourakis et al., 2018). Des enregistrements *ex-vivo* ont permis la cartographie des projections des neurones MeApd-GABA qui a révélé que la stimulation optogénétique induisait des courants inhibiteurs IPSCs évoqués dans les neurones glutamatergiques des noyaux VMHvl et PMv, ce qui suggère un mécanisme possible de la suppression de l'agressivité. L'activation optogénétique *in-vivo* des axones de neurones MeApd-GABA dans les noyaux VMHvl ou PMv n'a montré aucun effet sur l'agressivité, mais a en revanche induit une augmentation du comportement d'accouplement envers l'intrus (en le montant), ce qui est possiblement causé par l'implantation de la fibre optique dans l'hypothalamus. Pour éviter ce comportement artificiel, nous avons combiné l'utilisation d'un AAV rétrograde avec une approche Cre ON/Flip ON, ce qui a permis la stimulation spécifique des neurones MeApd-GABA projetant des axones dans le noyau VMHvl. Cette approche a révélé que, dans une souris agressive, la stimulation de cette connexion permettait de réduire l'agressivité. Enfin, nous avons utilisé l'imagerie calcique *in-vivo* dans les neurones MeApd-GABA projetant des axones dans le noyau VMHvl dans des souris libres de mouvement durant un test RI, et nous avons montré que ces neurones s'activaient pour différents sous-types de comportements sociaux, notamment durant l'agressivité.

Cette étude montre que la connexion inhibitrice directe reliant les neurones MeApd-GABA aux neurones se trouvant dans le noyau VMHvl pourrait directement empêcher le comportement agressif. Ainsi, le travail de cette thèse fournit une avancée dans notre compréhension des régions du cerveau contrôlant l'agressivité.

Mots clés: amygdale médiale, hypothalamus, agression territoriale, connexion inhibitrice, optogénétique

Contents

Chapter 1: Introduction

1.1 Innate and learned behaviours

Emotions are core elements of our existence that help us to thrive and enable us to create relationships. Their profound complexity to this day is challenging researchers to scientifically explain the underlying specific circuits and mechanisms in the brain. Ubiquitous across species emotions are responsive and can be expressed through behaviours which can be further subdivided into learned, versus innate (also termed instinctive) (Brigandt, 2005). While learned behaviours, such as fear learning or operant conditioning, require training and experience and are often aimed toward completion of a task, innate behaviours are genetically pre-programmed in early development and are based on evolution and inheritance (Ralph Adolphs and David J. Anderson, 2018; Tierney et al., 2000). It was postulated that innate behaviours cost less than the learned behaviours if measured by the use of genetic information (George C. Williams, 1992), which may be the reason for the generational transfer of innate, but not learned behaviours. Since early 1930s innate behaviours became a major interest of ethologists, among them Konrad Lorenz, Karl von Frisch and Nikolaas Tinbergen who observed animals in their natural habitat and tried to understand and classify their behavioural patterns (Altenberg, 1950; Karl von Frisch, 1967; Lorenz, 2005, originally published 1963; Tinbergen, 1951). Tinbergen noted that while innate behaviours are highly abundant across species, an external trigger must be present for them to be executed (Tinbergen, 1951). This observation is summarized in a model called “Innate Releasing Mechanism” that describes innate behaviour as a reproductive center which is required for the survival of the species, and only upon the specific set of motivational stimuli this behaviour can be to activated (“released“). Thus, these studies showed that while at the first sight innate behaviours appear to be basic (less complicated than learned), they are rather comprised of multiple layers of control, external stimuli and patterns resulting in a complexity that makes them a fascinating subject to be studied.

1.2 Aggression

Aggression is one of the key innate behaviours, described by ethologists as a biological necessity for the survival of the fittest animals in a population and for the preservation of the species at large (Lorenz, 2005). It is directed toward another individual with the intention to cause immediate harm (Anderson and Bushman, 2002). There are different forms of aggression such as territorial, maternal, predatory and abnormal (Haller, 2018). While these forms of aggression are evolutionary conserved and present across all species, they have been best studied in mice, rats, fruit flies, cats, chicken and humans (Averill, 1983; Hall, 1937; Putkonen, 1966). Territorial, maternal and predatory forms of aggression are directed towards the survival of species and transmission of genes to the next generation by defending the territory, protecting the offspring and killing of other animal species to obtain food, respectively. In contrary, abnormal aggression is associated with various psychopathologies and is often misregulated in certain psychiatric disorders such as schizophrenia (Swanson et al., 2006; Volavka et al., 1997), manic bipolar disorders (Ballester et al., 2012), or in such society-threatening conditions as alcohol or drug abuse (Brady et al., 1998; Bushman, 1997). Violent crimes that are mostly triggered by anger account for an estimated 1.43 million deaths worldwide annually (Siever, 2008). The resources required to address the consequences of these acts are high and bring substantial costs to our society. The importance of aggression for evolution and its impact on our quotidian life is evident, and therefore it is important to understand in detail the neural circuits mediating aggression.

Territorial aggression is one of the most abundant forms of aggression that is directed against the neighbouring group of male conspecifics and has been a major driving force for the survival of the species (Scott and Fredericson, 1951). Since the XXth century it has been widely studied in the laboratory environment (Miczek et al., 1974; Parmigiani et al., 1998; Takahashi and Miczek, 2013). The resident intruder (RI) test is commonly used as an assay to study territorial aggression in laboratory mice. During this test, an intruder male mouse is placed into the home cage of a singly housed resident male mouse. The resident mouse will try to protect its territory and will start attacking the intruder by biting from the top or laterally, chasing, trying to grasp with paws or standing up (Catlett, 1961; Koolhaas et al., 2013). In the early studies, brain lesions or electrical stimulations were performed on mice, rats and cats to assess the role of the certain brain areas in aggression control. Electrical stimulation of cat hypothalamus induced attack, and thus, hypothalamus was the first brain area shown to be required for attack

generation by Hess in 1927 (Miczek and Meyer-Lindenberg, 2014). The following hypothalamic stimulation studies in cats and rodents, confirmed that hypothalamus plays a crucial role in attack generation and found that anterior, lateral and ventromedial parts of hypothalamus are key areas involved in attack generation (Kruk, 1991; Lammers et al., 1988; Panksepp, 1971). The amygdala is another important center for aggression control discovered by early lesion and electrical stimulation studies (Egger and Flynn, 1963; Miczek et al., 1974). Lesion studies of amygdala, more specifically the medial amygdala (MeA), provided rather inconsistent results, as in some studies the lesions of the MeA decreased aggressiveness (Emery et al. 2001; Kemble et al., 1984; Miczek et al., 1974; Takahashi and Miczek, 2013; Vochteloo and Koolhaas, 1987; Wang et al., 2013) or had no effect on aggression (Blanchard and Takahashi, 1988; Busch and Barfield, 1974; Oakes and Coover, 1997). However, it is important to note that Kemble et al. (1984) tested defensiveness and not territorial aggression while Takahashi and Gladstone (1988) investigated male-female fighting during mating. Electrical stimulations of the amygdala in cats at subseizure levels on the one hand produced suppression of predatory attack (Egger and Flynn, 1963), and on the other hand facilitated a behaviour called “defensive rage” (Stoddard-Apter and MacDonnell, 1980), suggesting a functional antagonism in the roles of the amygdala within different types of aggression. Han et al., (1996), using electrical stimulation of the MeA and the lateral hypothalamus in cat, together with infusions of the substance P receptor antagonist or agonist, showed that defensive rage behaviour was mediated by a mechanism involving the release of substance P from the MeA in the medial hypothalamus via fibers of the stria terminalis. Interestingly, the amygdala region was also activated when aggression was induced by electrical stimulation of the hypothalamus (Halász et al., 2002). Taken together, lesion and electrical stimulation studies in different animal models strongly suggested that the MeA and hypothalamic nuclei such as the ventromedial and the lateral hypothalamic nuclei are key areas in regulation of aggression, yet these results have to be evaluated with caution as the electrical stimulation lacks cell type specificity and could co-stimulate the fibers of passage, while the lesion experiments could often damage the neighbouring brain areas. For a more comprehensive understanding of neural circuits of aggression, more specific tools are required to identify the exact subdivisions and the cell types of the MeA and the hypothalamus involved in control of aggression.

1.3 Optogenetics

One of the biggest challenges in understanding how neural circuits control behaviours has been to specifically stimulate defined types of cells or brain areas with a precise temporal resolution. The classical techniques such as lesions, electrical stimulations or infusions using cannula lack the precision and often provide inconclusive or even misleading results. In the last 15 years optogenetics has greatly helped researchers to understand how the brain is controlling various behaviours. It works by expressing the light-gated ion channels/transporters in the cell membrane of neurons which, upon light application, will open to depolarize or hyperpolarize neurons within their native circuitry (Deisseroth, 2015). The first ion channel used in the animal studies is Channelrhodopsin-2 (ChR2) (Nagel et al., 2003) (Figure 1.1). It was derived from the green alga *Chlamydomonas reinhardtii* and is a light-gated cation channel, encoded by a single open reading frame of 315 amino acids, that can produce inward currents within 50 µs of a flash of blue light, leading to depolarization of the membrane potential and subsequently causing an action potential (AP) via activation of the neuron intrinsic voltage-gated Na^+ channels (Boyden et al., 2005; Nagel et al., 2005).

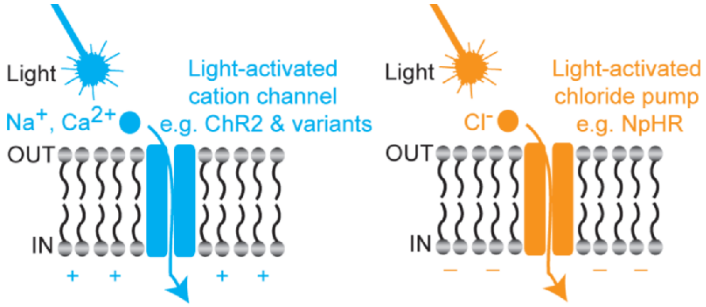

Figure 1.1 | Optogenetic approaches to control neuronal activity. Channelrhodopsin-2 (ChR2) is a nonselective cation channel which opens upon illumination with blue-light (450-470 nm). The influx of cations (mostly Na^+) leads to depolarization of the ChR2 expressing neurons. Halorhodopsin (NpHR) is a yellow-light-activated chloride pump. Effective outward current carried by the chloride ions entering the cell leads to hyperpolarization of the NpHR expressing neurons (adapted from (Ferenczi et al., 2019).

As a further refinement, a point mutation H134R was introduced into the wild type channelrhodopsin-2, resulting in the increased stationary photocurrent (Nagel et al., 2005). Using this improved ChR2 in excitable mechanosensory neurons of the nematode *Caenorhabditis elegans*, the stimulation with blue light evoked withdrawal behaviours that are

normally elicited by mechanical stimulation (Nagel et al., 2005). However, there were certain properties of ChR2 that still limited the stimulation precision. For example, when the stimulation is strong enough, extra action potential spikes can occur in response to a single light pulse. The maximum frequency of stimulation is limited to 40Hz with acceptable failure rate, and plateau offset potentials of 10 mV or more can occur when using ChR2^{H134R} under the stimulation using light train pulses (Boyden et al., 2005; Gunaydin et al., 2010; Mattis et al., 2012) (Figure 1.2). To circumvent these limitations, Gunaydin et al. (2010) introduced a family of further mutants to speed up the opsin kinetics. One of them, E123T, resulted in a double mutant of chennelrhodopsin-2 named ChETA$^{E123T/H134R}$. This double mutant showed accelerated channel closing kinetics which allowed to achieve rapid repolarization of neurons following a brief light pulse (Berndt et al., 2011; Mattis et al., 2012; Ting et al., 2014). Also upon longer light stimulation, ChETA$^{E123T/H134R}$ had increased steady-state to peak current ratio, and strongly diminished plateau offset potentials across all tested frequencies, thus it enabled following of the light stimulation train up to 200Hz depending on the cell type (Berndt et al., 2011; Gunaydin et al., 2010; Mattis et al., 2012).

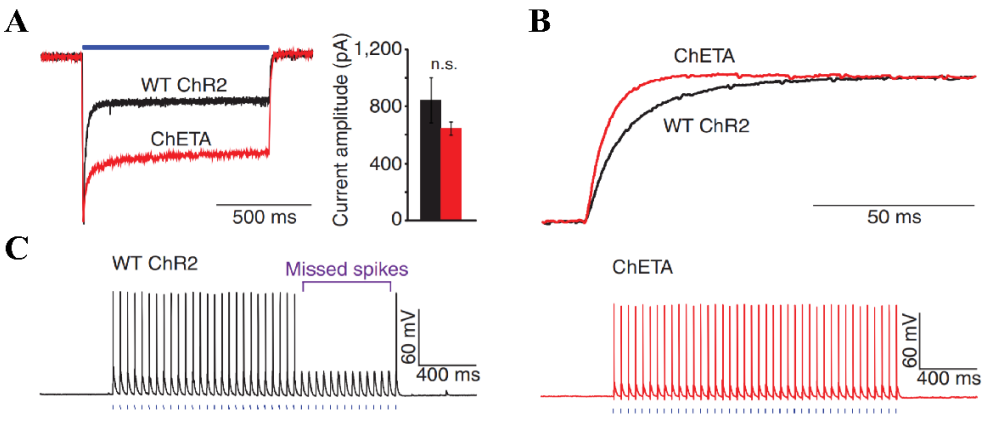

Figure 1.2 | Eletrophysiological properties of wild type ChR2 (black) and ChETA^{E123T,H134R} (red). **(A)** Left, traces of photocurrents evoked by a 1-s pulse of 472-nm blue light stimulation of ChR2 and ChETA expressed in parvalbumin (PV) interneurons. Right, summary of steady-state current amplitudes for ChETA and ChR2**. (B)** Expanded photocurrents from **(A)** normalized to steady-state current to show accelerated off-kinetics in ChETA expressing neurons **(C)** Whole-cell current-clamp recordings from ChR2 expressing (left trace) and ChETA expressing (right trace) PV neurons that respond to 2 ms 20-Hz light stimulation **(D)** (from Gunaydin et al., 2010)

To achieve inhibition in neurons, a light-driven chloride pump called halorhodopsin (NpHR) from *Natronomonas pharaonic* was isolated (Zhang et al., 2007). It enables membrane hyperpolarization, and thereby leads to inhibition of action potential firing or sustained

blockade of spiking. Halorhodopsin is a yellow-light driven chloride pump that activates upon light stimulation and transports the chloride ions from the outside to the inside of a neuron thus generating a hyperpolarization of the cell membrane potential (Zhang et al., 2007).

A variety of tools exists for delivering the opsin encoding genes to specific neuron (sub)populations in the brain (Luan and White, 2007). To achieve conditional expression in certain cell types, the Cre/lox recombinase system can be employed (Gong et al., 2007; Kim et al., 2018). First, a Cre-recombinase expressing mouse line has to be generated by inserting a Cre-encoding expression cassette next to the desired gene, which will drive the expression of the recombinase only in the neurons that express this gene. Adeno-associated viral vectors (AAV) delivering opsin-encoding DNA into the neurons, can be rendered Cre-recombinase dependent if a combination of Cre-specific recognition sites ("lox" sites) encompasses the opsin expression cassette. For example, using two different lox sites and an inverted expression cassete in a DIO/DIO design (Schnütgen et al., 2003), expression of the viral transgene will be enabled only in the neuronal cell types that express Cre-recombinase . Further combinations of advanced genetic systems can lead to combinatorial expression of opsins in genetically- and/or projection-specific manner (Fenno et al., 2014), providing specificity for studying neuronal circuits responsible for specific behaviours *in-vivo* and *in-vitro* (Yizhar, 2012).

1.4 Medial amygdala

The amygdaloid complex was first identified by Burdach in the early 19th century (Sah et al., 2003). It is located in the medial temporal lobe and is comprised of 13 structurally and functionally diverse nuclei that can be distinguished on the basis of cytoarchitecture (striatal, claustral and cortical), histochemistry, their local and long-range connectivity and function (Krettek and Price, 1978; Sah et al., 2003).

The medial amygdala (MeA) is a part of the amygdaloid complex and is situated more medially compared to other amygdalar subdivisions (Sah et al., 2003) (Figure 1.3). It begins at the level of the lateral olfactory tract (LOT) and extends caudally (Sah et al., 2003). The MeA can be divided into anteroventral (MeAav), anterodorsal (MeAad), posteroventral (MeApv) and posterodorsal (MeApd) subdivisions (Canteras et al., 1995). The posterior MeAp (MeApd and MeApv) receives socially relevant sensory information from the vomeronasal organ which expresses vomeronasal receptors (VRs) for detection of pheromonal cues emitted during social

interaction and sends its axons to the glomeruli of the accessory olfactory bulb (AOB) (Dulac and Torello, 2003). The AOB directly projects to the MeA, and after integrating this sensory information, the MeA further relays it to hypothalamic nuclei that control instinctive behaviours such as mating and aggression (Cadiz-Moretti et al., 2016; Canteras et al., 1995; Choi et al., 2005; Stowers et al., 2002).

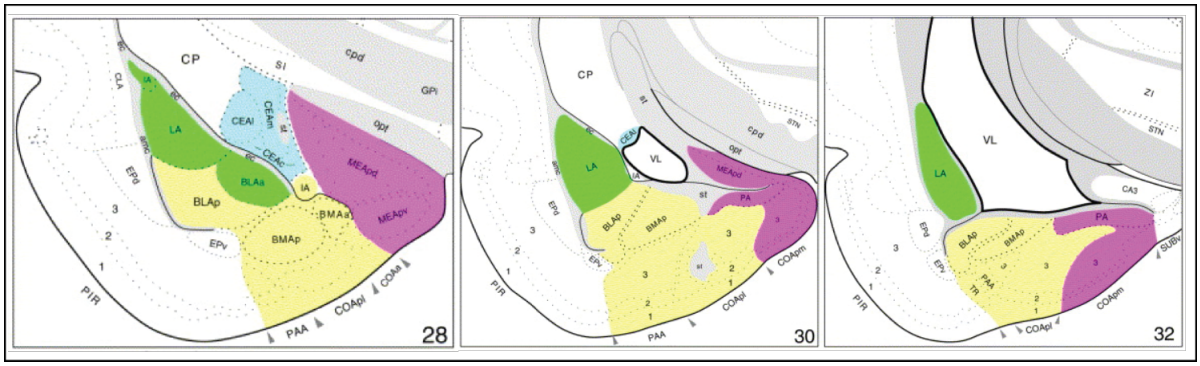

Figure 1.3 | Topograpical iliustration of the amygdaloid complex. Subsequent coronal sections through the left temporal region of the cerebral hemisphere showing amygdalar structures that are most closely associated with the accessory olfactory system (MeA; violet), with the main olfactory system (cortical amygdalar nulei; yellow), with the autonomic system (central amygdalar complex; blue), and with the frontotemporal association system (lateral amygdalar complex; green). (adapted from (Dong et al., 2001)

1.4.1 Neuron types in the MeA

The MeA contains a heterogeneous group of inhibitory and excitatory neurons (Choi et al., 2005) (Figure 1.4). Immunohistochemistry and in situ hybridization studies showed that a relatively high number of neurons in the MeAp express the inhibitory neuron marker glutamic acid decarboxylase 65/67 (Gad65/67) (Bian et al., 2008; Keshavarzi et al., 2014; McDonald and Augustine, 1993). Quantification of Gad67+ revealed that inhibitory neurons are more prevalent in the MeApd with the expression in 66 % of the total population, whereas only 32 % of MeApv neurons were Gad67 positive (Keshavarzi et al., 2014). A high diversity of inhibitory neurons is present in the MeAp. For example, a study of various inhibitory interneuron markers showed that GABAergic neurons most frequently express calbindin (45%), SOM (18%), calretinin (12%) while cholecystokinin (CCK) and vasoactive intestinal polypeptide (VIP) positive neurons were at much lower percentage, and parvalbumin (PV) neurons were virtually absent (Keshavarzi et al., 2014) (Figure 1.4). Wu et al. (2017) explored neuronal diversity in the MeA using a modification of single cell RNA sequencing (Act-seq)

system and classified 8 inhibitory, 4 excitatory and 4 mixed clusters of neurons that express neuropeptides such as Tac1 (encoding substance P), Cartpt (encoding CART peptide), SOM which did not overlap with Tac1 and Cartpt), CCK and several transcription factors with cluster restricted expression patterns such as Lhx1, Lhx5, Nhlh2, Mef2c and Bcl11b. Furthermore, using dual-color fluorescence-based in-situ hybridization (FISH), some studies have shown that mutually exclusive Cartpt and SOM are expressed largely in subsets of inhibitory neurons (Wu et al., 2017).

Heterogeneity of the MeA was also investigated in developmental studies (Carney et al., 2010; Choi et al., 2005; Hirata et al., 2009; Lischinsky et al., 2017). The embryonic telencephalic preoptic area (POA) has been shown to give rise to two distinct subclasses of inhibitory neurons: developing brain homeobox 1 (Dbx1) and forkhead box protein P2 (Foxp2) positive neurons that comprise majority of the MeA neurons (Hirata et al., 2009; Lischinsky et al., 2017). Progenitors from the ventral telencephalic Shh+ and Nkx2.1+ lineages also contribute to inhibitory neuronal diversity in the MeAp by generating calbindin, neuronal nitric oxide synthase (nNOS), Foxp2 and somatostatin (SOM) -expressing neurons (Carney et al., 2010). Gene expression profiling in the MeA revealed that two LIM homeodomain genes, Lhx6 and Lhx9, are differentially expressed in the posterior MeAp (Choi et al., 2005). Using in-situ hybridization and the genetically encoded axonal tracer placental alkaline phosphatase (PLAP) that targeted Lhx6 chromosomal locus, the authors showed that the majority (~80%) of the neurons in the MeApd expressed Lhx6, while Lhx9 was almost exclusively detected in the MeApv (Choi et al., 2005). This bimodal distribution of two major LIM homeodomain genes in the ventral and dorsal MeAp suggests different genetic profiles of the dorsally and ventrally residing neurons and possibly their involvement in divergent neuronal circuits.

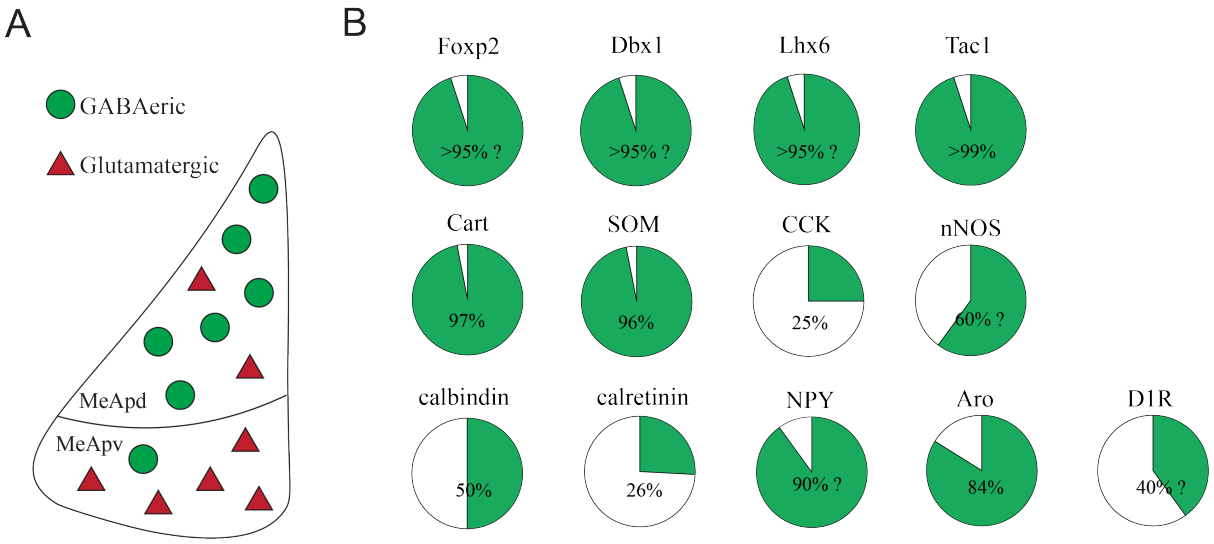

Figure 1.4 | Inbibitory cell distribution and their genetic profiles in the MeAp. (A) Schematic representation of excitatory and inhibitory cells in the ventral and dorsal parts of the MeAp. **(B)** MeAp contains heterogeneous group of inhibitory neurons. Pie charts for the some relevant marker genes of inhibitory neurons in the MeA. Green sectors show the fraction of inbibitory neurons within the respective genetically identified groups, as indicated in the available literature sources. Remaining white fractions represent the neuronal populations that were not studied in all cases, but most likely represent glutamatergic neurons. Question mark shows that the provided quantifications in the original study were not precise and are subject to possible errors. Quantifications were obtained (or deduced) from the following original publications by (Keshavarzi et al., 2014; Miller et al., 2019; Padilla et al., 2016; Unger et al., 2015; Wu et al., 2017).

1.4.2 Local connectivity in the MeA

The MeA has been shown to contain local interneurons that provide inhibition on neighbouring excitatory and inhibitory neurons (Bian et al., 2008; Keshavarzi et al., 2014). Whole-cell patch clamp recordings were performed in a previous study that described intrinsic electrophysiological properties of GABAergic neurons in adult knock-in mice expressed GFP in GABAergic neurons (Bian, 2013). Based on the electrophysiological and anatomical information, MeA neurons were classified as long range projection neurons, Type I and Type II, and local interneurons, Type III (Bian, 2013). These Type III multipolar stellate neurons were located along the edges of the MeA, had lower input resistance (<400 MΩ) than the other two types, had a small or no hyperpolarization-induced sag indicative of I_h currents, and had relatively small multipolar dendritic trees with axonal collaterals close to the cell body (Bian, 2013). Another study also has identified a local inhibitory neuron type in the MeApv electrophysiologically, and classified it as a "Type 2" that unidirectionally inhibited principal glutamatergic neurons of the MeApv (Keshavarzi et al., 2014). However, neither of these

studies described local inhibition in the MeApd, and thus it remains a very important question to be addressed as the local inhibition could potentially have a strong effect by modulating the behavioural outcomes.

1.4.3 Afferent innervation of the MeA

Social recognition and communication in mammals start from the integration of multimodal sensory information such as olfactory, visual, auditory and others (de la Zerda et al., 2020). Aggression is strongly regulated by pheromones across multiple species (Chamero et al., 2007). Olfactory information processing starts from activation of the primary chemosensory systems such as the vomeronasal organ (VNO) and the main olfactory epithelium (MOE) which send their axons to the accessory olfactory bulb (AOB) and the main olfactory bulb (MOB), respectively (Lledo et al., 2005). Multiple tracing studies have shown that the MeA is the primary recipient of glutamatergic inputs from the AOB, which innervates the molecular layer of the MeAav (von Campenhausen and Mori, 2000; Mohedano-Moriano et al., 2007). Furthermore, the AOB can also send projections to the MeA via the posterior medial subdivision of the cortical amygdala (COApm) (Alheid and Heimer, 1988). It was shown that the principal neurons of the MeApv receive convergent AOB and CoA inputs that are differentially segregated on their dendrites and display distinct temporal integration, with a larger summation and higher output gain for the AOB inputs (Keshavarzi et al., 2015). Interestingly, evoked synaptic currents from the AOB and CoA were followed by a disynaptic inhibitory component which is likely mediated by local inhibitory interneurons (Keshavarzi et al., 2015), reminiscent of the feedforward inhibition in the cortical circuits. Only sparse direct and indirect projections from the MOB and olfactory cortex were described in the MeA (Bergan et al., 2014; Cadiz-Moretti et al., 2016).

A highly detailed tracing study by Cádiz-Moretti et al. (2016) found that other strong inputs to the MeA arise from the piriform cortex, the posterior part of the BNST, the hippocampal CA1 area and posterior intralaminar thalamus while minor projections come from the basolateral and lateral amygdala (electrophysiologically described by (Twining et al., 2017), septum, ventral striatum, claustrum, various hypothalamic structures such as VMH, MPA, AH and PMv, raphe nucleus and parabrachial complex. Knobloch et al., (2012) also showed that the MeA receives a high density of oxytocinergic fibers from the hypothalamic paraventricular nucleus (PVN).

1.4.4 The outputs of the MeA

After processing the primary olfactory information, the MeA sends its output axons to various hypothalamic nuclei via long-range projections (Canteras et al., 1995) (Figure 1.5). The neurons of the MeApd mainly project to the bed nucleus of stria terminalis (BNST) and to hypothalamic subdivisions implicated in reproductive and aggressive behaviours, while the MeApv axons innervate hypothalamic nuclei that are involved in defensive behaviour and aggression (Bian et al., 2008; Choi et al., 2005; Swanson, 2000). More specifically, Keshavarzi et al. (2014) showed that both excitatory and inhibitory neurons of the MeApd and MeAv project to the anterior hypothalamus, the medial preoptic nucleus, the VMH and the ventral premammillary nucleus (PMv). Padilla et al. (2016) observed that MeA Npy1r-expressing neurons densely innervate the posterior principal region of the bed nucleus of the stria terminalis (pBNST), the lateral hypothalamus, the periaqueductal gray, the parabrachial nucleus, the ventromedial hypothalamus and the anterior olfactory bulb. In turn, the MeA is also indirectly connected to hypothalamus via the BNST.

While it is clear that some of the inhibitory neurons in the posterior MeA take part in the local inhibitory networks (Bian, 2013; Keshavarzi et al., 2014) and also project to the distant downstream areas (Choi et al., 2005; Keshavarzi et al., 2014), it is not yet know whether these are the same neurons with divergent connectivity patterns or rather two distinct populations (Figure 1.5, C).

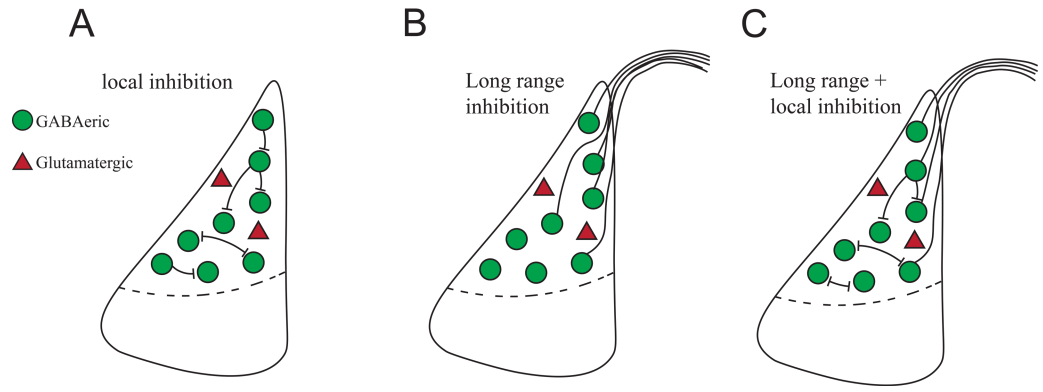

Figure 1.5 | Schematic representations of connectivity scenarios of the inhibitory neuron in the MeApd. (A) Certain types of MeApd neurons have been shown to provide local inhibition on their neighbouring inhibitory neurons. Local inhibitory intputs onto the excitatory principal neurons of the MeA have also been documented (not shown in the scheme). **(B)** The MeApd inhibitory neurons send their long-range axons to the BNST and to multiple hypothalamic nuclei. **(C)** Possibly, both connectivity types (local and long-range) co-exist at the level of single neurons in the MeApd.

1.4.5 The posterior MeA in aggression control

The studies that were conducted over the last few years used optogenetic tools to stimulate the posterior MeA and its subdivisions, allowing dissection of the role of neuronal circuits in modulation of aggression in a cell-specific manner.

Hong et al. (2014) used optogenetic tools to identify neuronal populations in the MeApd which are responsible for promoting social and non-social behaviours. The authors showed that optogenetic stimulation of the MeApd inhibitory neurons, using Cre-dependent expression of $ChR2^{H134R}$ in vesicular GABA transporter (VGAT) Cre mouse line, triggered aggression against an intruder animal during the RI test, upon stimulation with the train of light pulses (20 Hz, 20 ms pulse duration). Reducing the laser intensity without changing other parameters led to mating (mounting) behaviour of the resident male towards the intruder male. This suggested that the net output of the MeApd depended on the stimulation intensity of VGAT+ neurons. Silencing the same neurons for 3s using halorhodopsin eNpHR3.0 after the onset of attack towards a male intruder, stopped ongoing attacks with an average latency of <0.5 s. Furthermore, the authors have shown that optogenetic activation of glutamatergic neurons in the MeApd, using a similar optogenetic setup in the $VGluT2^{Cre}$ mice, led to self-grooming and suppression of social interactions. Therefore, GABAergic and glutamatergic neurons in the MeApd seem to antagonistically influence different modes of social behaviours, while optogenetic stimulation of the MeApd GABA neurons seemed to stimulate aggression by an unknown downstream mechanism (Hong et al., 2014). Social interaction that provides a rewarding experience (social reinforcement) has also been linked to the MeAp inhibitory neurons (Hu et al., 2021). In this study, again using the $VGAT^{Cre}$ mouse line and $ChR2^{H134R}$ it was shown that the MeA to medial preoptic area (MPOA) inhibitory projection mediates social reinforcement in mice of both sexes (Hu et al., 2021).

In another study, the role of MeApd neurons was also assessed in modulating territorial aggression (Unger et al., 2015). The authors used inhibitory chemogenetics that utilized a modified G_i-coupled human muscarinic receptor 4 (hM4Di) (DREADD-Gi) activated by a designer compound CNO, to understand the role of aromatase expressing (Aro+) neurons in the MeApd. The population of Aro+ neurons was shown to contain ≈84% GABA neurons (Unger et al., 2015; see also Fig 1.4). Chemogenetic inhibition of these neurons significantly increased the latency of attack initiation and the tail rattle towards the intruder males, without a change of attack duration and inter-attack interval. Other behaviours such as mating,

courtship vocalization, urine marking, anxiety-type behaviour, food finding, or locomotion were not affected (Unger et al., 2015). These results in general supported the positive role of MeApd-GABA neurons in aggression suggested in (Hong et al., 2014), however the differences in the type of manipulation and in the strength/quality of behavioural effect make it difficult to make strong mechanistic conclusions.

Padilla et al. studied the role of neuropeptide Y receptor expressing (Npy1R+) neurons in the MeA in feeding, aggression and fear. Overall, ≈64% of the Npy1R+ MeA cells were estimated to be GABAergic; they are anatomically distributed throughout the MeA, with a slight bias toward the anteroventral subdivision, thus this study was focused on the whole MeA nucleus rather than on one of the subdivisions. The authors showed that chemogenetic activation of Npy1R+ neurons in the MeA stimulated attack in four out of nine animals, while the rest were engaged in other aggressive behaviours including nudging, aggressive grooming and holding. Furthermore, optogenetic activation of the axonal terminals of the MeA Npy1R+ cells in their projection area (posterior BNST) increased the overall attack duration in mice (Padilla et al., 2016). Interestingly, the authors showed that a large fraction of Npy1R+ neurons expressed GAD67. This led to the idea of an existing MeA-GABA→BNST→VMH disinhibitory pathway that functions via BNST which in turn sends inhibitory axons to the VMH. This pathway could potentially stimulate aggression as suggested in a review (Chen and Hong, 2018), but this needs further experimental evidence.

Another population of neurons in the MeApv expresses the dopamine receptor Type 1 (D1R), and 40% of these D1R+ neurons were estimated to be GABAergic (Miller et al., 2019). D1R+ neurons send their axons to the VMH and the BNST and were shown to regulate social behaviours during the resident intruder assay (Miller et al., 2019). Both GABAergic and glutamatergic neurons were shown to exert opposite effects on investigation or avoidance of threatening stimuli based on their projection target (Miller et al., 2019). Stimulation of MeApv-D1R→VMH projections in mice showed decreased aggression and significantly increased non-aggressive social behaviours such as grooming of the male intruder, while stimulation of the MeApv-D1R→BNST pathway led to a significantly increased aggression phenotype (Miller et al., 2019).

The MeApv has also been studied in the presence of abnormal aggression. It has been thought that traumatic stress can lead to abnormally increased aggression which may be a symptom of psychiatric condition such as the post-traumatic stress disorder (PTSD) (McHugh and

Treisman, 2007). Nordman et al. (2020) studied how the plasticity of synapses between MeApv neurons and their target nuclei VMH and BNST, underlies aggression escalation induced by the prior attacking behavior and the traumatic stress. They have shown that the MeApv→BNST and MeApv→VMH circuits influence different stages of attack: the MeApv→BNST connection regulate attack initiation, whereas the MeApv→VMH connection mainly acts on the maintenance of attack (Nordman et al., 2020). However, no careful distinction between the excitatory and inhibitory neurons of the MeApd were made in their experimental design.

Altogether, these studies have shown that the MeA is a heterogeneous nucleus that contains different GABA neuron populations that are involved in aggression control. Nevertheless, the current consensus based on the studies using optogenetic and chemogenetic stimulation of VGAT+, Aro+, Npy1R+ and D1R+ neurons (the latter three to a large degree also comprise of GABAergic neurons) in the MeApd and MeApv, is that activity of various MeA-GABA neurons leads to increased aggressive behaviour. However, while MeApv regulates different aspects of aggression via BNST or VMH, it remains unclear through which downstream nuclei the MeApd acts. Moreover, it is unknown with which cells the MeApd-GABA neurons make synapses in the BNST and the VMH, and how these specific connections can influence aggressive behaviour.

1.5 Optogenetic aggression studies in other nuclei

1.5.1 Ventrolateral part of the ventromedial hypothalamus (VMHvl)

A key area that receives inputs from the MeAp and is crucial for aggression regulation is the hypothalamus (Figure 1.6). The hypothalamus contains highly conserved neural circuits that control basic functions essential or life such as energy homeosthasis (incl. feeding), thermoregulation, fluid and electrolyte balance (incl. drinking), rhythmic activity (sleep/wake cycle), reproduction and fertility, visceral motor control, defence (aggression), and emergency responses to the stressors in the environment (Saper and Lowell, 2014). It integrates various sensory inputs, behavioural information and computes motor signals. With the help of novel techniques the ventrolateral part of the ventromedial hypothalamus (VMHvl) has been identified as an exact hypothalamic location required for male aggression (Lee et al., 2014; Lin

et al., 2011; Yang et al., 2017). Lin et al. (2011) showed that optogenetic stimulation of the VMHvl neurons with a train of 20 ms long light pulses delivered at 20 Hz in male mice using $ChR2^{H134R}$ led to attack of other males, females and inanimate objects, while chemogenetic silencing of the same area using ivermectin-gated Cl^--channel reversibly inhibited inter-male aggression. Interestingly, the authors have also shown by the early response gene expression analysis that the neurons activated during attack were inhibited during mating (Lin et al., 2011). Further, VMHvl activity can also predict upcoming aggressive action such as the latency and duration of the next attack (Falkner et al., 2014). VMHvl contains ~4,000 neurons which are predominantly excitatory, as defined by expression of vesicular glutamate transporter 2 (vGlut2); a sub-population of these neurons partially co-express estrogen receptor alpha (ERα, encoded by the Esr1 gene) (Kim et al., 2019; Krause and Ingraham, 2017). These ERα expressing neurons (Esr1+) code for the intruder sex identity and activate during aggression bouts of the resident mouse (Lee et al., 2014; Remedios et al., 2017). Another study in the VMHvl found that progesterone receptor (PR)-expressing neurons are critical for male territorial aggression in solitary but not in socially housed males, and that this behavioural difference becomes smaller by disabling chemosensation in the latter group (Yang et al., 2017). These findings broaden the previous beliefs of predetermined circuits by showing that social contexts can override developmentally hard-wired neural pathways.

It has been suggested that attack is stimulated by VMHvl neurons projecting downstream to the midbrain periaqueductal gray (PAG) (Gregg and Siegel, 2001). A recent study revealed that VMHvl vGlut2-positive neurons target the lateral PAG (lPAG) of the midbrain and this excitatory connection is required to coordinate the biting jaw movements during attack(Falkner et al., 2020). Taken together, the experiments that I have discussed above have shown a key role of VMHvl in aggression control.

In my PhD thesis I am interested to characterize the upstream neuronal structures that regulate the VMHvl which in turn stimulates attack in mice.

1.5.2 Ventral premammillary nucleus (PMv)

The ventral premammillary nucleus (PMv) is another hypothalamic area important for aggression control that is highly connected to the medial and periventricular zones of the

hypothalamus, septum, and parts of the amygdala (Canteras et al., 1992; Cavalcante et al., 2014; Lin et al., 2011; Motta et al., 2013) (Figure 1.6). In male mice, aggression and mating results in strong c-Fos activation in the PMv (Lin et al., 2011). In female mice, lesions of the PMv resulted in significantly reduced maternal aggression (Motta et al., 2013). Dopamine transporter positive (DAT+) neurons make up to 34% of PMv neurons and optogenetic stimulation of DAT+ neurons in the PMv triggers attack and further leads to a long-lasting switch of intermale hierarchy positions (Stagkourakis et al., 2018). These neurons have also been shown by antero-/retrograde tracing experiments to innervate the VMHvl, and by the optogenetic circuit mapping experiments - to provide a strong monosynaptic glutamatergic input to the VMHvl (Stagkourakis et al., 2018). Moreover, it was shown that VMHvl and PMv excitatory neurons are reciprocally connected, a network which largely forms a positive feedback loop driving aggressive behaviour (Stagkourakis et al., 2018). While these results provided a strong evidence for the PMv involvement in aggression control in both males and females, it is still undetermined which afferents relay aggression-relevant input onto the PMv DAT+ neurons.

1.5.3 Bed nucleus of the stria terminalis BNST

The bed nucleus of the stria terminalis (BNST) is an anatomically highly diverse, sexually dimorphic branch of the extended amygdala that plays a role in fear and anxiety (Davis et al., 2010) and in social behaviours such as social bonding, mating and aggression (Lebow and Chen, 2016). Its role in intermale aggression has been partially addressed by some recent studies (Bayless et al., 2019; Lin et al., 2011; Masugi-Tokita et al., 2016; Padilla et al., 2016). Masugi-Tokita et al. (2016) found a severe reduction of intermale attacks in metabotropic glutamate receptor subtype 7 (mGluR7) null mutant (KO) mice. Reduced c-Fos activation in the posterior BNST (BNSTp) of mGluR7 KO mice after placing urine sample of another male (which normally produces an agonistic reaction such as aggression in male mice) suggested that mGluR7-mediated olfactory processing in this brain region is essential for intermale aggression. Pharmacological block of mGluR7 in the BNSTp during RI test significantly reduced the duration of aggressive behaviour (Masugi-Tokita et al., 2016). Another study used a fiber photometry measurements of a population Ca^{2+}-dynamics in aromatase expressing (Aro+) neurons of the principle (sub)nucleus of the medial BNST (BNSTpr), and found that these neurons in sexually naive males were active upon introduction of another male, but not

during attacks (Bayless et al., 2019). Since Aro+ BNSTpr neurons are mostly inhibitory (Bayless et al., 2019) and project to the VMHvl (Lo et al., 2019), it is not straightforward to conclude on their role in regulating aggression via the VMH. Overall, these studies suggest that the BNST plays a role in mating and territorial aggression.

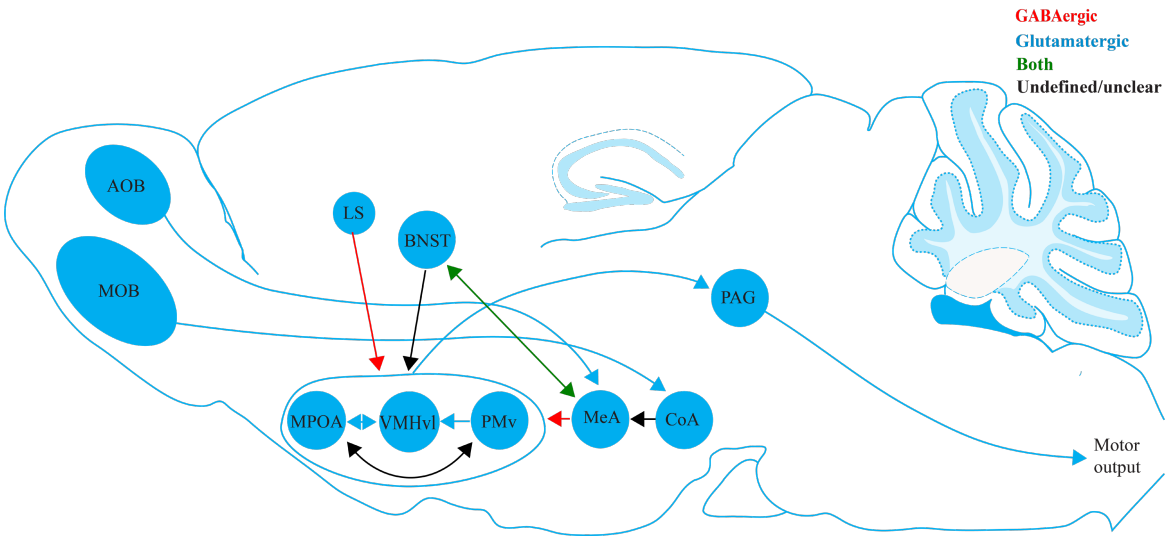

Figure 1.6 | Neural circuits of aggression in mice. Olfactory information is first detected and processed by the accessory and the main olfactory bulbs. Then this information is relayed to amygdala nuclei (MeA and CoA, respectively), and from there – to the hypothalamic nuclei directly or via the BNST. The lateral septum (LS, not shown on the scheme) is another upstream controller of aggression, negatively modulating it by inhibiting the VMHvl. (adapted from (Lischinsky and Lin, 2020)).

Taken together, the neural circuits of innate behaviours, including aggression, has seen a surge of interest by many researchers in the recent years. However, despite a few decades of efforts to identify molecular markers and the brain areas required to initiate aggressive behaviour (attack), the circuit mechanisms that underlie territorial male aggression remain not well understood. This was in part caused by a large molecular complexity of inhibitory neurons in the MeA connecting to various hypothalamic areas involved in the aggression control.

In my thesis work I have studied the neural circuits of aggression, initially attempting to further subdivide molecularly defined, or projection-area defined subpopulations of the MeApd inhibitory neurons. In the initial *in vivo* optogenetic stimulation experiments, a paradoxical difference between the stimulation of MeA GABA neurons using ChR2 ($ChR2^{H134R}$) versus ChETA ($ChR2^{E123T,H134R}$) was found. This has called for re-interpretation of the earlier results by Hong et al. (2014). Therefore, in the first part of the thesis I will show how two widely used channelrhodopsin variants can lead to opposing modulation of aggressive behaviours. In the second part of my thesis, using *in-vivo* and *in-vitro* optogenetic and imaging tools, I will

describe the possible mechanism of how MeApd inhibitory neurons can control mouse aggressivity via the downstream connections to the VMHvl and PMv.

Chapter 2: Results I

Optogenetic stimulation of medial amygdala GABA neurons with kinetically different channelrhodopsin variants yield opposite behavioral outcomes

Aiste Baleisyte[1], Ralf Schneggenburger[1*], Olexiy Kochubey[1*]

[1] Laboratory of Synaptic Mechanisms, Brain Mind Institute, School of Life Science, École Polytechnique Fédérale de Lausanne (EPFL), 1015 Lausanne, Switzerland

Author contribution:

A.B. and O.K. performed the experiments and analyzed the data; O.K., R.S., and A.B. conceived the study and wrote the manuscript.

Introduction

The advent of optogenetic methods about a decade ago has allowed researchers to manipulate the electrical excitability and AP-firing of genetically-specified neuron populations by light, and to observe the influence of this manipulation on animal behavior (Deisseroth, 2015; Tye and Deisseroth, 2012; Zhang et al., 2007). The "excitatory" cation channel channelrhodopsin-2 from *Chlamydomonas reinhardtii* has been amongst the first light-sensitive ion transporters from single-cell organisms made available for optogenetic studies (Boyden et al., 2005; Nagel et al., 2002, 2005; Sineshchekov et al., 2002). After its initial description, the properties of channelrhodopsin-2 were optimized for *in-vivo* use by introducing engineered mutations. A histidine to arginine mutation was introduced to increase the stationary photocurrent (H134R; Nagel et al., 2005), giving rise to the channelrhodospin-2^{H134R} variant (called here "ChR2"), which has been widely used for *in-vivo* optogenetic stimulation experiments. In subsequent work, additional mutations were introduced with the aim to increase the off-kinetics of the light-gated channel; one of the resulting variants carries an additional E123T mutation (channelrhodopsin-$2^{H134R,\ E123T}$) and has been called "ChETA" (Gunaydin et al., 2010). In addition, other light-gated ion channels with fast kinetics have become available, like for example Chronos and ChIEF (Klapoetke et al., 2014; Lin et al., 2009). The kinetic differences between ChR2, and the faster ChETA, ChIEF and Chronos have been well documented (Berndt et al., 2011; Gunaydin et al., 2010; Klapoetke et al., 2014; Lin et al., 2009; Mattis et al., 2012), and it was shown that blue light stimulation of ChR2 expressing neurons can lead to a light-induced depolarization block, especially in some classes of interneurons (Herman et al., 2014). Nevertheless, fundamentally conflicting behavioral outcomes after the *in-vivo* use of different channelrhodopsins have, to our knowledge, not been found.

The medial amygdala, and especially its postero-dorsal division (MeApd) contains a large fraction of GABA neurons (Choi et al., 2005; Keshavarzi et al., 2014). Of these, many neurons are long-range projection neurons that send axons to hypothalamic nuclei and other targets (Bian et al., 2008; Canteras et al., 1995; Choi et al., 2005; Keshavarzi et al., 2014). Early lesion studies showed a role of the MeA in social behavior and aggression control (Miczek et al., 1974; Vochteloo and Koolhaas, 1987; reviewed in Haller, 2018). More recent optogenetic and chemogenetic studies in mice have further defined the role of the MeA in aggression control (Hong et al., 2014; Nordman and Li, 2020; Padilla et al., 2016; Unger et al., 2015). Particularly,

Hong et al. (2014) have shown, using a *VGAT*^{Cre} mouse line to target GABA neurons in the MeApd, that optogenetic stimulation of these neurons using ChR2 led to a marked increase of attacks in the resident-intruder test (Hong et al., 2014). This finding has given rise to the generally accepted view that MeApd GABA neurons have a *stimulatory* role in aggression control (see reviews by Aleyasin et al., 2018; P. Chen & Hong, 2018; Hashikawa et al., 2016; Lischinsky & Lin, 2020).

We now report that using ChR2 and ChETA for optogenetic stimulation of MeApd-GABA neurons gives rise to a paradoxical *opposite* behavioral outcome in a social behavior test. In initial experiments in which we wished to follow-up on the role of MeApd GABA neurons in aggression control, we accidentally used ChETA and observed an *inhibition* of aggression, opposite to the previous study that had employed ChR2 (Hong et al., 2014). We therefore systematically compared the behavioral effects of optogenetic stimulation with ChR2 *versus* ChETA. This revealed that under otherwise identical conditions, activating MeApd GABA neurons with ChETA *suppressed* aggression, whereas optogenetic stimulation with ChR2 led to an *increase* of aggression as reported earlier (Hong et al., 2014). *Ex-vivo* electrophysiological recordings showed that optogenetic stimulation of MeApd GABA neurons expressing the slower ChR2 showed significantly larger plateau depolarizations than with ChETA. The plateau depolarizations caused a time-dependent decrease of AP amplitudes during prolonged stimulation trains, and a larger charge transfer during optogenetically-evoked inhibition of neighboring MeApd GABA neurons, as compared to stimulation using ChETA, differences which might explain the opposite behavioral outcomes *in-vivo*. Our study shows that care has to be taken when selecting channelrhodopsin variants for *in-vivo* optogenetic experiments, especially in mixed populations of GABA neurons. Given these conflicting results with two channelrhodopsin variants, the role of MeApd GABA neurons in controlling aggressive behavior should be newly investigated.

Materials and Methods

Laboratory mice

All procedures with laboratory mice (*mus musculus*) were authorized by the Service of Consumption and Veterinary Affairs (SCAV), Canton of Vaud, Switzerland (authorizations VD2885.0 and VD2885.1). We used the $VGAT^{Cre}$ mouse line, which is a VGAT-internal ribosome entry site (IRES)-Cre line (STOCK $Slc32a1^{tm2(cre)Lowl}$/J; RRID:IMSR_JAX:016962), first described in Vong et al. (2011). In some experiments (Fig. 2.1, Suppl. Fig. 2.4H, 2.4I), we used $VGAT^{Cre}$ × tdTomato mice, which were the offspring of a cross between $VGAT^{Cre}$ line and a Cre-dependent tdTomato reporter mice Ai9 (B6.Cg-$Gt(ROSA)26Sor^{tm9(CAG-tdTomato)Hze}$/J; RRID:IMSR_JAX:007909), described in (Madisen et al., 2010). $VGAT^{Cre}$ mice were back-crossed to the C57Bl6/J line (RRID:IMSR_JAX:000664) for 2-3 generations; similarly, the tdTomato line was maintained on C57Bl6/J background. Healthy adult, virgin male mice were used in a resident-intruder aggression tests. The animals were group-housed in cages with a maximum of five individuals at the specific pathogen free animal facility at EPFL under a 12/12 hr light/dark cycle, with food and water ad libitum. The animals were separated into single cages one day before surgery. BALB/cByJ male mice (RRID:IMSR_JAX:001026) were purchased from Charles River (Écully, France) and were group-housed until used as intruder mice in the resident-intruder test.

Viral vectors. To target channelrhodopsin and/or fluorophore expression to MeApd GABA neurons for *in-vivo* and *ex-vivo* experiments, we used Cre-recombinase dependent (DIO/DIO; Schnütgen et al., 2003) adeno-associated viral vectors (AAV) of the serotypes 2/8, 2/2 and 2/1 (referred to as AAV8, AAV2, AAV1; see Table 1). We used two modifications of the original wildtype ChR2 (Boyden et al., 2005; Nagel et al., 2003): a speed-optimized $ChETA^{H134R,E123T}$ (Gunaydin et al., 2010), and an enhanced $ChR2^{H134R}$ (Nagel et al., 2005) version. For production of the AAV8:hSyn:DIO:ChETA-eYFP and AAV8:hSyn:DIO:eGFP vectors used for our initial experiments (Fig. 2.1), the DNA plasmids were respectively derived from the plasmids pAAV:EF1α:DIO:ChETA-eYFP (plasmid #26968; Addgene, Watertown, MA, USA) and pAAV:EF1α:DIO:eYFP (Addgene plasmid #27056) by custom cloning, and verified by sequencing. These two AAV8 vectors were packaged by the lab of Dr. Bernard Schneider (EPFL).

Because the previously used custom-made AAV2:EF1α:DIO:ChR2-2A-hrGFP vector (Hong et al., 2014) was not publically available, we purchased a vector driving the Cre-dependent expression of $ChR2^{H134R}$ as close as possible to Hong et al. (2014): AAV2:EF1α:DIO:ChR2-eYFP (see Table 1). Indeed, with this vector, and with AAV8:EF1α:DIO:ChR2-eYFP, we were able to reproduce the previously reported stimulatory effect on aggression (Hong et al., 2014; see Fig. 2.4). DNA sequence alignment has confirmed that all the channelrhodopsin-encoding vectors used in our study had the sequences downstream of promoters identical to plasmids pAAV:EF1α:DIO:ChETA-eYFP (Addgene #26968) and pAAV:EF1α:DIO:ChR2-eYFP (Addgene #20298), respectively, which were originally donated by the lab of Dr. Karl Deisseroth. Other viral vectors were purchased from various suppliers (see Table 1).

Table 2.1. List of the viral vectors used in the study.

Vector	**Figure**	**Source/Supplier**	**Catalog number / Other ID**
AAV8:hSyn:DIO:ChETA-eYFP	Fig. 2.1 Fig. 2.2 Fig. 2.4	AAV packaging made by the lab. of Neurodegenerative Studies Laboratory (LEN), Dr. Bernard Schneider	Coding sequence identical to Addgene plasmid #26968
AAV8:EF1α:DIO:ChR2-eYFP	Fig. 2.4 Suppl. 2.4	University of Zürich Viral Vector Facility, Zürich, Switzerland	Cat# v214-8
AAV2:EF1α:DIO:ChETA-eYFP	Fig. 2.4 Fig. 2.5 Suppl. 2.4 Suppl. 2.5	University of North Carolina Vector Core, Chapel Hill, NC, USA	In-stock vector (contributed by Dr. Karl Deisseroth)
AAV2:EF1α:DIO:ChR2-eYFP	Fig. 2.3 Fig. 2.4 Fig. 2.5 Suppl. 2.2 Suppl. 2.5	University of North Carolina Vector Core	In-stock vector (contributed by Dr. Karl Deisseroth)

AAV1:EF1α:DIO:ChETA-eYFP	Suppl. 2.1	University of Pennsylvania Vector Core, Philadelphia, PA, USA	Cat# AV-1-26968P; now available from Addgene as Cat# 26968-AAV1
AAV8:hSyn:DIO:eGFP	Fig. 2.1 Fig. 2.4 Suppl. 2.4	AAV packaging made by the lab. of Neurodegenerative Studies Laboratory (LEN), Dr. Bernard Schneider	Coding sequence identical to Addgene plasmid #50457
AAV8:CAG:DIO:tdTomato	Suppl. 2.3	University of North Carolina Vector Core	In-stock vector (contributed by Dr. Ed Boyden)
AAV2:EF1α:DIO:eYFP	Fig. 2.3 Fig. 2.4 Suppl. 2.3 Suppl. 2.4 Suppl. 2.5	University of North Carolina Vector Core	In-stock vector (contributed by Dr. Karl Deisseroth)

Stereotactic surgery procedures. VGAT^{Cre} male mice (8-10 weeks old) in cohorts of 5-6 animals were randomly assigned to a test or to a control group. They were stereotaxically bilaterally injected in the MeApd with an AAV vector encoding for a channelrhodopsin-fluorophore fusion construct (test group) or fluorophore only (control group). All procedures were identical between the control - and the test groups. Stereotaxic surgeries were made using a model 942 small animal digital stereotaxic instrument (David Kopf Instruments, Tujunga, CA, USA) under continuous anesthestesia (1-1.5% isoflurane in O_2) and pre-operative local analgesia (a mix of bupivacaine and lidocaine subcutaneously). For additional analgesia, paracetamol was provided in the drinking water (1 mg/ml) starting one day before, and during five days post-surgery. For *in-vivo* optogenetic stimulation experiments (Fig. 2.1, 2.3, 2.4; Suppl. Fig. 2.1, 2.4), 200 nl of virus suspension was injected on each brain side into the MeApd with a pulled glass capillary at the following coordinates (in mm from bregma skull surface): ML ±2.3, AP -1.7, DV -5.3. Optic fiber implants, custom made of 200 □m core / 0.39 NA optic fiber (FT200UMT; Thorlabs Inc, Newton, NJ, USA; implant transmission >70% at 473 nm) as previously described (Sparta et al., 2012; Tang et al., 2020), were vertically advanced to 500

μm above the injection sites and secured to the skull with a dental cement cup (Jet denture repair package; Cat#1234FIB; Lang Dental, Wheeling, IL, USA), and an anchoring screw (Cat#AMS90/1B-100; Antrin Miniature Specialties, Fallbrook, CA, USA). For *ex-vivo* patch-clamp recordings (Fig. 2.5; Suppl. Fig. 2.5), the injected suspension (200 nl) consisted of a 1:1 mix of two viral vectors as indicated, and no optic fibers were implanted. For histological analysis of AAV2 and AAV8 vector tropism (Suppl. Fig. 2.3), 100 nl of a 1:1 mix of indicated viral vectors was unilaterally injected into the left MeApd.

Behavioral testing. Following the surgery, the mice were housed individually. 4-5 weeks after surgery, a resident-intruder test was performed under optogenetic stimulation. The testing was performed at the beginning of the dark cycle in the home cages of the operated mice under minimal ambient light levels. No change of bedding was made for a week before testing; enrichment materials (nesting material, plastic shelter and cardboard tunnel) were removed for the experiment. There was no pre-selection of animals based on their basal aggression or hierarchy rank. Prior to the resident-intruder test, the operated $VGAT^{Cre}$ resident mice were habituated to handling (being held in experimenter's hands, constraining and patch cord attachment). Furthermore, the mice were habituated to the head tethering imposed by the optic patch cords while exploring the home cage, during 4-5 daily sessions 15 min long each. The resident-intruder experiment consisted of a 5 min baseline when the resident animal was exploring its home cage alone, followed by introducing an unfamiliar BALB/cByJ male intruder (8-9 weeks old) for the next ~25 min. Each mouse underwent two sessions of resident-intruder testing on subsequent days using different intruders; each intruder animal was used maximally twice. The behavior was continuously recorded with two synchronized CMOS cameras (acA1300-60gc; Basler AG, Ahrensburg, Germany) providing top- and side views, equipped with infrared long-pass filters and under infrared light illumination, at 30 fps under control of EthoVision XT 13 software (Noldus Information Technologies, Wageningen, The Netherlands). The same software recorded a TTL signal from a Master-8 stimulator (A.M.P.I., Jerusalem, Israel) representing the gate for the trains of blue light pulses. The blue light pulses were produced by a 473 nm diode pumped solid state laser (MBL-FN-473-150mW, Changchun New Industries Optoelectronics, Changchun, China) triggered with TTL pulse trains from the Master-8 stimulator, and directed towards the optic fiber implants through 200 μm core / 0.22 NA optic patch cords (FC connector to 1.25 mm ferrule; Doric Lenses, Quebec, Canada) attached to a 1x2 intensity dividing fiber optic rotary joint (Doric Lenses). For each mouse, the laser power was adjusted to obtain 10 mW at the tip of the optic fiber implant; in some

experiments we adjusted to other light power levels (Suppl. Fig. 2.1). Light stimuli were 5 ms long, repeated at 20 Hz. We used a regular pattern of light trains (30-60 s long) interleaved with dark periods of fixed length (60 s), to avoid possible experimental bias. Such a bias could arise if the experimenter would trigger the light train manually during a short aggression bout, resulting in a trend of the light trains starting towards the end of the aggression bout.

Histology. For the post-hoc validation of channelrhodopsin expression and optic fiber placement above the MeApd (Fig. 2.2, Suppl. Fig. 2.2), the animals were deeply anesthetized with intraperitoneal injection of pentobarbital, and transcardially perfused with 4% paraformaldehyde in PBS. After 24h post-fixation in 4% PFA and dehydration in 30% sucrose in PBS, 40 µm thick coronal brain sections were cut using a freezing microtome (Hyrax S30; Carl Zeiss, Oberkochen, Germany).

For analysing the distribution of AAV2- and AAV8-infected GABA neurons in the MeApd, one VGAT^{Cre} mouse was injected with a mix of AAV2:EF1α:DIO:eYFP and AAV8:CAG:DIO:tdTomato viruses. Two other mice were injected with AAV8:EF1α:DIO:mCherry instead of the latter vector (Suppl. Fig. 2.3). The animals were sacrificed 3 and 4 weeks after injection, respectively, and coronal sections of the MeA were prepared as described above. Immunohistochemistry was performed using 1:1000 diluted chicken anti-GFP (ab13970; Abcam, Cambridge, United Kingdom; RRID:AB_300798) and 1:500 rabbit anti-RFP antibodies (ab62341; Abcam; RRID:AB_945213) to stain against eYFP and tdTomato or mCherry, respectively. As the secondary antibodies, goat anti-chicken Alexa-488 (A11039; Thermo Fisher Scientific, Waltham, MA, USA; RRID:AB_2534096) and donkey anti-rabbit Alexa-568 antibodies (A10042; Thermo Fisher Scientific; RRID:AB_2534017) were used at 1:200 dilution.
In all cases, free-floating brain sections were mounted on glass slides and embedded in DAPI containing mounting medium (Fluoroshield with DAPI; F6057-20ML; Merck/Sigma-Aldrich, Darmstadt, Germany).

Image acquisition. Brain sections for post-hoc validation of fiber placements (Fig. 2.2, Suppl. Fig. 2.2) were imaged with a slide scanning microscope (VS120-L100; Olympus, Tokyo, Japan) employing a 10x/0.4 NA objective. To analyze the distribution of AAV2- and AAV8-transduced neurons (Fig. 2.5, Suppl. Fig. 2.3), tile images of up to 3 focal planes were acquired using an inverted confocal microscope (LSM 700; Carl Zeiss) equipped with a 40x / 1.3 NA

oil objective (Fig. 2.5A, 2.5B, Suppl. Fig. 2.3A-2.3C), or with a 20x / 0.8 NA air objective (Suppl. Fig. 2.3D-2.3I) and 405, 488 and 555 nm laser lines for exciting DAPI, YFP and tdTomato/mCherry, respectively. Image acquisition was done at the Bioimaging and Optics Platform (BIOP), EPFL.

Patch-clamp electrophysiology. A mouse at a time was sacrificed by decapitation after a brief anaesthesia with 3% isoflurane in O_2 (according to the authorized protocol; see above), and 300 µm thick coronal brain slices containing the MeApd were made with a Leica VT1000S vibratome (Leica Microsystems, Wetzlar, Germany). The experiments were done 4-5 weeks following injection with the respective virus mix (Fig. 2.5; see Table 1). Slicing was done in N-methyl-D-glutamine (NMDG) based solution containing (in mM): 110 NMDG, 2.5 KCl, 1.2 NaH_2PO_4, 25 $NaHCO_3$, 20 HEPES, 25 D-glucose, 5 sodium ascorbate, 2 thiourea, 3 sodium pyruvate, 10 $MgCl_2$, 0.5 $CaCl_2$ (pH 7.3; Ting et al., 2014). The slices were then kept in a holding solution containing (in mM): 92 NaCl, 1.2 NaH_2PO_4, 30 $NaHCO_3$, 20 HEPES, 25 D-glucose, 5 sodium ascorbate, 3 thiourea, 3 sodium pyruvate, 2 $MgCl_2$, 2 $CaCl_2$ (pH 7.3). Whole-cell patch clamp recordings were performed using an extracellular solution containing (in mM): 124 NaCl, 2.5 KCl, 1.2 NaH_2PO_4, 30 $NaHCO_3$, 20 HEPES, 10 D-glucose, 5 sodium ascorbate, 2 thiourea, 3 sodium pyruvate, 2 $MgCl_2$, 2 $CaCl_2$ (pH 7.4, continuously bubbled with 95% O_2 / 5% CO_2). Recording pipettes were filled with a low-chloride solution, containing in (mM): 8 KCl, 145 K-gluconate, 10 HEPES, 3 Na-phosphocreatine, 4 Mg-ATP, 0.3 Na-GTP, 5 EGTA (pH 7.26, with KOH; 315 mosm). All recordings were done under an upright BX50WI microscope (Olympus) equipped with a 60x / 0.9 NA water-immersion objective (LUMPlanFl, Olympus), using an EPC-10 patch-clamp amplifier under control of PatchMaster software (HEKA Elektronik, Reutlingen, Germany). A near-physiological temperature control of the recording bath (34-36°C) was done using a PM-1 heated platform, a SHM-6 inline solution heater and a TC-344B controller (Warner Instruments, Holliston, MA, USA). The slices were illuminated with a Dodt IR gradient contrast and imaged using a CMOS camera (C11440-52U; Hamamatsu Photonics, Hamamatsu City, Japan) under control of MicroManager software (Edelstein et al., 2014). To visualize the eYFP or tdTomato/mCherry fluorescence, the fluorophores were excited using custom-fitted high-power LEDs (CREE XP-E2 Royal blue, 465 nm, and Green, 535 nm, respectively; Cree Inc, Durham, NC, USA) controlled with a BioLED driver (BLS-SA02-US; Mightex Systems, Toronto, Canada), and imaged using appropriate dichroic mirrors and emission filters. Short pulses (5 ms) of a blue LED at maximal

power (~80 mW/mm^2 at the focal plane with 60x objective) were used for exciting ChETA or ChR2. oIPSCs were measured at 0 mV holding potential (Fig. 2.5).

Analysis of behavior data. The behavioral data was manually scored using the video annotation tool Anvil (https://www.anvil-software.org/; Kipp, 2001). During analysis, the scorer was blind to the timing of the optogenetic light train. During manual scoring, each video frame was exclusively classified as one of 23 elementary behaviors of the resident mouse: 1) attack; 2) tail rattle; 3) catching with paws; 4) proactive approach; 5) sniffing/touching the intruder's body; 6) sniffing the body while following the intruder; 7) mouse/nose sniffing; 8) anogenital sniffing; 9) anogenital sniffing while following; 10) tail sniffing; 11) licking the intruder; 12) mounting the intruder; 13) being sniffed by intruder; 14) being followed; 15) being attacked; 16) being licked; 17) escaping from intruder; 18) grooming; 19) digging; 20) moving at a distance from the intruder; 21) resting at a distance; 22) rearing; 23) active avoidance. Display and averaging of the resulting behavioral traces was done using custom routines in IgorPro 7.08 (WaveMetrics, Lake Oswego, OR, USA). We combined the traces of elementary behaviors (see above) into the following six groups using a logical "OR": "aggression" (behaviors #1-3), "following" (#6, 8-9), "social contact" (#4, 5, 7, 10, 11), "asocial" (#18, 19, 22, 23), "passive" (#13-17) and "resting/moving" (#20, 21). Note that mounting (#12) was not included in any of these groups because we have virtually never observed spontaneous nor light-evoked mounting in these experiments. The resulting six behavior traces were aligned to the onsets of the blue light trains and averaged across repeated trains for a given mouse (see e.g. Fig. 2.1E, 2.1G). To quantify the effect of blue light exposure (e.g. Fig. 2.1E), we compared the relative time of aggressive behavior during the first 30 s of the light train, to the last 30 s of the preceding dark period. The results of this analysis were averaged for each animal between two consequent days of resident-intruder testing, yielding one final data point per animal in the summary bar plot graphs (e.g. Fig. 2.1H).

About one third of the behavioral experiments, performed towards the end of the study, was analyzed with an automatic procedure as described by Nilsson et al. (2020), using top-view videos and a DeepLabCut (Mathis et al., 2018; run on Google Colab platform) - SimBA behavior classification framework. The predictions of behaviors generated by SimBA (Nilsson et al., 2020) were analyzed in IgorPro the same way as the manually scored behaviors.

Analysis of illuminated brain areas. The slide scanner images of brain sections for post-hoc validation of fiber placement were manually aligned into a serial stack using FIJI TrackEM2 (Cardona et al., 2010; Schindelin et al., 2012). A custom IgorPro macro was used for navigation through the stack and for fitting a model of the optic fiber into the fiber track visible on the images, in order to calculate the 3D location of an idealized light cone emanating from the fiber, thereby taking into account the fiber tilt. For computing a cone-shaped 3D light cone, we used the core diameter and numerical aperture of the fiber, and assumed a 500 □m limit for the light propagation in brain tissue (Aravanis et al., 2007). The contours of a brain atlas (Franklin and Paxinos, 2013) were overlaid onto the images using Adobe Illustrator (Adobe Inc, Mountain View, CA, USA). Finally, the areas of the relevant brain nuclei, their overlap with the extent of the channelrhodopsin expression, and the percentage overlap with the light cone were quantified in IgorPro. Before calculating the fr s, the respective areas were summed across the serial brain sections to approximate the fractions of volume (see Fig. 2.2B, 2.2C, Suppl. Figure 2.2B-2.2C).

Analysis of AAV vector tropism. For analysis of distribution of AAV2- and AAV8-transduced neurons (Suppl. Fig. 2.3), non-overlapping ROIs were manually drawn using FIJI on confocal tile images around each neuron expressing any of the reporters (eYFP or tdTomato/mCherry), and the mean intensities and centroid coordinates of these ROIs were imported into IgorPro for analysis. The cells were classified as either expressing, or non-expressing the fluorescent reporter protein when the mean ROI fluorescence intensity exceeded a threshold value set at 150% and 200% of the mean background fluorescence in the whole MeApd for the red and the green channels, respectively. Based on this classification, binary maps of reporter (co-) expression by individual cells were generated (Suppl. Fig. 2.3).

Electrophysiological data analysis. Electrophysiological recording data were imported into IgorPro for analysis using custom routines. Peak amplitudes of light-gated channelrhodopsin currents and of oIPSCs (Fig. 2.5C-2.5F) were measured at -70 mV and 0 mV holding potential, respectively, in response to the first light pulse in a train (Fig. 2.5A, 2.5B; the second from top and the bottom panels, respectively). For some cells, the first light pulse evoked an unclampable Na^+-current; in those cases, the value of the light-gated current was read out at the point of the falling slope change (if apparent; see Fig. 2.5B insets), or as the peak of the next well-clamped channelrhodopsin-mediated current. The ChR2 or ChETA-evoked plateau potential during the 20 Hz / 5 ms light trains, was quantified as the average voltage offset over

resting V_m, after low-pass filtering <10 Hz to remove the action potential (AP) transients. Deactivation time constants of the two channelrhodopsin variants (see Results) were estimated by single-exponential fits to the decay of light-gated currents upon the last pulse in a train. Synaptic charge transfer (Fig. 2.5 G) was estimated by integrating the oIPSC trace over 1 s long train of light pulses (Fig. 2.5 A, 2.5 B, bottom panels) after the baseline current subtraction; cells with the negative integral values due to negligible IPSC amplitudes were excluded. Analysis of the APs during the 30s trains of light pulses (Fig. 2.5 H-2.5 J) was limited to cells expressing the direct current >50 pA, which lead to exclusion of n=2 and n=4 cells from ChR2 and ChETA groups, reducing the sample to n=25 and 18 recordings, respectively. For the absolute AP peak amplitude measurements during 30 s light trains (Fig. 2.5 H, 2.5 I), fast voltage transients time-locked to the light pulses were first classified as APs only if exceeded 20 mV threshold relative to the passive membrane response level; the latter was estimated by filtering the voltage trace <10 Hz in a procedure identical to determination of the plateau potential. Only the cells that displayed no failures during the indicated time periods were admitted for analysis in Fig. 2.5 I; note that the cell numbers contributing to the average traces dropped faster for ChR2 than for ChETA, respectively, due to the failures in ChR2 expressing cells. For quantification of the number of successful APs generated during optogenetic trains (Fig. 2.5 J), APs were detected based on a threshold of 0 mV (see dashed line in Fig. 2.5 H) and considered as failure if the AP peak amplitude dropped below this threshold during the train.

Classification of the cells into intrinsic AP firing types (Suppl. Fig. 2.5) was performed manually by an observer, based on the cell membrane voltage response to the step current injections (from -100 to +320 pA in 30 pA increments relative to the holding current; Suppl. Fig. 2.5 B). For this, the passive and active (AP firing dynamics) membrane properties were first analyzed with custom routines in IgorPro to extract information on the time course of AP frequency during the current step depolarizations, and on the maximal firing frequency as a function of injected current (Suppl. Fig. 2.5 B). Passive membrane properties such as the input resistance and membrane time constant were also documented, as well as the presence of a negative voltage sag (quantified as a "sag ratio"). The following definitions of the firing types were then used for classification (see Suppl. Fig. 2.5 B for examples). Type 1: a neuron responded with only a single AP to depolarizing current steps, then the AP firing ceased. Type 2: a neuron that slowly adapts to low spiking frequency at small injected currents, but which can only generate a short burst (a few APs) upon intermediate to large current steps. Type 3: a

neuron generating a brief high-frequency burst of APs which then rapidly adapts to a low (<50 Hz) steady-state frequency. Type 4: a neuron showed no clear adaptation of the AP firing frequency, and in some cases – augmentation of instantaneous AP frequency showing a maximum between the 2nd and the 3rd APs. Type 5: a high-frequency spiking neuron slowly adapting to the high (≥ 50 Hz) AP frequency steady state at intermediate injected currents, and expressing no negative voltage sag. Type 6: AP firing dynamics as for the type 5 neurons, but expressing a negative voltage sag (a signature of I_h current, in some cases leading to post-hyperpolarization rebound AP). Note that at the largest amplitudes of tested depolarizing current steps, some neurons of the types 5 and 6 ceased AP firing after a short period of AP frequency adaptation (Suppl. Fig. 2.5B).

Statistical data analysis. No prior sample size calculation was performed. Resident-intruder experiments with optogenetic modulation were usually performed in small cohorts at a time of N = 3 and N = 3 mice for the test group (expressing ChETA or ChR2) and for the control group (expressing eYFP or eGFP); experiments were repeated with several cohorts for each condition. Statistical tests were performed using GraphPad Prism 9 (GraphPad Software, USA). A Shapiro-Wilk test for normality was made to determine if the data was normally distributed before choosing a parametric or non-parametric test type. In case of two-sample datasets, either a paired or two-sample t-test, or Wilcoxon or Mann-Whitney U tests were performed as indicated in the Results (Fig. 2.1, 2.3, 2.4, 2.5 C-2.5G, Suppl. Fig. 2.1, 2.5). To compare the timecourses of AP amplitudes (Fig. 2.5 I; n=20 data points per cell in each time range), two-way repeated-measures ANOVA was performed for each time range to analyse effects of the channelrhodopsin variant and of the time, followed by Holm-Šidák's multiple comparison test. For the analysis of AP following (Fig. 2.5 J), the average firing frequency was calculated in two 15s bins for each group, and a two-way repeated measures ANOVA analysis was performed followed by Šidák's multiple comparison test. Significance levels were reported in the Results text and additionally indicated in the Figures by star symbols according to: $p < 0.05$, *; $p < 0.01$, **; $p < 0.001$, ***.

Results

Optogenetic stimulation of MeApd GABA neurons with ChETA reduces aggression

Following a previous pioneering study which showed a *stimulatory* role of MeApd GABA neurons in the control of aggression (Hong et al., 2014), we originally wished to investigate the role of molecularly - and projection-defined MeApd GABA neurons in this social behavior. For this, we first attempted to reproduce the earlier findings, in which MeApd GABA neurons were optogenetically stimulated using the $VGAT^{Cre}$ mice, leading to the targeting the entire GABA neuron population (Fig. 2.1 A, B; see also Hong et al., 2014). Male *$VGAT^{Cre}$ x tdTomato* mice were bilaterally injected with an AAV vector driving the Cre-dependent expression of ChETA (AAV8:hSyn:DIO:ChETA-eYFP; see Table 2.1). Control mice received a vector driving the expression of eGFP (AAV8:hSyn:DIO:eGFP), but underwent otherwise identical procedures. Optic fibers were implanted bilaterally in the MeA, targeting the postero-dorsal subnucleus (Fig. 2.1 B; Fig. 2.2). Four weeks later, the mice were subjected to a resident-intruder test in their home cage using an adult male BALB/cByJ mouse as an intruder. We used trains of blue light pulses (5 ms, 10 mW, 20 Hz, length of 30s or 60s) delivered at regular intervals (60s dark periods), to avoid a possible bias by experimenter-driven stimulation.

We observed that aggression bouts occurred mostly in the dark periods (60s) in-between light stimulation, and that blue light often led to a stop of aggression (Fig. 2.1 C-2.1 E). Aligning and averaging the behavioral scores from individual mice showed that blue light reduced the time that a mouse spent attacking, from 2.55 s per 30 s of dark period (averaged over n = 10 dark periods), to 0.6 s per 30s of light period (n = 10; Fig. 2.1E). Blue light stimulation reduced the time mice spent attacking in all animals of the ChETA group (Fig. 2.1H; $p = 0.039$, N = 5 mice; two-tailed paired t-test). Control mice expressing eGFP did not show a modulation of aggression by light, as shown in Fig. 2.1 F, G for an example animal (N = 7 mice, $p = 0.73$; two-tailed paired t-test, Fig. 2.1 H). These findings, unexpectedly, suggest that optogenetic stimulation of MeApd GABA neurons leads to a *decrease* of aggression, opposite to the previous results (Hong et al., 2014).

Our experimental mice were single-housed after surgery and were not further selected according to their aggression levels (see Materials and Methods). In some mice, we found low levels of aggression and no spontaneous attacks against the intruder. In none of these non-aggressive mice did optogenetic activation of MeApd GABA neurons induce attacks (see Fig. 2.1 I for an example; N = 3 non-aggressive mice). This finding is also different from the previous study, in which blue light readily triggered attacks in non-aggressive mice (Hong et al., 2014; their Fig. 2). Furthermore, in an additional N= 2 mice in which ChETA was expressed by an AAV1 serotype vector, we similarly observed that blue light suppressed aggression (Suppl. Fig. 2.1). In the latter experiments, we also varied the intensity of blue light stimulation, and observed that the inhibition of aggression depended on light intensity, with no other obvious behaviors stimulated at low light intensities (Suppl. Fig. 2.1). These observations further support our finding that optogenetic stimulation of MeApd - GABA neurons *inhibits* aggression (Fig. 2.1), opposite to the previous report (Hong et al., 2014).

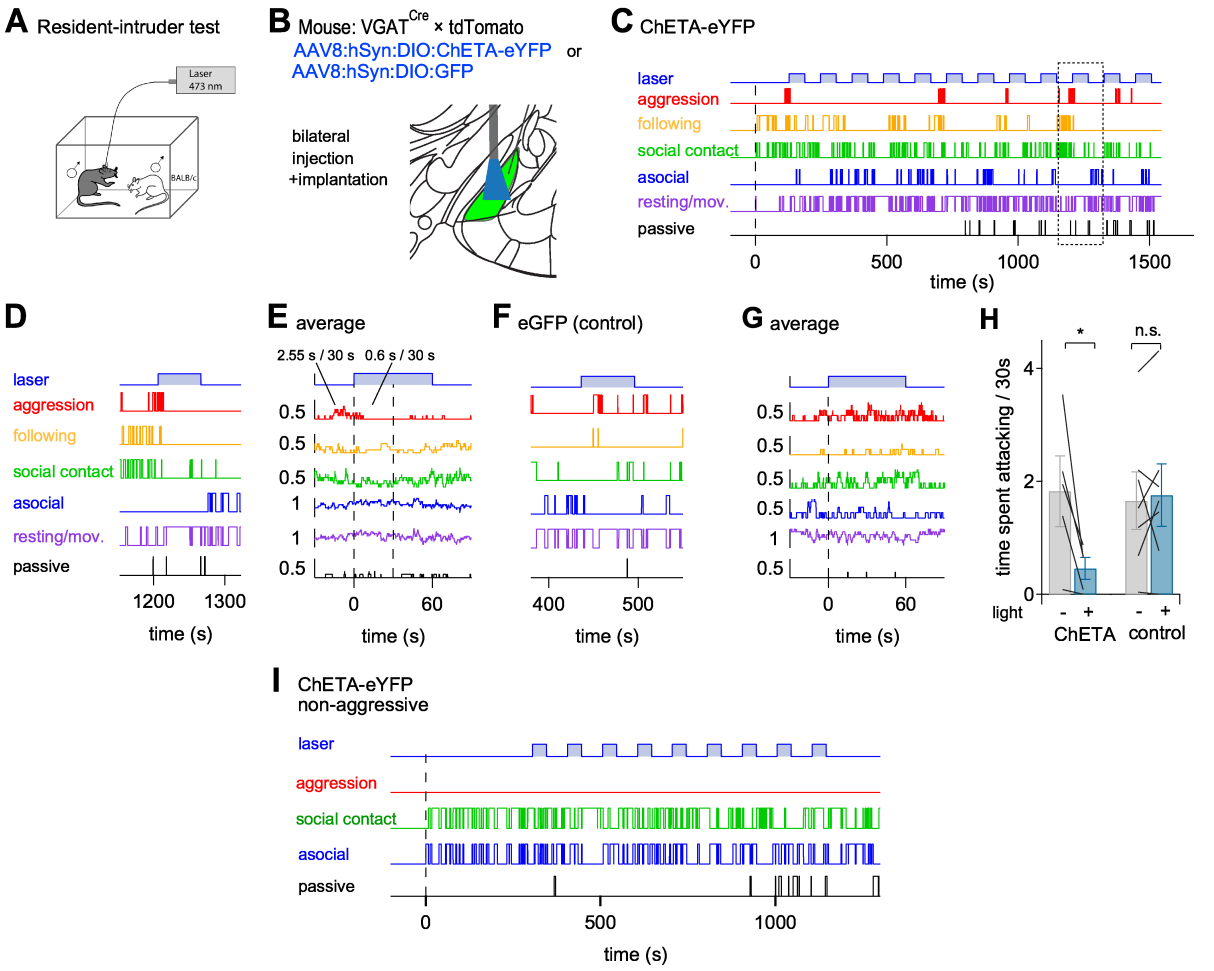

Figure 2.1 | In-vivo optogenetic stimulation of MeApd GABA neurons using ChETA inhibits inter-male aggression. (A) Scheme of a resident-intruder test with optogenetic stimulation of the MeApd in the resident male. BALB/cByJ male mice (one at a time) were used as intruders. **(B)** Schematic of the experimental approach for expression of ChETA and optic fiber implantation targeting. **(C)** Traces showing various quantified behaviors of a resident mouse during a resident-intruder test (see Materials and Methods). An intruder was introduced at t = 0. Trains of laser light pulses (5 ms, 20 Hz repetition rate, 10 mW intensity) were applied for 60s, interleaved by 60s dark periods. Note that the aggression bouts (red trace) preferably occurred *outside* the light trains. **(D)** An example light train episode marked by the dotted rectangle in **(C)**. **(E)** Aligning the behavior traces to the onsets of light trains with subsequent averaging showed a reduction of aggression after the start of the light train. The average time spent attacking during the last 30s of darkness, and during the first 30s of light stimulation, is indicated. Data in **(C-E)** are from a single ChETA-expressing example mouse. **(F, G)** Behavioral data from a control mouse expressing eGFP, both before and during a single light train **(F)** and corresponding average behavior traces for n = 7 light trains **(G)**. As expected, in this eGFP-expressing control mouse, blue-light stimulation did not modulate aggressive behavior. **(H)** Quantification of the time spent attacking during the 30 s before (-), and 30 s into (+) the light stimulation in mice expressing ChETA (N = 5) or eGFP (N = 7). For each mouse, the individual values are averages across two tests performed on subsequent days. Note the significant inhibition of aggression by blue light in the ChETA group ($p = 0.0385$), but not in the eGFP group ($p = 0.73$). **(I)** An example mouse expressing ChETA, which showed no aggression against the intruder (non-aggressive mice were not included in in the data pool shown in H). Note that optogenetic stimulation with ChETA did not induce aggression. Similar observations were made in N = 3 non-aggressive mice expressing ChETA. Error bars are ± s.e.m. See also Suppl. Figure 2.1.

A factor that may explain the opposite outcome of optogenetic stimulation between the present and the previous study (Hong et al., 2014) is that different brain areas might have been targeted between the two studies. We therefore reconstructed the regional expression of ChETA-eYFP, and the fiber placements for the experimental mice shown in Fig. 2.1C-2.1I (Fig. 2.2 A; see Materials and Methods). We found that 90 ± 5% and 89 ± 4 % of the cumulative area of the MeApd located in the vicinity of the optic fiber expressed ChETA (Fig. 2.2A and 2.2B; for the left and the right brain side respectively, N = 5 mice). The expression of ChETA was not limited to the MeApd but extended into the adjacent areas of neighboring subnuclei of the amygdala, albeit filling smaller percentages of those areas (Fig. 2.2A, 2.2 B; MeApv, posterioventral MeA; CeA, central amygdala; STIA, bed nucleus of the stria terminalis, intraamygdaloid division; BMA/BMP, basomedial amygdaloid nuclei, anterior or posterior; I, intercalated nuclei of amygdala). Next, we estimated the percentages of the ChETA-positive brain areas which, based on the position and angle of the optic fiber, were likely illuminated by blue light (see Materials and Methods). The largest fractional overlap between the area of ChETA expression and the calculated light cone was found for the MeApd (19.0 ± 2.8 % and 20.7 ± 3.1 % for the left and right brain side; Fig. 2.2 C), whereas the overlap was negligible in the MeApv, CeA, and BMA (~3.1%, ~0.08% and ~3.8%, respectively). The STIA region had a somewhat larger overlap of ChETA expression and illumination (8.0 ± 2.9 % and 5.7 ± 3.0 % of STIA volume for the left and right brain side; Fig. 2.2 C). However, it is possible that a significant part of ChETA-eGFP positive tissue in STIA originates from axons that project away from the MeApd. Taken together, post-hoc histological validation showed that we have primarily targeted the MeApd. Thus, we conclude that optogenetic stimulation of MeApd GABA neurons, using ChETA expressed by an AAV8 vector, suppresses aggression (Fig. 2.1, 2.2).

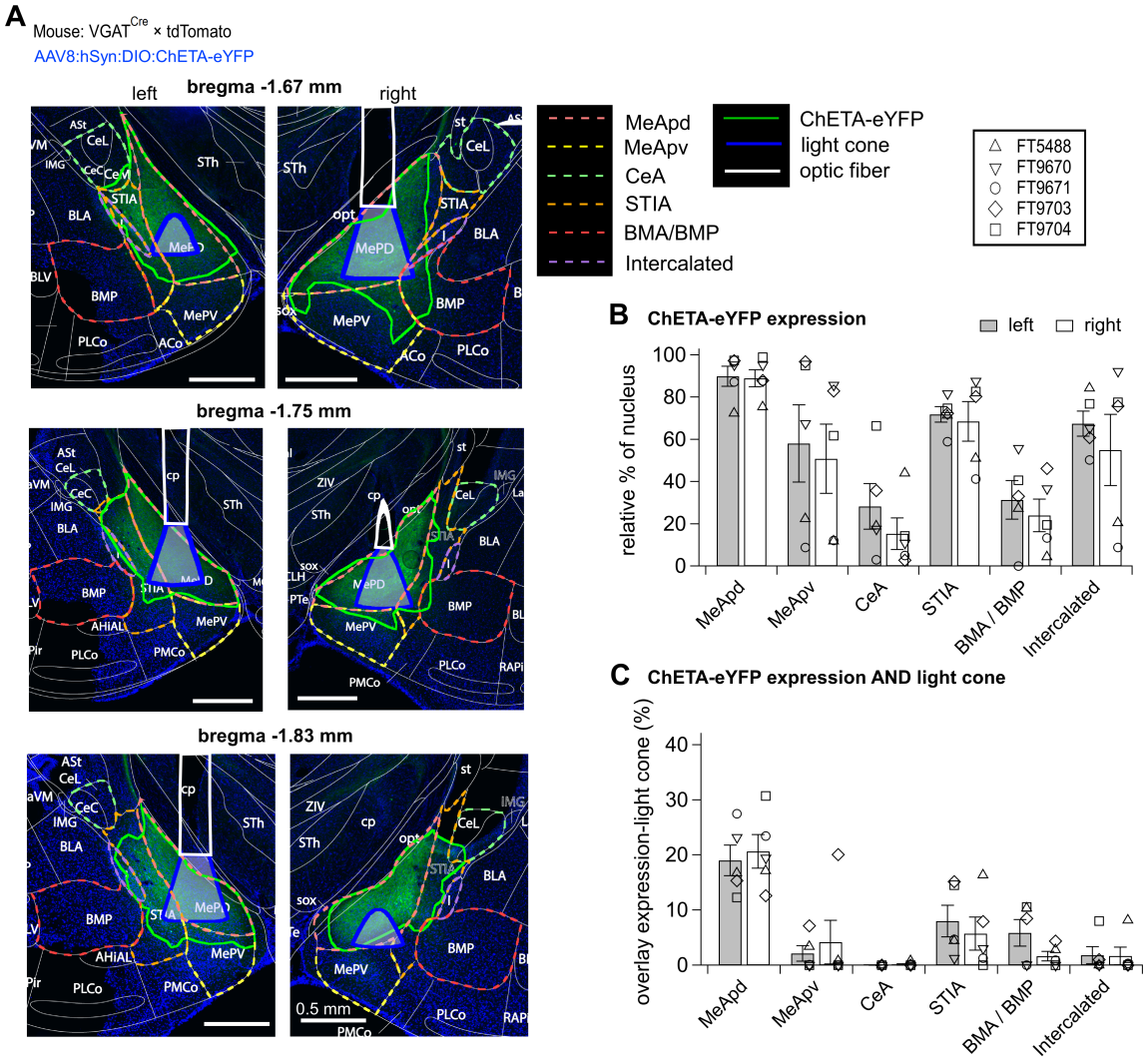

Figure 2.2 | Histological reconstructions of ChETA-eYFP expressing brain areas and optic fiber placement confirm optogenetic stimulation of the MeApd. (A) Fluorescent images on the level of the left and the right MeApd (bregma levels indicated), obtained from a ChETA-expressing mice after the behavior experiments (Figure 2.1). The regions of ChETA-eYFP expression (fluorescence in green channel) were outlined (solid green lines). Reconstructed contours of cross-sections through the optic fiber (solid white lines) and the brain atlas outlines (dashed lines; Franklin and Paxinos, 2013) were overlaid. The area of effective illumination (blue shading) was derived as explained in Materials and Methods. **(B)** The percentage of the area expressing ChETA-eYFP in the MeApd and neighboring brain structures, integrated across serial brain sections (N = 5 mice). See Results for abbreviations.
(C) The percentage of each nucleus which expressed ChETA-eYFP *and* overlapped with the effective illumination area (see A). Note that, despite an expression of ChETA-eYFP expression in some neighboring structures **(B)**, the volume of efficient optogenetic stimulation is predominantly located in the MeApd.

Optogenetic stimulation of MeApd GABA neurons with ChR2, independent of AAV serotype, leads to increased aggression

We next looked for other factors that might be different between our experiments (Fig. 2.1, 2.2) and the previous study (Hong et al., 2014). The previous study had used an AAV2 serotype, driving the expression of the slower channelrhodopsin variant ChR2 (channelrhodopsin-2^{H134R}; see Introduction). We therefore next performed optogenetic stimulation experiments of MeApd GABA neurons, using AAV2:EF1α:DIO:ChR2-eYFP (Fig. 2.3 A), a commercial vector as close as possible to the previously used custom construct (see Materials and Methods). With this vector, under otherwise identical conditions as in Fig. 2.1, we found that optogenetic activation of MeApd GABA neurons *stimulated* attack behavior. In an example animal, the time spent attacking increased from an average of 0.22 s per 30 s of dark periods, to an average of 4.86 s per 30 s of light-stimulation period (Fig. 2.3 B-D). Across all mice in which we employed AAV2:ChR2, blue-light stimulation significantly increased aggression (Fig. 2.3 G, left; N = 7 mice; p = 0.012; two-tailed paired t-test). On the other hand, in control mice expressing eYFP under an AAV2 vector, stimulation with blue light did not modulate the attack frequency (Fig. 2.3 G, right; p = 0.35).

It might be noted that in the ChR2 - and ChETA groups of mice, the baseline frequency of attacks in the non-stimulation epochs was different (ChR2:0.28 ± 0.09 s / 30s; N = 7 mice, Fig. 2.3G; ChETA: 1.82 ± 0.63 s / 30s; N = 5 mice; Fig. 2.1H; p = 0.038; see also Fig. 2.4). Thus, under conditions under which optogenetic stimulation *increases* aggression (using AAV2:ChR2; Fig. 2.3), aggressive behavior preferentially seems to occur during the stimulation with blue light, and vice-versa. Conversely, with AAV8:ChETA, a condition under which aggression was reduced by blue light, attacks occurred preferentially during the non-stimulation periods (AAV8:ChETA; see Fig. 2.1). Thus, the stimulation of aggression observed with AAV2:ChR2 (Fig. 2.3) seems to draw aggressive behaviors towards the light periods and presumably "depletes" the amount of aggression in the absence of light. Therefore, the period of non-stimulation across channelrhodopsin variants cannot be used to define a common "baseline" level of aggression.

One of the mice did not show spontaneous baseline aggression. In this mouse, in remarkable contrast to our results with ChETA (Fig. 2.1 I), the first 2-3 blue light stimulation trains triggered time-locked attacks (Fig. 2.3 H). This result further demonstrates the opposite

direction in aggression control when using ChR2 versus ChETA for the optogenetic stimulation of MeApd GABA neurons. Histological reconstructions showed that we had successfully targeted the MeApd in the experiments with AAV2:ChR2 (Suppl. Fig. 2.2), quantitively similar to our previous experiments with ChETA (see above, Fig. 2.2). Therefore, the experiments with AAV2:ChR2 in Fig. 2.3 suggest that with ChR2 for optogenetic stimulation, the behavioral outcome is opposite from what is observed with ChETA.

The experiments performed in Fig. 2.1 and 2.3, however, were also different in terms of the AAV serotype. Thus, while we had performed our initial experiments with an AAV8 serotype (Fig. 2.1), we used an AAV2 serotype in Figure 2.3 to enable a direct comparison with the previous study (Hong et al., 2014). Additional experiments showed that AAV2 infected a larger number of MeApd GABA neurons than AAV8 (207 ± 19 %; n = 7 sections from N = 3 mice; Suppl. Fig. 2.3). We found that only few neurons were infected by AAV8 *alone* and thus, AAV8-transduced neurons were essentially a subpopulation of the AAV2-transduced MeApd GABA neuron population (see Venn diagrams in Suppl. Fig. 2.3).

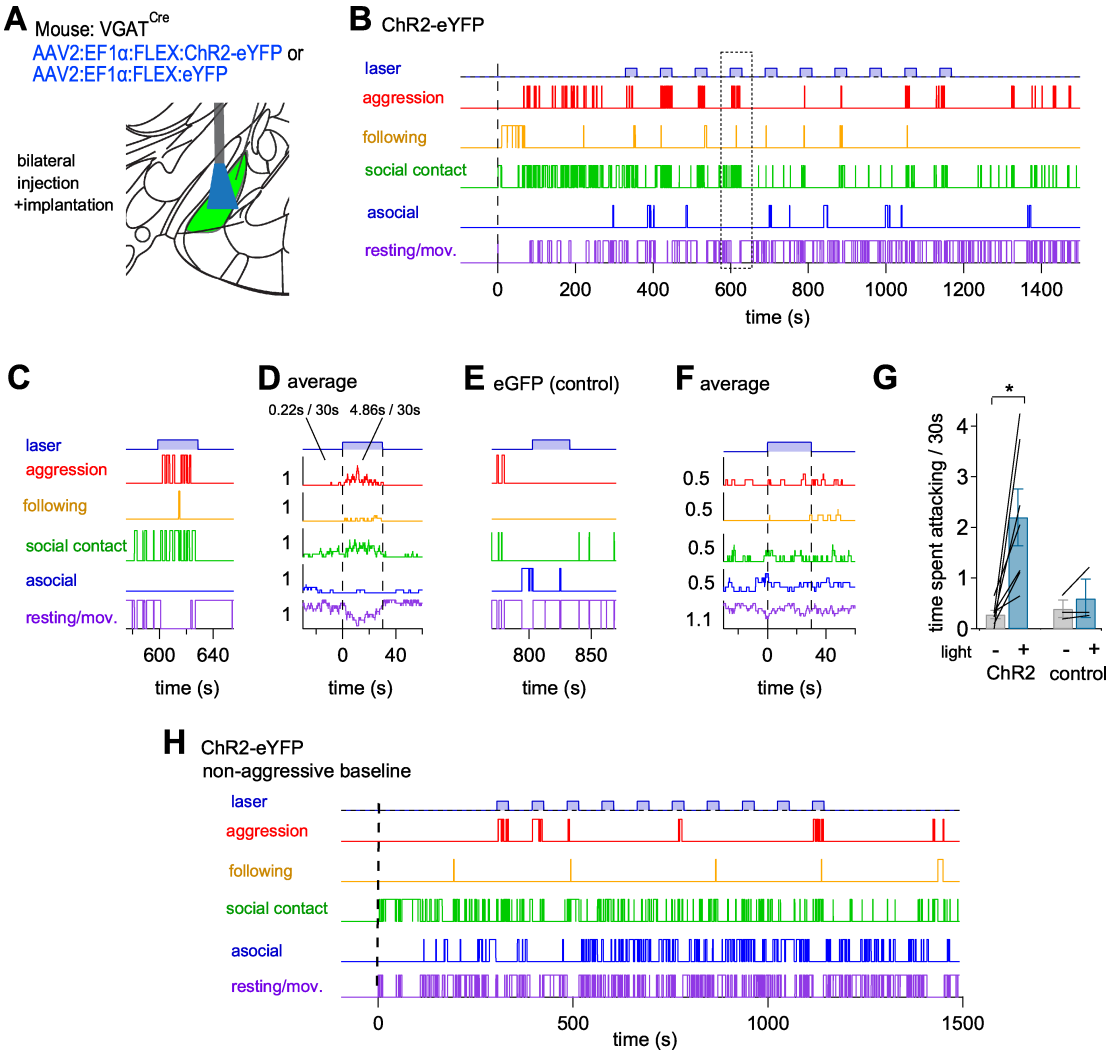

Figure 2.3 | In-vivo optogenetic activation of MeApd GABA neurons using ChR2 stimulates inter-male aggression. (A) Scheme of the approach to express ChR2-eYFP and for optic fiber placement. **(B)** Behavior traces during the resident-intruder test with a mouse expressing ChR2 in the MeApd GABA neurons. 30s-long trains of blue-light pulses (1 ms, 20 Hz, 10 mW) were interleaved with 60 s dark periods. Note that under these conditions, attacks occurred preferentially *during* illumination, in contrast to the experiments with ChETA (Figure 2.1). **(C - D)** Example light episode from **(B)** marked with a dotted rectangle **(C)**, and average behavior traces after alignment to the light onsets for n = 10 consecutive light trains **(D)**. Numbers indicate average time spent attacking 30s before the light, and during the 30s light train. Note the increase of aggression during the light stimulation. **(E-F)** Behavior data for a VGAT^{Cre} mouse expressing eYFP (a control mouse). **(G)** Quantification of the effect of optogenetic stimulation on aggression in mice that expressed ChR2 (N=7) as compared to eYFP (N=3 control mice). Individual data are averages across two resident-intruder tests made on subsequent days. **(H)** An example mouse expressing ChR2, which was initially non-aggressive against the intruder mouse. Note that from the first trains of blue light pulses, this mouse started attacks against the intruder mouse. This observation further indicates that optogenetic activation of MeApd GABA neurons under ChR2 *stimulates* aggression. Error bars are ± s.e.m. See also Suppl. Figure 2.2.

To investigate whether the AAV serotype, or rather the expressed channelrhodopsin variant (ChR2 versus ChETA) determined the behavioral outcome, we next performed experiments with the two missing combinations of AAV serotypes and channelrhodopsin variants. These experiments unambiguously showed that the channelrhodopsin variant, but not the AAV serotype, determined the behavioral outcome (Suppl. Fig. 2.4, and Fig. 2.4). Thus, when ChETA was expressed with an AAV2 vector, a significant *decrease* in aggression was observed (Fig. 2.4, third dataset; N = 9 mice; p = 0.0039; Wilcoxon two-tailed test; see Suppl. Fig.2.4A-2.4D for an example mouse). This finding thus confirms the results of Fig. 2.1 with AAV8:ChETA; the latter results are re-plotted in Fig. 2.4, leftmost dataset. Conversely, when we expressed ChR2 using an AAV8 vector, blue light led to a significant *increase* in aggression as compared to dark periods (Fig. 2.4, fourth data set from left; N = 8 mice; p = 0.0391; Wilcoxon two-tailed test; see Suppl. Fig. 2.4E-2.4G for an example mouse). This experiment confirms our results in Fig. 2.3 with AAV2:ChR2; the latter results are re-plotted in Fig. 2.4, second dataset. In mice expressing the inert eGFP or eYFP under the AAV8 or AAV2 serotype respectively, blue light stimulation was inefficient as expected (Fig. 2.4, fifth and sixth datasets; N = 11 and 7 mice for AAV8 and AAV2 respectively; p = 0.41 and 0.53; two-tailed Wilcoxon test and paired t-test).

Taken together, the experiments in Fig. 2.1 – 2.4 show that optogenetic stimulation of MeApd GABA neurons with ChETA versus ChR2 produce opposite behavioral outcomes: an *inhibition* of aggression with ChETA, versus a *stimulation* of aggression with ChR2 (Fig. 2.4). This, obviously, presents a problem for the interpretation of these optogenetic stimulation experiments, because it cannot be assigned whether MeApd GABA neurons have a *stimulatory* - or else a *suppressing* role - in aggression control.

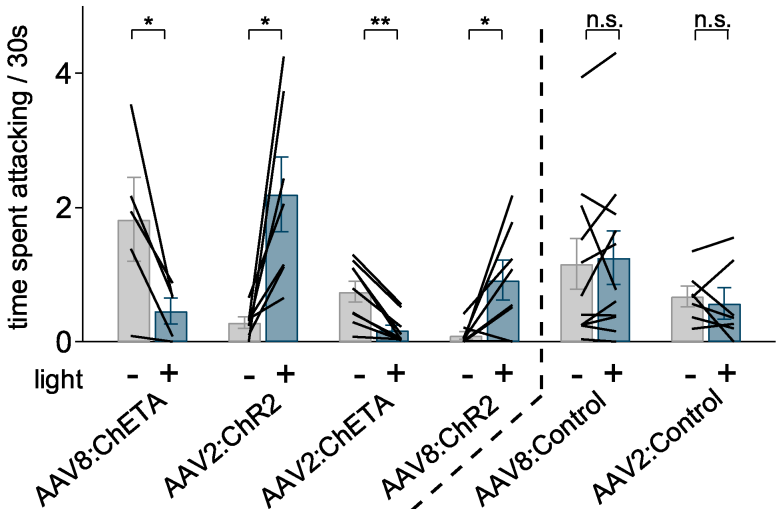

Figure 2.4 | Channelrhodopsin variant, but not AAV serotype, determines the opposite behavioral outcome of optogenetic stimulation of MeApd GABA neurons. Quantification of time spent attacking during 30 s immediately before-, or during light train stimulation (grey and blue bars, respectively), for all experimental conditions. The leftmost, and the second datasets (AAV8:ChETA and AAV2:ChR2 respectively) are re-plotted from Figures 2.1H and 2.3G. The third and the fourth datasets show the other two combinations of channelrhodopsin variants and AAV-serotypes: AAV2:ChETA (N=9), and AAV8:ChR2 (N=8 mice); example behavior traces are shown in Suppl. Figure 2.4. The two rightmost datasets represent the pooled AAV8 and AAV2 control groups, in which blue-light stimulation was ineffective (N = 11 and N = 7 mice, respectively). Note that irrespective of AAV serotype, optogenetic stimulation with ChETA resulted in *inhibition* of aggression, whereas optogenetic stimulation with ChR2 resulted in *stimulation* of aggression. See also Suppl. Figures 2.3, 2.4.

ChR2 causes large plateau depolarizations, AP amplitude decrements and increased local inhibition

We next investigated the membrane potential changes driven by ChETA and ChR2 in MeApd GABA neurons, in order to correlate possible differences with the opposite behavioral outcomes of the two channelrhodopsin variants. For this, we expressed ChR2, or ChETA in a Cre-dependent manner using AAV2:EF1α:DIO:ChETA-eYFP and AAV2:EF1α:DIO:ChR2-eYFP (the same AAV2 vectors as used above for the behavioral experiments). In addition, we expressed cytosolic eYFP with a second, co-injected AAV2 vector (see Materials and Methods) to facilitate the targeting of transfected neuron in subsequent slice electrophysiology recordings, which were performed at near-physiological temperature (34-36°C).

We first recorded the responses of MeApd neurons to short trains of blue light (5 ms pulse length, 20 Hz, duration of trains 1s). Under voltage-clamp, we observed robust light-induced currents (Fig. 2.5A, B; top) which had larger amplitudes in neurons expressing ChR2 - than ChETA (Fig. 2.5C; $p < 10^{-4}$; Mann-Whitney test), in keeping with previous work (Berndt et al., 2011; Mattis et al., 2012). The decay of the light-evoked currents was faster for ChETA than for ChR2 ($p < 10^{-4}$; Mann-Whitney test; Fig. 2.5D), as expected based on the engineering of the faster ChETA variant (Gunaydin et al., 2010). With repeated light stimuli, ChETA- and ChR2-expressing neurons fired APs reliably during the 1s trains (Fig. 2.1A, B; middle). In ChR2-expressing neurons, however, a high plateau depolarization of 30.4 ± 1.9 mV was observed (analyzed over the first second of stimulation; n = 39 recordings; Fig. 2.5E), significantly larger than in ChETA-expressing neurons (7.7 ± 0.9 mV; n = 25 cells; $p < 10^{-4}$; two-tailed t-test; Fig. 2.5E). One consequence of the plateau potential was a time-dependent decrease of the AP amplitudes from the first few stimuli onwards in ChR2-expressing neurons (Fig. 2.1B, arrow), which was likely caused by voltage-dependent Na^+-channel inactivation. An analysis of the time-course for AP amplitudes during the first 1s of light stimulation trains showed a significant effect of time in both the ChETA and ChR2 groups ($p < 10^{-4}$ for ChETA and ChR2; one-way repeated measures ANOVA followed by a linear trend test), and the AP-amplitudes were significantly smaller in the ChR2 group as compared to the ChETA group (difference of ~ 17 mV; p = 0.0096 for the channelrhodopsin variant effect; two-way repeated measures ANOVA followed by Holm-Šidák's test for multiple comparisons; Fig. 2.5I, left).

GABA neurons in the medial amygdala establish local inhibitory connections (Bian et al., 2008; Keshavarzi et al., 2014). We therefore next recorded optogenetically-evoked IPSCs (oIPSCs) at the reversal potential of the ChR2/ChETA currents (0 mV; Fig. 2.5A, B; bottom), to compare the amount of optogenetically evoked mutual inhibition of MeApd GABA neurons with each channelrhodopsin variant. The first oIPSC amplitudes were not significantly different between the two groups (Fig. 2.5F; p = 0.224). However, oIPSCs decayed more slowly after individual light pulses in preparations expressing ChR2, as compared to ChETA (Fig. 2.5A, B, bottom). To quantify this effect, we analyzed the charge transported during the 1s-stimulation trains, which revealed a significantly, ~ 2.5-fold larger inhibitory charge in the ChR2 group as compared to the ChETA group (Fig. 2.5G; p=0.029; Mann-Whitney test; n = 33 and 25, respectively). Thus, a difference in optogenetically-stimulated local inhibition might contribute to the opposite behavioral outcomes between the two channelrhodopsin variants (see Discussion).

We next applied longer trains of blue light pulses, designed to mimic the *in-vivo* stimulation conditions (5 ms pulse width, 20 Hz, duration of 30s; Fig. 2.5H). We again found a strong plateau depolarization in ChR2-expressing neurons, both during the first second as well as during the last 10 s, and this plateau depolarization was significantly smaller with ChETA ($p < 10^{-4}$; two-way repeated measures ANOVA with Šidák's multiple comparison test for 20 - 30 s; n = 17 and 24 recordings). Also, the AP amplitudes decreased in ChR2-expressing neurons to a stronger degree than in ChETA-expressing neurons, such that AP-amplitudes were smaller with ChR2 than with ChETA at various time points of the 30s-trains (Fig. 2.5I; p=0.0096, p=0.011, and p=0.0113 in the three indicated time ranges for the channelrhodopsin factor in a two-way repeated measures ANOVA followed by Holm-Šidák's multiple comparison test). Note that in the time range of 0-1s, AP amplitudes at every time point except t=0 were significantly lower in ChR2 expressing cells ($p<0.05$). With ChR2, we often observed that during the second half of the train, the peak of the APs dropped below 0 mV and in many instances blue light pulses failed to trigger APs (Fig. 2.5H; stars). Correspondingly, during the second half of the trains, the average AP-frequency attained by the 20 Hz stimulus trains was only about 10 Hz in the ChR2-expressing neurons (Fig. 2.5J). This was lower than in the ChETA-expressing neurons (~ 15 Hz), but the difference did not reach statistical significance ($p = 0.11$; two-way repeated measures ANOVA; Fig. 2.5J). This data shows that with long trains of blue-light stimuli as applied *in-vivo*, i) the plateau depolarization caused by ChR2 persists and becomes even larger (data not shown), ii) AP amplitudes were significantly smaller for stimulation with ChR2 than with ChETA, and iii) the AP-failure rate is higher for ChR2 than for ChETA during long trains, but the latter effect did not reach statistical significance.

We furthermore measured the intrinsic AP-firing properties in response to step current injections, and classified the AP-firing of the recorded MeApd GABA neurons to six types (Suppl. Fig. 2.5). We found two types of MeApd GABA neurons with remarkably low rates of AP-firing even with high current injections (Suppl. Fig. 2.5, AP-firing types 1 and 2; see also Lischinsky et al., 2017; Matos et al., 2020). In these neurons, optogenetic stimulation under ChR2 was often not able to trigger APs during the second half of trains (Suppl. Fig. 2.5C). Nevertheless, the data set was too small to test for possible differences in AP-following, stratified for the six different AP-firing types of the MeApd GABA neurons.

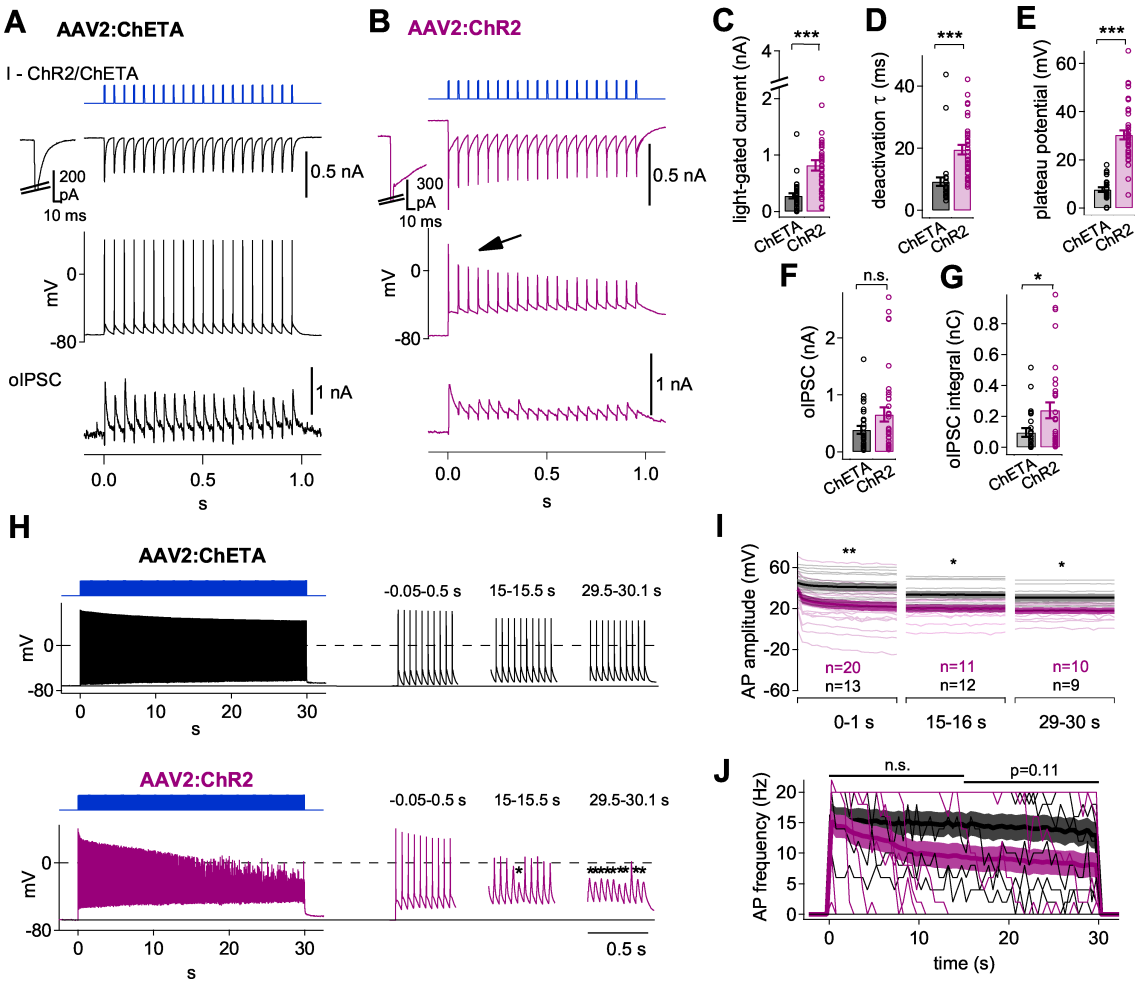

Figure 2.5 | Optogenetic stimulation with ChR2 causes plateau depolarizations, AP decrements, and eventual failure of AP-triggering in MeApd GABA neurons. (A, B) Whole-cell recordings from example MeApd GABA neurons expressing either ChETA **(A)** or ChR2 **(B)**. Cre-dependent expression was driven by the AAV2 vectors in VGAT^{Cre} mice (see Materials and Methods). Short (1s) trains of blue-light stimuli were applied (5 ms duration; 20 Hz repetition rate). Traces from top to bottom show: light-gated currents recorded at -70 mV holding potential (insets show the response to the first pulse; unclamped Na^+ current components are clipped); current-clamp recording of membrane potential response (AP firing); optogenetically-evoked IPSCs (oIPSCs) recorded at 0 mV holding potential. **(C - G)** For each channelrhodopsin variant, we quantified the light-gated current amplitudes b, the decay time constant of the light-gated current currents (τ; **D**), the plateau depolarizations **(E)**, the first oIPSC amplitudes **(F)**, and the integral of the oIPSCs **(G)**. For statistical tests and statistical significance, see Results. **(H)** Example traces of AP-firing induced by in-vivo like trains (5ms, 20 Hz, 30s duration) at near-physiological temperature (35°C), in a MeApd GABA neurons expressing ChETA (top) or ChR2 (bottom). Insets to the right show traces during 0.5 s stretches at the start, middle, and end of the blue-light trains (corresponding times are indicated). Note the stronger decay of AP-amplitudes, and eventual AP-triggering failures in the ChR2-expressing neuron compared to the ChETA-expressing neuron. **(I)** Analysis of peak AP amplitudes at three times during the 30s light trains. Note a more pronounced time-dependent decrease of AP-amplitudes in ChR2-expressing neurons at the start of the train, and that the peak AP-amplitudes remain significantly smaller for ChR2 than for ChETA throughout the train. For statistical significance, see Results. **(J)** Plot of average AP-frequency attained by 20 Hz light pulse stimuli with ChETA (black traces) and ChR2 (violet traces), quantified for 500 ms bins. Shown are both individual traces, and the average ± s.e.m trace for each group. During the second half of the trains, the difference in attained AP-frequency (~ 10.1 and 14.6 Hz for ChR2 and ChETA, respectively) did not reach statistical significance ($p = 0.11$). Error bars or color shadings are ± s.e.m. See also Suppl. Figure 2.5.

Discussion

The MeApd contains a majority of GABAergic neurons and has a crucial role in the control of social behaviors (Aleyasin et al., 2018; Haller, 2018; Hashikawa et al., 2016; Hong et al., 2014; Padilla et al., 2016; Unger et al., 2015). Previous work has suggested that optogenetic activation of these neurons, using the slow channelrhodopsin^{H134R} variant (ChR2), *stimulates* inter-male aggression (Hong et al., 2014). However, we found that optogenetic stimulation of MeApd GABA neurons, initially using the faster channelrhodopsin-2^{H134R,E123T} variant (ChETA; Gunaydin et al., 2010) produced the opposite behavioral outcome, i.e. an *inhibition* of aggression. We therefore compared the optogenetic activation of MeApd GABA neurons with ChR2 and ChETA in behavioral experiments side-by-side, using two widely-used AAV serotypes to express the channelrhodopsins. These experiments showed unambiguously that with ChETA, aggression was *reduced* during the time of light stimulation (Fig. 2.1), whereas with ChR2, an *increase* in aggression was observed (Fig. 2.3, 2.4). To our knowledge, this is the first demonstration of how kinetically different channelrhodopsin variants used to stimulate the same neuronal population *in-vivo* can lead to diametrically opposite behavioral outcomes.

An *ex-vivo* electrophysiological analysis of optogenetic stimulation of MeApd GABA neurons showed two main differences between the two channelrhodopsin variants: ChR2-expressing neurons showed a pronounced plateau depolarization of ~ 30 mV, and, probably as a consequence, a decrement of the optogenetically-triggered AP-amplitudes. Plateau depolarizations have been observed previously with ChR2, and are a consequence of the slow light-off kinetics of ChR2 (Berndt et al., 2011; Gunaydin et al., 2010; Herman et al., 2014; Mattis et al., 2012). It is safe to assume that the decrease in AP-amplitudes, and the partial failure of AP-triggering late during the trains, are caused by the inactivation of voltage-gated Na^+-channels (Hodgkin and Huxley, 1952), driven by the elevated plateau depolarization in ChR2- expressing neurons. Nevertheless, this difference in AP-triggering between ChR2 and ChETA, which was more apparent in the second half of the *in-vivo*-like trains and which did not reach statistical significance, is probably not the most important explanation for the different behavioral outcomes between the channelrhodopsin variants. Hong et al. (2014) found with shorter light trains of only 15 s length (20 ms pulse duration, 20 Hz), that activation of MeApd GABA neurons under ChR2 produced an almost immediate, but lasting increase of attacks (Hong et al., 2014; their Fig. 1). In our experiments with ChR2, we could reproduce the

stimulatory effect of blue light trains on aggression; nevertheless, we did not observe a similarly fast increase in aggression (Fig. 2.3D) as was observed by Hong et al. (2014) (their Fig. 1). This difference might lie in the fact that Hong et al. used longer blue light pulses than we did (20 ms vs 5 ms, i.e. 40% vs 10% duty cycle, respectively). Increased pulse duration might have caused even stronger plateau depolarizations than we measured here, and potentially could lead to a partial light-induced depolarization block of certain MeApd GABA neuron sub-populations, as was demonstrated for different cell types in other brain regions (Herman et al., 2014). Taken together, these considerations suggest that a difference between ChR2 and ChETA in the first 5 - 10 s of light train stimulation more likely accounts for the behavioral differences. The more efficient recruitment of local inhibition by ChR2 (Fig. 2.5G) might be among the factors that causes the behaviorally different outcomes within the first 5-10s of blue light stimulation.

The MeApd consists of a majority (~70%) of inhibitory neurons. Many of these neurons are long-range projection neurons to hypothalamic and other targets (Bian et al., 2008; Choi et al., 2005; Keshavarzi et al., 2014). Concomitantly, local inhibition described before for the MeApv (Keshavarzi et al., 2014) also likely occurs in the MeApd; our finding of optogenetically-evoked oIPSCs is consistent with local inhibitory circuits. Thus, while the activation of long-range inhibitory projection neurons to hypothalamic targets might drive an inhibition of aggression (see below), optogenetic activation under ChR2 leads to a stronger local inhibition than ChETA (Fig. 2.5F, G). Thus, it is conceivable that this local opposing inhibitory effect reverses the behavioral outcome during *in-vivo* optogenetic activation with ChR2. Indeed, it is well-known that optogenetic activation of inhibitory neurons in cortical circuits causes an *inactivation* of the corresponding cortical area (Li et al., 2019; Sachidhanandam et al., 2013), because of the local nature of inhibition in the cortex. In analogy, optogenetic activation of $VGAT^{Cre}$ positive neurons in the MeApd is expected to cause local inhibition in addition to the likely long-range inhibitory role of MeApd GABA neurons.

Hong et al. (2014) suggested a *stimulatory* role of MeApd GABA neurons in aggression control, which is now the predominant view in the literature (see reviews by Aleyasin et al., 2018; Chen and Hong, 2018; Hashikawa et al., 2016; Lischinsky and Lin, 2020). Nevertheless, Hong et al. did not identify the postsynaptic targets of inhibition by MeApd GABA neurons. Considering, however, that MeApd GABA neurons make a connection to hypothalamic nuclei including the VMH (ventromedial hypothalamus) and PMv (ventral pre-mammillary nucleus

(Canteras et al., 1995; Choi et al., 2005; Lo et al., 2019), and further considering that optogenetic stimulation of specific populations of excitatory neurons in the VMH or PMv leads to a *stimulation* of aggression (Chen et al., 2020; Falkner et al., 2020; Lee et al., 2014; Stagkourakis et al., 2018; Yang et al., 2017), it might be expected that optogenetic activation of MeApd GABA neurons *inhibits* aggression, as we have observed with ChETA. Indeed, Hong et al. (2014) had to postulate a *disinhibition* of VMH glutamatergic neurons following activity of MeApd GABA neurons in order to explain their observations; nevertheless, such a disinhibitory pathway has not yet been identified. In a study published after Hong et al. (2014), NPY-expressing neurons in the MeA, which were to a large part GABA neurons, were found to increase aggression via the BNST (Padilla et al., 2016). This pathway via the BNST has been discussed as a possible *disinhibitory* route from the GABAergic MeApd to the VMH, and it was proposed to explain the earlier results by Hong et al. (2014) (see review by Chen and Hong, 2018). However, the correspondence of NPY+ neurons and MeApd GABA neurons remains to be shown, and the mechanisms by which the BNST controls aggression is at present not well defined, although an involvement of the BNST in aggression control is evident (Chen et al., 2020; Masugi-Tokita et al., 2016; Miller et al., 2019; Nordman et al., 2020). Yet another study showed that optogenetic activation of an excitatory projection from the dorsal raphe nucleus to the MeA inhibits aggression (Nordman and Li, 2020). This finding is consistent with our observation of an inhibition of aggression after optogenetic activation of MeApd GABA neurons. Taken together, the possible long-range inhibitory, or else - disinhibitory output pathways via which MeApd GABA neurons control aggression in either direction, should be elucidated in future studies.

Taken together, the paradoxical opposite behavioral outcomes of the optogenetic "sufficiency" experiment under ChR2 versus ChETA, does not allow us at present to conclude whether MeApd GABA neurons are involved in a *stimulatory* (Hong et al., 2014), or else in an *inhibitory* control of aggression. Our study calls for caution when choosing channelrhodopsin variants for *in-vivo* optogenetic studies with mechanistic conclusions, maybe especially so when studying inhibitory projection neurons. Thus, we suggest that the role of the MeApd GABA neurons in aggression control should be newly addressed. Such studies should include carefully controlled optogenetic experiments, including experiments on the relevant long-range output targets of MeApd GABA neurons. In addition, the *in-vivo* activity of projection-defined MeApd GABA neurons should be recorded. Such experiments might be able to more

conclusively establish the role of the MeApd GABA system in the control of aggressive behavior.

Supplementary Figures

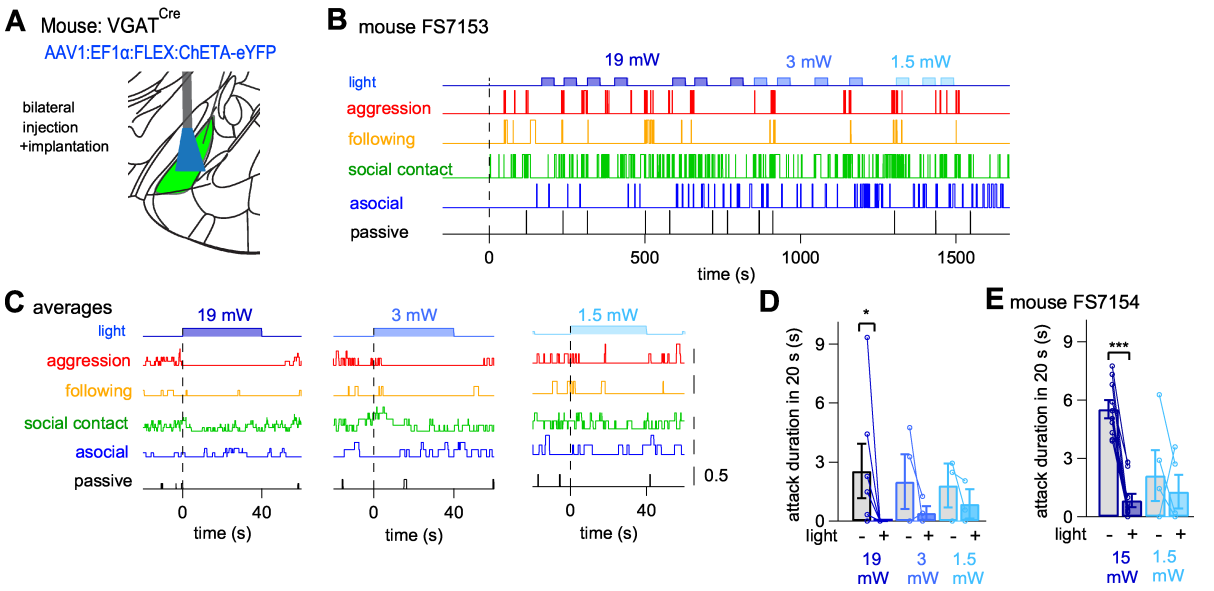

Suppl. Figure 2.1 | The inhibition of aggression by optogenetic activation of MeApd GABA neurons with ChETA depended on light power. Related to Figure 2.1. (A) Scheme of the approach for expression of ChETA and for optic fiber placement. In the experiments for this data set, an AAV1 vector was used to express ChETA. **(B)** Behavior traces during a resident-intruder test with a ChETA-expressing mouse. Trains of blue-light pulses (5 ms, 20 Hz, 40 s duration) were applied at varying intensities as indicated (19 mW, 3 mW and 1.5 mW; color-coded). **(C)** Average behavior traces aligned to the onsets of the light trains of different intensities (see B), as indicated. Note the clear interruption of ongoing aggression when using 19 mW light power and at 3 mW, whereas smaller light intensities of 1.5 mW did not have obvious effects. **(D, E)** Quantification of the time spent attacking during optogenetic stimulation with ChETA at different light intensities (D; same mouse as shown in B, C; for a second mouse see E). Note that significant differences ($p = 0.03$ and $p = 0.001$ in D and E, respectively; one-tailed Wilcoxon matched-pairs signed rank test) were observed at 19 mW and 15 mW, whereas behavioral changes were non-significant at lower light levels (3 and 1.5 mW).
Error bars are ± s.e.m.

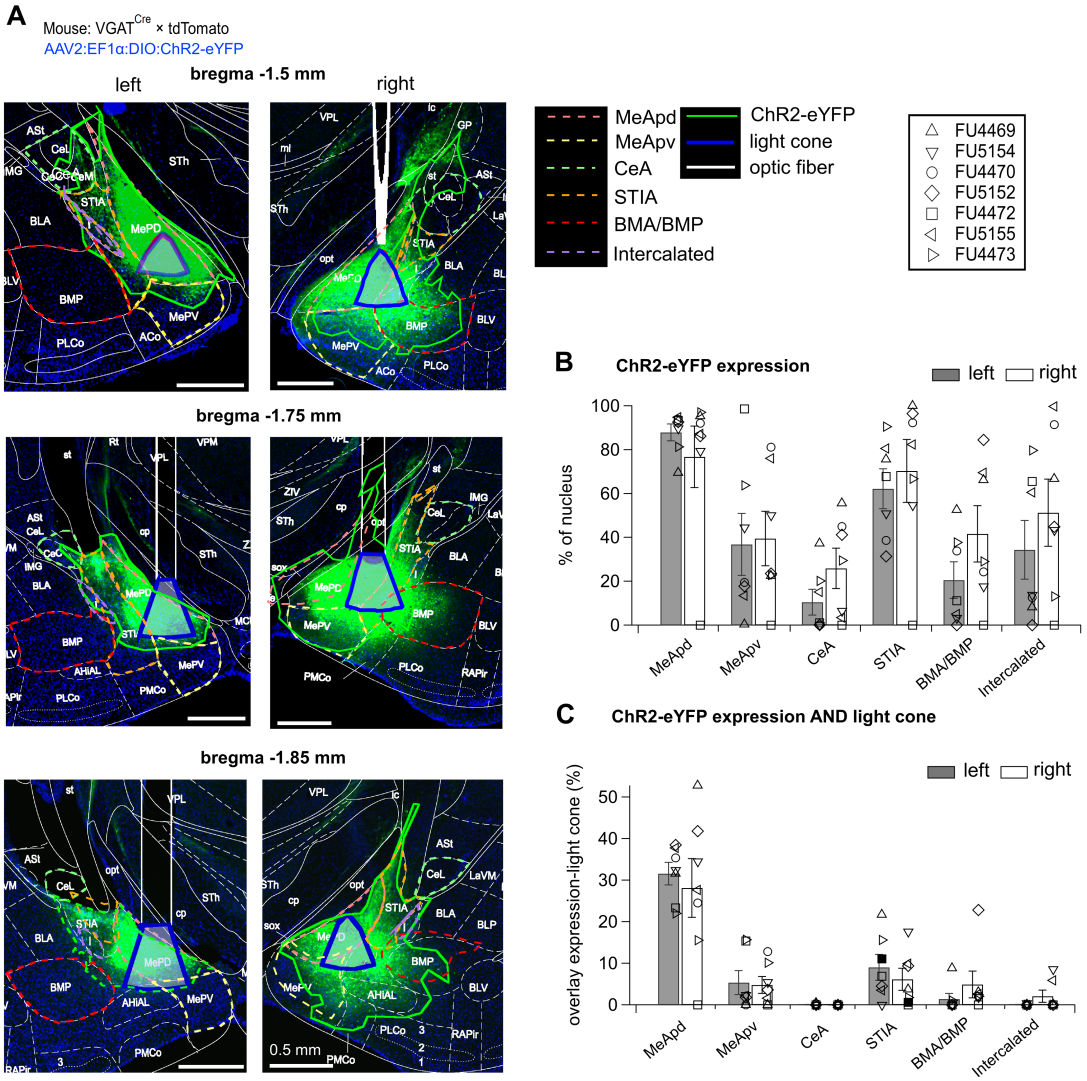

Suppl. Figure 2.2 | Histological analysis to identify the brain areas targeted by optogenetic stimulation with ChR2. Related to Figure 2.3. Here we performed a quantitative post-hoc histological analysis, analogous to that in Figure 2.2, in a cohort of N = 7 VGAT^{Cre} mice injected with AAV2:EF1α:DIO:ChR2-eYFP and subjected to a resident-intruder test with optogenetic stimulation of the MeApd GABA neurons (see Figure 2.3). The data of this histological analysis are presented in the same way as in Figure 2.2. Note that the results of the quantification **(B, C)** are very similar to those shown in Figures 2.2B, 2.2C for a cohort of ChETA expressing mice, and indicate that mainly the MeApd was targeted. We thus conclude that there were no gross differences in the targeting of the channelrhodopsin-variant expression, nor of the optic fiber placement, between optogenetic stimulation experiments using ChETA (Figure 2.1) and ChR2 (Figure 2.3). Error bars are ± s.e.m.

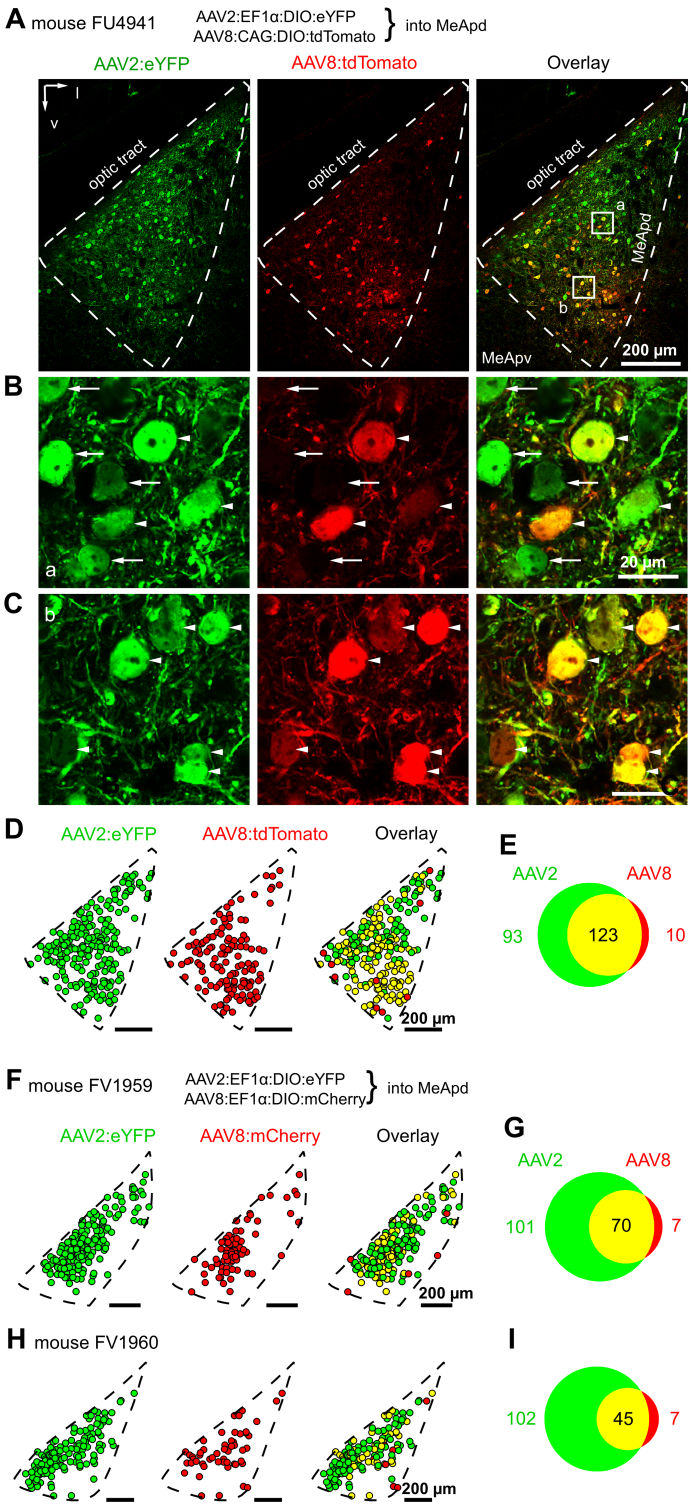

Suppl. Figure 2.3 | AAV8 vectors infect a sub-population of MeApd neurons transduced with AAV2 vectors. Related to Fig. 2.4. (A) Overview confocal images of a coronal brain section containing the MeApd (white dashed outline), obtained from a VGAT^{Cre} mouse after injection with a mix of viral vectors AAV2:EF1α:DIO:eYFP (green channel; eYFP) and AAV8:CAG:DIO:tdTomato (red channel; tdTomato). Final titers of the injected vectors were $2.25 \cdot 10^{12}$ and $3.25 \cdot 10^{12}$ ml^{-1}, respectively. **(B, C)** Zoomed-in images of the areas marked with the white rectangles in **(A)**. *Arrows* point out example neurons expressing *only* eYFP from AAV2 (green channel); *arrowheads* point out neurons expressing tdTomato under an AAV8 serotype vector (red channel). The tdTomato-positive neurons often co-

expressed eYFP (overlay, appearing yellow). **(D)** Binary maps showing the localization within the MeApd and identity of neurons in **(A)** that express either single marker (green or red), or both fluorescent proteins (yellow). **(E)** Venn diagram showing the proportions of neurons transduced by the AAV2 vector alone (green), by the AAV8 alone (red), or by both vectors (yellow). Same mouse as shown in (A-C); n = 2 sections were analyzed. **(F - H)** Binary maps and Venn diagrams as in **(D, E)**, obtained from another two $VGAT^{Cre}$ mice, four weeks after co-injection with AAV2:DIO:eYFP and AAV8:DIO:mCherry (n = 5 sections were analysed). Note the similarly of results obtained across N = 3 mice **(D-I)**, which suggest that AAV8-transduced neurons are essentially a sub-population (~ half) of the AAV2-transduced neurons. This finding is consistent with the behavioral findings, which did not reveal a fundamental difference in the behavioral outcome between the two AAV-serotypes, given that the same channelrhodopsin variant was used (Fig. 2.4).

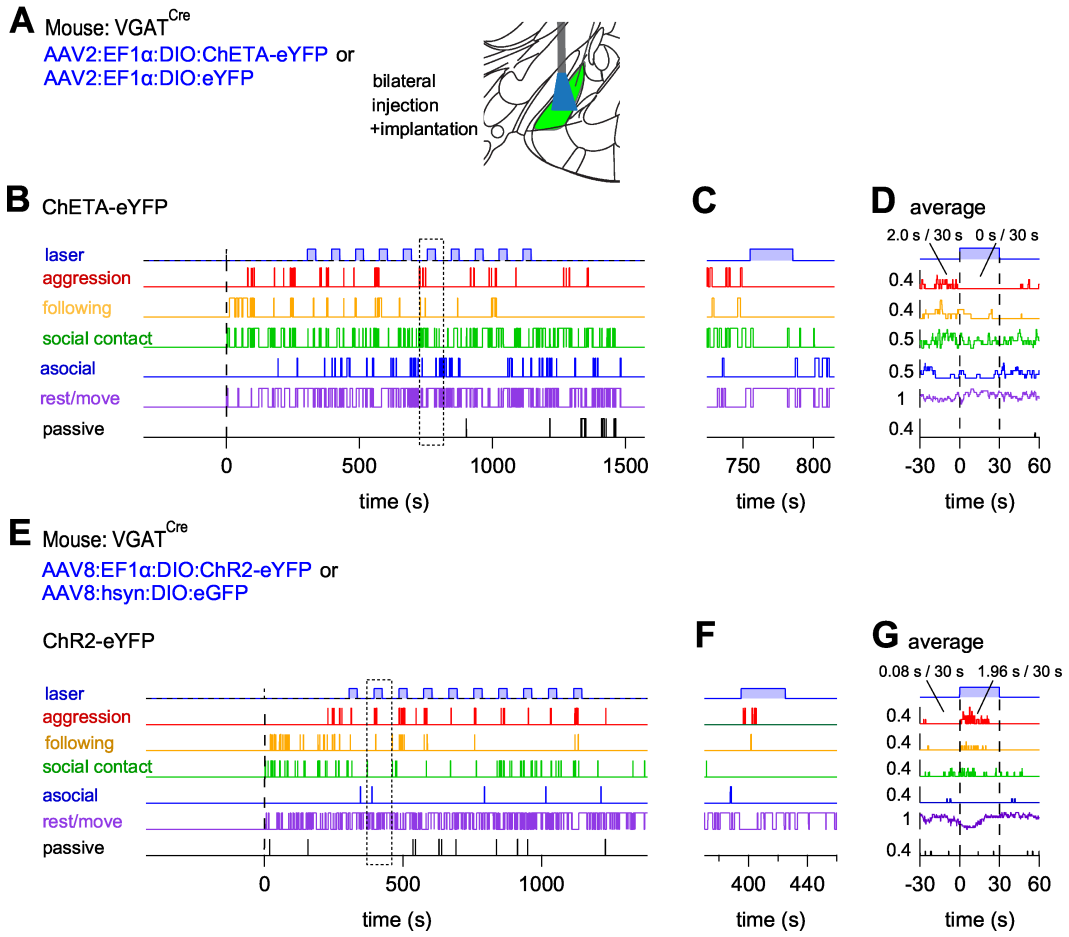

Suppl. Figure 2.4 | Example traces for optogenetic stimulation experiments under further combinations of AAV serotypes and channelrhodopsin variants. Related to Figure 2.4.
Here, we show example experiments underlying the third and the fourth datasets in Fig. 2.4 (AAV2:ChETA and AAV8:ChR2, respectively). **(A)** Schematic of the experimental approach to express ChETA, and for fiber placement. **(B)** Behavior traces during the resident-intruder test with a VGAT^{Cre} mouse expressing ChETA under an AAV2 serotype vector. **(C)** Example light episode marked with a dotted rectangle in **(B)**. **(D)** Average behavioral traces from the experiment shown in **(B)**, aligned to the onset of the light trains. Note the absence of aggressive behavior during the train of blue-light pulses. **(E-G)** Experimental data for a mouse expressing ChR2-eYFP under an AAV8 serotype vector. The expanded traces in **(F)** are taken from the area indicated by rectangle in **(E)**. Note that aggression bouts preferentially occurred during the light trains **(F)**, as reflected in the average aligned behavior traces **(G)**.

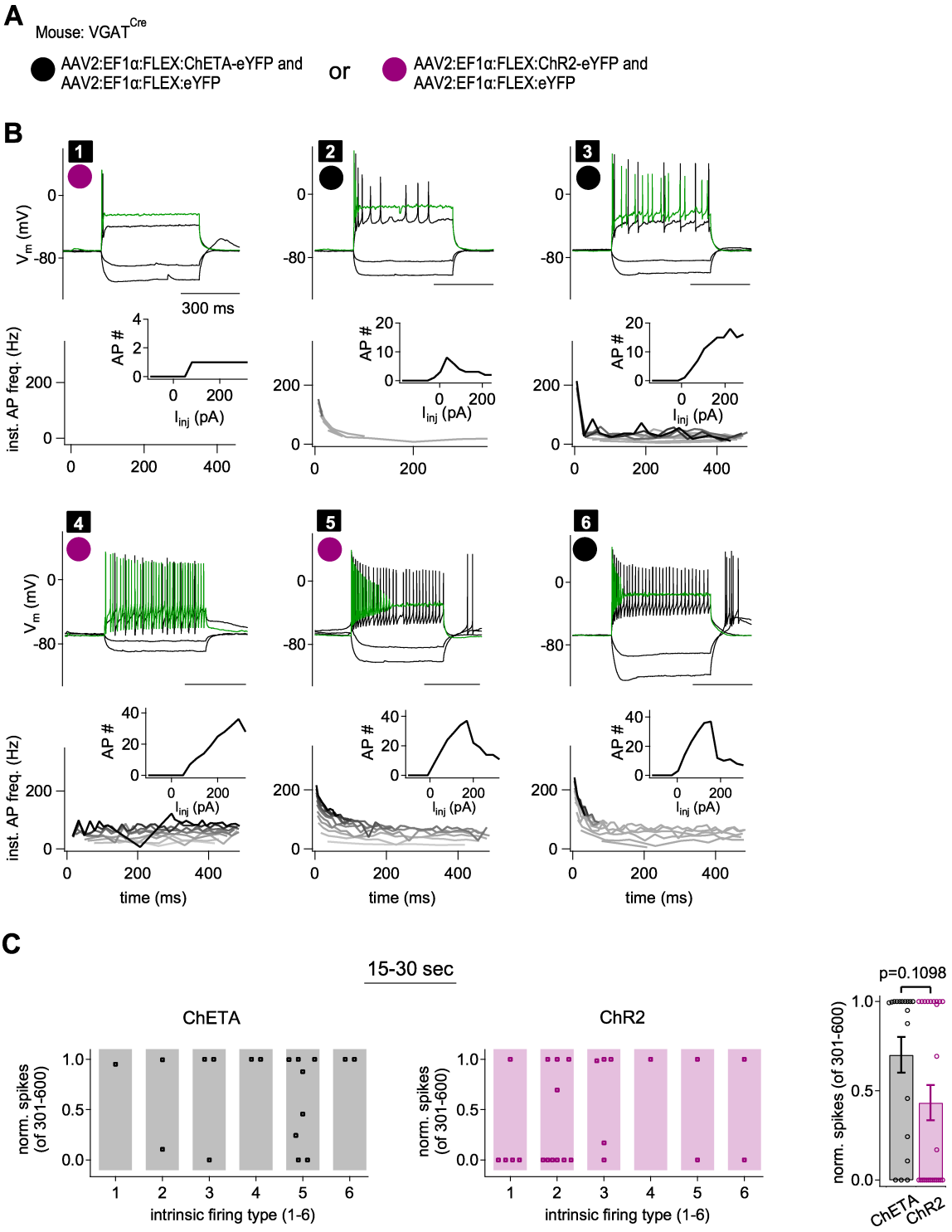

Suppl. Figure 2.5 | AP firing types identified amongst MeA GABA neurons, and distribution of channelrhodopsin variant - induced AP-firing across cell types. Related to Figure 2.5. (A) Experimental approach to express either ChETA or ChR2 in MeApd GABA neurons, co-expressing cytosolic eYFP from a co-injected second AAV2 vector for cell identification. **(B)** Examples of membrane potential (V_m) responses of MeApd GABA neurons for each identified AP firing type (types designated 1 to 6; black squares). Responses to two hyperpolarizing (-100 and -40 pA) and two depolarizing current injections are shown (+110 and +290 pA; the latter in green). The expression of ChETA or ChR2 is indicated by black or magenta circle, respectively. The graphs at the bottom of each panel show the time-course of instantaneous AP frequency (darker traces show responses to larger

depolarizing current steps), and AP-number as a function of the step current injection amplitude (insets). Materials and Methods describe the classification of the n = 6 AP-firing types in more detail. **(C)** Normalized number of APs during the second half of 30 s-long trains of blue light, segregated according to the AP-firing type of each neuron, both for MeApd GABA neurons expressing ChETA (left) and ChR2 (middle panel). Unfortunately, the number of recordings (n = 18 and 25 for ChETA and ChR2 in total) is too small to arrive at statistically meaningful difference in AP-following between the channelrhodopsins variants *and* across the n = 6 different AP-firing types. The quantification on the right shows the same data as on the left, collapsed over all AP-firing type cells in each group (p = 0.1098; Mann-Whitney test; see also Figure 2.5J).

Chapter 3: Results II

MeApd-GABA neurons inhibit aggression by modulating neurons in the VMH and the PMv

Aiste Baleisyte[1], Ralf Schneggenburger[1*], Olexiy Kochubey[1*]

[1] Laboratory of Synaptic Mechanisms, Brain Mind Institute, School of Life Science, École Polytechnique Fédérale de Lausanne (EPFL), 1015 Lausanne, Switzerland

Author contribution:

A.B. and O.K. performed the experiments and analyzed the data; O.K., R.S., and A.B. conceived the study and A.B. wrote the manuscript.

Introduction

Aggression is a highly demanding innate behavior that requires multiple regulatory mechanisms (Adams, 2006). While various brain nuclei have been shown to be involved in aggression control, early classical lesion- or electrical stimulation experiments in various animal models demonstrated that hypothalamic stimulation is key for attack initiation (Lammers et al., 1988; Siegel et al., 1999). More recently, the advent of circuit dissecting methods such as optogenetics and chemogenetics has significantly advanced our understanding of the neuronal circuits that underlie inter-male territorial aggression. Thus with the help of these tools, hypothalamic areas like the ventrolateral part of the ventromedial hypothalamus (VMHvl), ventral premammilary nucleus (PMv) and the medial preoptic area (MPOA) have been identified as sites for regulating inter-male aggression (Chen et al., 2020; Falkner et al., 2016; Hashikawa et al., 2017; Karigo et al., 2020; Lee et al., 2014; Lin et al., 2011; Stagkourakis et al., 2018). In vivo recordings showed that subpopulations of excitatory neurons in the VMHvl are active during inter-male aggression and code for upcoming attacks (Falkner et al., 2014), while optogenetic stimulation of the VMHvl elicited immediate attack toward males, females, and inanimate objects (Falkner et al., 2020; Lee et al., 2014). Thus, there is a substantial knowledge of how the VMHvl controls aggression. However, there is a lack of understanding of what are the upstream nuclei that gate the VMHvl activity and relay the necessary sensory information to the VMHvl, as it does not seem to receive direct inputs from the olfactory, visual or auditory systems.

The medial amygdala (MeA) has also been implicated in aggressive behaviors (Miczek et al., 1974; Vochteloo and Koolhaas, 1987). It receives direct pheromonal information about conspecifics from the accessory olfactory bulb and after integrating it, relays it to various hypothalamic nuclei, including the VMHvl (Cadiz-Moretti et al., 2016; von Campenhausen and Mori, 2000; Canteras et al., 1995; Choi et al., 2005; Keshavarzi et al., 2014; Lehman et al., 1980; Scalia and Winans, 1975). The MeA consists of both inhibitory GABA neurons and of excitatory glutamatergic neurons, with the postero-dorsal part of the MeA (MeApd) containing a majority of GABA neurons ~ 70% (Choi et al., 2005; Keshavarzi et al., 2014). Recent optogenetic and chemogenetic studies described the role of the MeA neurons in social behaviors and aggression (Chen et al., 2019; Hong et al., 2014; Li et al., 2017; Miller et al., 2019; Nordman et al., 2020; Padilla et al., 2016; Unger et al., 2015). Hong et al. (2014) found

that optogenetic stimulation of MeApd GABA neurons induces attacks in the resident-intruder test (Hong et al., 2014). On the contrary, in our recent study (Baleisyte et al., 2021) we found that aggression modulation in the MeApd depends on the channelrhodopsin variant. We found that when using channelrhodopsin variant ChETA, optogenetic stimulation of MeApd GABA neurons suppressed aggression, whereas optogenetic stimulation with ChR2 increased aggression. These opposing results could potentially be reconciled if a total population of MeApd GABA neurons comprised of a mix of intra-MeA inhibiting projector cells and of the cells providing long-range inhibition to distant targets involved in aggression control. In that case, different channelrhodopsin variants could shift the net effect of optogenetic stimulation between silencing the long-range inhibitory projections (local inhibition overrides light commands) or activating these projections (MeApd GABA cells follow the optogenetic stimulation; see Chapter 2 for discussion).

To better understand the role of the MeApd GABA neurons in aggression control, it is thus necessary to account for the connectivity of these neurons: whether they are locally inhibiting interneurons or/and long-range projecting neurons, and in the latter case - which other aggression-relevant nuclei they innervate. An earlier neuronal tracing study showed that Lhx6-positive neurons in the MeApd provide axonal outputs to the VMHvl; the population of Lhx6-derived neurons is probably largely GABAergic (Choi et al., 2005). These tracing results were later confirmed in another study (Keshavarzi et al., 2014). If MeApd GABA neurons indeed inhibit VMHvl excitatory neurons, then by stimulating MeApd-GABA projection neurons one would expect to interrupt aggression. On the other hand, there is a sparse population of GABAergic interneurons located in the VMH shell surrounding the nucleus (Choi et al., 2005; Fu and van den Pol, 2008) which allows for the possibility of a disinhibitory circuit, if these interneurons receive inhibitory inputs from the MeA. Hence, based on the current knowledge, the MeApd stands out as a potentially very important nucleus to gate the VMHvl during aggressive behaviour. However, to date there are no studies showing functional connectivity between the MeApd and the VMHvl, and the behavioural significance of this connection has yet to be assessed.

Here, we wished to investigate possible mechanisms of how MeApd GABAergic neurons that send their axons to the VMHvl control aggressive behaviour and to understand if this connection is indeed critical to modulate aggressive behaviour. In this part of my thesis, we performed anatomical experiments using anterograde and retrograde tracing techniques and found putative output synapses of MeApd GABA neurons in many hypothalamic nuclei,

including the ventro-medial hypothalamus (VMH), the ventral premammilary hypothalamic nucleus (PMv) and additionally in various subdivisions of the bed nucleus of stria terminalis (BNST). Further, in-vitro optogenetic mapping of synaptic connections made by the MeA-GABA projecting axons showed direct inhibition of glutamatergic neurons in the VMHvl and the PMv. On the other hand, in-vivo optogenetic stimulation of MeA-GABA axonal terminals in the VMHvl or PMv revealed unexpected technical difficulties (induction of mounting behaviour in case of optic fiber implantation in hypothalamus) and overall provided currently inconclusive data. Finally, we performed in-vivo Ca^{2+} imaging of the VMHvl projecting MeApd-GABA neurons during the resident-intruder test and found that these neurons are largely multimodal, activating during different social behaviours such as aggression, following and social investigation.

Materials and Methods

Laboratory mice

Please see Materials and Methods, Chapter 2

Viral vectors

To target channelrhodopsin, GCaMP6m and/or fluorophore expression to MeApd-GABA neurons for *in-vivo* and *ex-vivo* experiments, we used Cre-recombinase dependent (DIO/DIO; Schnütgen et al., 2003) adeno-associated viral vectors (AAV) of the serotypes 2/8 and 2/2 (referred to as AAV8 and AAV2 see Table 3.1). We used two modifications of the original wildtype ChR2 (Boyden et al., 2005; Nagel et al., 2003): a speed-optimized ChETA^{H134R,E123T} (Gunaydin et al., 2010), and an enhanced ChR2^{H134R} (Nagel et al., 2005) version. More information about the viral vectors used in this Chapter are given in the Table 3.1.

Table 3.1 | List of the viral vectors used in Chapter 3.

Vector	Figure	Source/Supplier	Catalog number / Other ID
AAV8:hSyn:DIO:ChETA-eYFP	Fig. 3.3 Fig. 3.4 Fig. 3.5 Fig. 3.6 Fig. 3.7	AAV packaging made by the lab. of Neurodegenerative Studies Laboratory (LEN), Dr. Bernard Schneider.	Coding sequence identical to Addgene plasmid #26968
AAV8:hSyn:DIO:eGFP	Fig. 3.6 Fig. 3.7	AAV packaging made by the lab. of Neurodegenerative Studies Laboratory (LEN), Dr. Bernard Schneider.	Coding sequence identical to Addgene plasmid #50457
AAV8:EF1α:DIO: mCherry	Fig. 3.4	University of Zürich Viral Vector Facility	Cat# v114-8
AAV2:EF1α:DIO:ChETA-eYFP	Fig. 3.4	University of North Carolina Vector Core	In-stock vector

			(contributed by Dr. Karl Deisseroth)
AAV2:EF1α:DIO:ChR2-eYFP	Fig. 3.3	University of North Carolina Vector Core	In-stock vector (contributed by Dr. Karl Deisseroth)
AAV8:hSyn:DIO: Synaptophysin-mCherry.IRES.EGFP.CW3SL	Fig. 3.1	DNA plasmid cloning by Dr. Olexiy Kochubey. AAV packaging made by the lab Neurodegenerative Studies Laboratory (LEN), Dr. Bernard Schneider.	Custom vector
AAV8:VGLUT2prom:eGFP	Fig. 3.3 Fig. 3.5	DNA plasmid cloning by Dr. Olexiy Kochubey. AAV packaging made by the lab Neurodegenerative Studies Laboratory (LEN), Dr. Bernard Schneider.	Custom vector
AAVretro:hSyn:mCherry.2A.FLPo	Fig. 3.8 Fig. 3.9 Fig. 3.10 Fig. 3.11	University of Zürich Viral Vector Facility	Cat# v150-retro
AAV8:EF1α:DIO:mCherry	Fig. 3.4	University of Zürich Viral Vector Facility	Cat# v114-8
AAV2:hSyn: Con/Fon: eYFP	Fig. 3.8	University of Zürich Viral Vector Facility	Cat# v403-2
AAV2:hSyn:Con/Fon: ChETA-eYFP	Fig. 3.8	University of Zürich Viral Vector Facility	Cat# v616-2
AAV2:hSyn:Con/Fon: GCaMP6m	Fig. 3.9 Fig. 3.10 Fig. 3.11	University of Zürich Viral Vector Facility	Cat# v571-2

Custom made viral vectors

The AAV8:VGLUT2prom:eGFP virus was custom packaged in B. Schneider lab from the vector DNA plasmid pAAV:VGluT2(1.8kb):eGFP:WPRE:hGh-pA cloned in our lab. The idea of using the 1.8 kb promoter came from Fu and van den Pol (2008).

Cloning of pAAV:VGluT2(1.8kb):eGFP:WPRE:hGh-pA vector: Forward and reverse primers VGluT2pr_MluI_for and VGluT2pr_AscIEcoRV_rev were used to directly amplify the 1794 bp sequence from genomic DNA of a C57Bl6/J mouse, corresponding to the 3' 1.8 kb portion of the 2.4 kb DNA promoter sequence of the VGluT2 gene, also known as Slc17a6 (see PubMed and GenBank entries NM_080853.3, DQ812098). The 5'-3' primer sequences were: "TTT ACGCGT ACGCACTCCCCTGGTTGATTTAG" and "TTT GATATC TT GGCGCGCCTCTTGTAAAGACTGGTGTCCAGCCTT" for the forward and reverse primers, respectively. Phusion(R) DNA polymerase with HF buffer (find supplier) was used to set up this PCR reaction, using 98C denaturing, 70C annealing, and 72C elongation temperatures, during 35 cycles. The reaction product was subcloned in between MluI - EcoRV sites of a standard pAAV:WPRE:hGH-pA vector (provided by B. Schneider) to obtain a pAAV:VGluT2(1.8kb):WPRE:hGh-pA plasmid. An insert encoding for eGFP reporter gene was amplified with a PCR reaction from another pAAV vector encoding for eGFP, using the forward GFP-AscI-for and reverse GFP-EcoRV-rev primers with the corresponding sequences: "TT GGCGCGCC ACC atg gtg agc aag ggc gag", "TTT GATATC tta ctt gta cag ctc gtc cat gcc g". The PCR eGFP PCR product, containing a Kozak sequence immediately upstream the eGFP ORF, was subconed in the VGluT2(1.8kb) promoter containing vector in between the AscI and EcoRV sites, to obtain the final pAAV:VGluT2(1.8kb):eGFP:WPRE:hGh-pA vector. The vector DNA was propagated in the NEB5alpha cells (find provider), and verified by Sanger sequencing at the Microsynth company. The primers were also ordered from Microsynth AG (Balgach, Switzerland).

***Stereotactic surgery procedures*.**

Surgery procedures for the *in vivo* optogenetic stimulation experiments (Fig. 3.6-3.8; were performed as it is described in the Methods part of Chapter 2 with a few exceptions. For optogenetic stimulation above the VMHvl, bilateral injections were executed as follows: 300 nl of virus suspension was injected on each brain side into the MeApd at the following coordinates (in mm from bregma skull surface): ML ±0.6, AP -1.4, DV -5.9 and bilaterally implanted with 12° angle (tilted) 500µm above the VMHvl at ML ±2.3, AP -1.7, DV -5.3; for

unilateral stimulation injection coordinates remained the same but the implantation had 0° angle (straight). For optogenetic stimulation above the PMv, ipsilateral injections were executed as follows: 300 nl of virus suspension was injected unilaterally in the MeApd at the following coordinates (in mm from bregma skull surface): ML ±2.3, AP -1.7, DV -5.3 and ipsilaterally implanted with 500µm above the PMv area at ML ±0.47, AP -2.3, DV -5.2.

For *ex-vivo* patch-clamp recordings (Fig. 3.3-3.5) MeApd was injected with the same coordinates as described above in the Methods part of Chapter 2. For labelling glutamatergic or GABAergic neurons in the VMHvl (Fig. 3.3-3.4), 100 nl of virus suspension was injected bilaterally at ML ±0.6, AP -1.5, DV -5.9. For labelling glutamatergic neurons in the PMv (Fig. 3.5), 200 nl of virus suspension was injected bilaterally at ML ±0.48, AP -2.2, DV -5.75.

For histological analysis of projection areas of MeApd-GABA neurons (Fig. 3.1), 100 nl (diluted 1:1 in PBS) of Synptophysin expressing virus was injected in the MeApd at coordinates: ML ±2.3, AP -1.7, DV -5.3. Immunohistochemistry was performed using 1:1000 diluted chicken anti-GFP (ab13970; Abcam, Cambridge, United Kingdom; RRID:AB_300798) and 1:400 rabbit anti-RFP antibodies (ab62341; Abcam; RRID:AB_945213) to stain against eGFP and mCherry, respectively. As the secondary antibodies, goat anti-chicken Alexa-488 (A11039; Thermo Fisher Scientific, Waltham, MA, USA; RRID:AB_2534096) and donkey anti-rabbit Alexa-568 antibodies (A10042; Thermo Fisher Scientific; RRID:AB_2534017) were used at 1:200 dilution.

For histological analysis of retrograde tracing from the PMv and the VMHvl (Fig. 3.2), we used Alexa Fluor-conjugated cholera toxin subunit B (CTB–Alexa 488 and CTB–Alexa 647; Thermo Fisher Scientific). 50 nL of CTB–Alexa 488 or CTB–Alexa 647 was unilaterally injected in the VMHvl or the PMv of the $VGAT^{Cre}$ mouse, respectively.

Patch-clamp electrophysiology.

In vitro electrophysiology experiments were performed as described in the Methods part of Chapter 2 with the following exceptions:

Recording pipettes were filled with a high-chloride solution, containing in (mM): 140 KCl, 20 K-gluconate, 10 HEPES, 5 Na-phosphocreatine, 4 Mg-ATP, 0.3 Na-GTP, 5 EGTA (pH 7.25, with KOH).

Recordings were done at the room temperature (20-24°C)

Inscopix: Surgeries and the behavioral testing.

The procedures of stereotactic surgery for the virus injection and implantation of a GRIN lens for microendoscopic Ca2+ imaging, were in general similar to the procedures followed during stereotactic surgeries for the optic fiber implantation described above (see Chapter 2, Materials and Methods), with a few differences. In brief, a GRIN lens was implanted during the same surgery session as the virus injection. For the experiments described in Figs. 3.9-3.11, a single bolus of AAVretro:hsyn:mCherry-ires-FlpO viral particles (250 nl of suspension containing 7.7·1012 particles/ml) was injected into the left VMHvl of a VGAT-ires-Cre mouse under isoflurane anesthesia at the following stereotactic coordinates: 1.4 mm posterior, 0.75 mm lateral, 6.0 mm ventral from the bregma skull surface. Next, a bolus of AAV2:EF1a:con/fon:GCaMP6m (Cre-ON/Flp-ON) viral suspension (250 nl of 4.4·1012 particles/ml) was injected into the ipsilateral MeApd at the following coordinates: 1.7 mm posterior, 2.3 mm lateral, 5.3 mm ventral from the bregma skull surface. In the next step, before implanting a GRIN lens, a vertical tract was first made in the brain tissue above the MeApd by insertion till 5.1 mm ventrally, and removal of a 25G medical injection needle, with its sharp end pointing laterally. The purpose if this manipulation was to penetrate through the optic nerve so that a blunt-ended GRIN lens would reach the MeApd without a thick myelinated structure of the nerve in between. Then, a docking platform-integrated GRIN lens (600 µm diameter/7.3 mm long; Inscopix Inc, USA) was slowly advanced ventrally along this vertical tract (with the lens axis at 2.4 mm lateral, 1.7 mm posterior from the bregma skull), using a cycling technique: moving in cycles of 100 µm forward/50 µm backward until the last 150 µm before the target depth, then continuously till the final position 5.05 mm ventrally from the bregma skull level. The lens was then first secured to the skull with a drop of cyanoacrylate gel glue, followed by treatment of the lens and the microscope docking platform with an adhesive iBond Total Etch (Kulzer AG, Germany), and by embedding into the UV-curable dental ceramic Tetric EvoFlow (Ivoclar Vivadent, Lichtenstein). The docking platform was then filled with a Kwik-Sil silicone compound (World Precision Instruments, USA) to prevent dust deposition on the lens aperture; the skin was stitched, and the mice were removed from isoflurane to wake up.

The animals were allowed to recover from surgery for 3 weeks in a single-housed cage, then habituation to handling and microscope dummy attachment/detachment was performed during 5 consequent days. At the end of habituation cycle, the mice were briefly brought to sleep using isoflurane to replace the silicon plug in the docking platform with a magnetized cover (Inscopix). During this procedure, the lens was inspected for dust particles, cleaned if necessary, and the expression of GCaMP6m in the MeApd neurons was examined using a microendoscope of nVista3.0 system (Inscopix Inc). The optimal LED intensity, camera gain and three focal planes were then chosen during this session.

Next, the animals were subjected to a standard RI test as described above, using an unfamiliar Balb/cByj male mouse as an intruder. During the RI test, in-vivo GCaMP6m fluorescence was continuously recorded with the camera of nVista3.0 microendoscope at 30 fps, however at three interleaved focal planes (see Fig. 3.9 C) using elens focusing capability of the system. Thus, effective sampling frequency per focal plane was 10 frames per second. Behaviour of the mouse was monitored using two CCD cameras as previously under control of EthoVision XT 13.0 software (Noldus) at 30 fps. Synchronization between the behavioral and in-vivo Ca2+ video streams was achieved by generation of 0.3s long TTL pulses every 2s by the EthoVision XT system, which were then recorded by both nVista3.0 and EthoVision systems. Comparing the timestamps of these TTL signals as recorded by two systems allowed alignment of the Ca2+ activity traces with behavior.

Initial processing of in-vivo Ca^{2+} imaging data was done using built-in analysis pipeline of Inscopix Data Processing Software (IDPS; Inscopix Inc). This included: 1) deinterleaving of the videos into the frames taken at individual focal planes; 2) spatial filtering; 3) motion correction. Next, the motion-corrected videos were exported into multiplane TIFF files and processed using an automated CaImAn pipeline (Giovannucci et al., 2019 eLife) for the source separation and ROI assignment based on constrained nonnegative matrix factorization (Pnevmatikakis et al., 2016 Neuron; Zhou et al., 2016 eLife). The output from CaImAn analysis was imported into the IgorPro 7, and custom-written routines were further used for user-supervised removal of the duplicate cells (those appearing on neighboring focal planes) based on the spatial X-Y proximity of their centroids and on the cross-correlation of their fluorescent traces. The timestamps for every data point, as well as sync signals for alignment with the cameras monitoring behavior, were imported into IgorPro from IDPS.

Next, from the intensity traces for each i-th cell ($F_i(t)$), Z-score traces were calculated as $Z_i(t) = \frac{F_i(t)-\langle F_i(t)\rangle}{\sigma(F_i(t))}$, where $\langle F_i(t)\rangle$ and $\sigma(F_i(t))$ are the mean and the standard deviation of the fluorescence intensity, respectively, calculated from the whole duration of the experiment. The timestamps of the onsets/offsets of behavioral bouts were used to produce excerpts of event-aligned $Z_i(t)$ traces, that in turn gave rise to individual rows on the color-coded raster plots illustrating the population activity correlated with a certain behavior (e.g. see Fig. 3.10). To quantitatively analyze cellular responses, $Z_i(t)$ traces were deconvolved using Fourier transform with a kernel function approximating a unitary fluorescence response to a single spike, similar to an approach used in (Yaksi and Friedrich 2006). For the kernel, a function $z(t) = (1 - e^{-t/\tau_{rise}}) \cdot e^{-t/\tau_{decay}}$ was assumed with the time constants τ_{rise} =0.08s and τ_{decay}=2.5s, respectively, with the peak amplitude scaled to 2. Prior to deconvolution, $Z_i(t)$ traces were denoised with a low-pass FIR filter (end of the pass and start of the reject bands, 2 and 4 Hz respectively; 101 coefficient), and Fourier transform-based deconvolution was performed on filtered traces $\acute{Z}_i(t)$ yielding an approximation for the cellular spiking rate $R_i(t) = FFT^{-1}\left[FFT\left[\acute{Z}_i(t)\right]/FFT[z(t)]\right]$ in s^{-1}. These $R_i(t)$ traces were smoothed with a 3-points boxcar filter, and the local peaks exceeding a given amplitude threshold (generally set to 1.0) were detected using a first-derivative method. The time location and the amplitude of the peaks thus defined discrete spiking "events" $E_i(t_j)$, which aligned to the start of the rising phase of the j-th fluorescent transient seen in $F_i(t), Z_i(t)$, and the amplitudes of the events (in units of Z/s) were proportional to the amplitude of the transients. In this study, we did not aim to accurately infer AP spiking of cells with an accuracy down to single spikes, but rather we interpreted each event as a burst of several APs, considering that the event amplitude scales with the underlying number of APs in such a burst. Next, based on the timing and amplitudes of discrete events $E_i(t_j)$, we performed a receiver operating characteristic (ROC) analysis for sorting the cells by their properties to discriminate different behaviours. In brief, we calculated an auROC value for each cell (Britten et al, 1992) by comparing the distribution of its responses (taken as a sum of the amplitudes of occurring events) during the defined "test" time windows (usually a 0.5s window centered at the onset or offset of each individual behavioural bout), with the distribution of the "baseline" responses during equivalent time windows selected at time points supposedly irrelevant for the MeA function (here, 0.5s windows centered at the middle of the resting/moving bouts longer than 2s). To estimate the significance of the resulting auROC value for each cell for a given behaviour type, we compared these values with auROCs

obtained by random (1000x) shuffling of the "test" and "baseline" time windows. The cell was considered negatively or positively discriminative, if its auROC was below or exceeded, respectively, 5% or 95% quantile of shuffled auROCs, as was described in (Li et al., 2017). For convenience, we also converted auROC values into the response strength values as $RS = (2 \cdot auROC - 1)$ (Li et al., 2017). RS values were used to determine the cell order (row position) in the color-coded raster plots of cell activity, sorted in decreasing order of responsiveness to a given stimulus as indicated (e.g. see Fig. 3.10). The triangle plots (Fig. 3.11) were constructed, and response selectivity indices were calculated as described in (Bergan et al., 2014; Li et al., 2017), using RS values for the aggressive, following or investigation behaviors as orthogonal coordinates; only the cells significantly responsive to at least one type of behaviour were considered for this analysis.

Results

GABAergic neurons from the MeApd strongly inervate the VMHvl, the PMv and the BNST

We first investigated the MeApd to hypothalamus projections anatomically using anterograde and retrograde tracing techniques. In order to visualize the axonal projections of the MeApd GABA neurons, we stereotaxically injected a Cre-inducible adeno-associated virus vector expressing eGFP and a mCherry-labelled synaptic marker Synaptophysin (AAV8:hsyn:DIO:Synaptophysin-mCherry-IRES-eGFP) into the MeApd, of transgenic mice expressing Cre recombinase under the control of the vesicular GABA transporter ($VGAT^{Cre}$) (N=2 animals) (Fig 3.1 A). Three weeks later immunohistochemistry staining with an anti-RFP antibody to enhance Synaptophysin-mCherry labelling was performed. Widefield fluorescense images of the injection site in the MeApd (Fig 3.1 B) and of the whole brain (data not shown) were generated to verify the specificity of the injection site and to screen for the target areas, respectively. In the ventromedial hypothalamic region, confocal fluorescence images showed strongest Synaptophysin expression in the VMHvl (Fig 3.1 C), compared to medial and central parts of the VMH. Another strongly targeted nucleus in the hypothalamus was the PMv (Fig 3.1 D), while in the extended amygdala region, the most intense labeling was observed in multiple subdivisions of the BNST, particularly the medial division, posteromedial part (STMPM) and medial division, posterior intermediate part (STMPI) (Fig 3.1 E), according to the brain atlas by Franklin and Paxinos (Franklin and Paxinos, 2013). Other less innervated nuclei were found to be the medial preoptic nucleus (MPON), the lateral hypothalamus (LH), the anterior hypothalamus (AH), the lateral septum (LS) and the cortical amygdala (CoA) (data not shown). However, nuclei with the strongest Synaptophysin signal and with a known role in aggression control are VMHvl, PMv, BNST, and thus, they remain as our major interest areas in this paper.

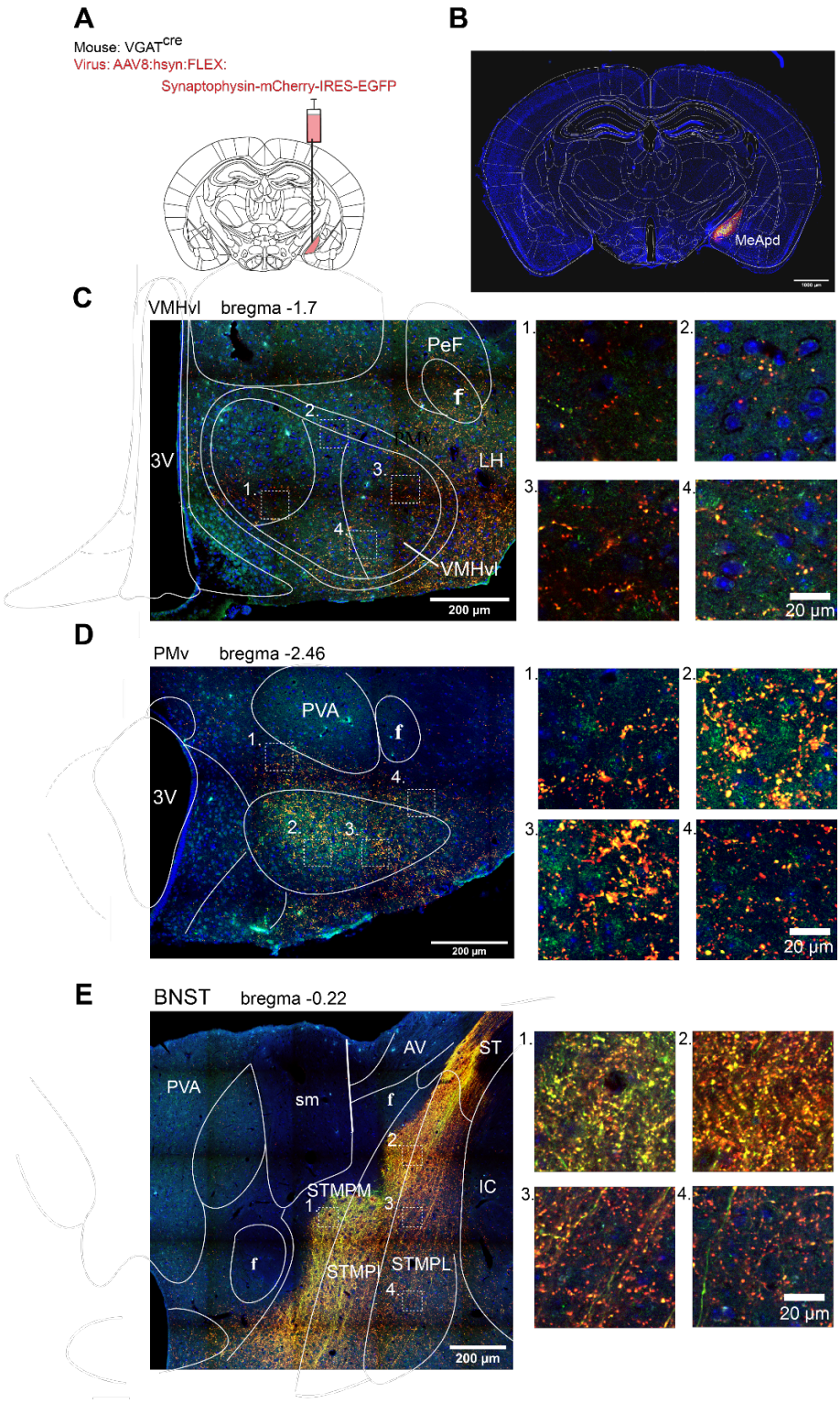

Figure 3.1 | MeApd-GABA neurons produce long range divergent axonal projections : anterograde labelling approach. (A) Schematic of unilateral stereotactic injection of the Cre-dependent AAV8 expressing a presynaptic vesicular marker Synaptophysin tagged with mCherry, along with the cytosolic eGFP, into the MeApd of VGAT^{Cre} mice. **(B)** A slide scanner widefield fluorescent image of a coronal brain section from a VGAT^{Cre} mouse injected into the MeApd as shown in (A), after enhancement using immunostaining against mCherry (red), eGFP (green) and DAPI (blue). Scale bar, 1000 µm. **(C-E)** Confocal images of the brain areas most intensely labelled with Synaptophysin-mCherry. *Left panels*, confocal (40x objective) tile overview images of VMHvl (C), PMv (D), BNST (E) from the coronal sections taken at the indicated distance posterior from the bregma level. White outlines of the most relevant brain nuclei were overlaid from the brain atlas (Fr(Franklin and Paxinos, 2013)anklin and Paxinos, 2004). Scale bar: 200 µm. *Right panels*, enlarged views onto the numbered areas (white

squares) in the respective overview images shown in the left panels. Note the size of single Synaptophysin puncta, compatible with the typical dimensions of small presynaptic terminals, ≈1 μm.
Abbreviations: 3V, 3rd ventricle; AV, anteroventral thalamic nucleus; f, fornix; IC, internal capsule; LH, lateral hypothalamic area; PeF, perifornical nucleus; PVA, paraventricular thalamic nucleus, anterior part; sm, stria medullaris; ST, stria terminalis; STMPI, bed nucleus of the stria terminalis, medial division, postero intermediate part; STMPM, bed nucleus of the stria terminalis, medial division, posteromedial part; STMPL, bed nucleus of the stria terminalis, medial division, posterolateral part; VMHvl, ventromedial hypothalamic nucleus, ventrolateral part

Next, we investigated the location of VMHvl and PMv-projecting MeApd neurons in the MeApd. Retrograde tracer CTB-Alexa488 or CTB-Alexa647 were injected into the VMHvl or PMv, respectively, of $VGAT^{Cre}$ ×tdT mice (Fig. 3.2 A, C). The injections were mostly limited to the VMHvl, with some spill into the central part of the VMH (VMHc) (Fig. 3.2 A, right), and to the PMv (Fig. 3.2 C, right). From the VMHvl, retrogradely labeled neurons were found in the BNST, the anterior, medial and lateral preoptic area, the anterior hypothalamus, the lateral septum, the extended amygdala, the cortical amygdala, the central amygdala, the basomedial amygdala and all subdivisions of the MeA (data not shown). In the MeAp, many retrogradely labeled neurons were situated at the boundary region between the dorsal and ventral subdivisions with a higher density in the MeApv (Fig. 3.2, B). In the MeApd, retrogradely labelled neurons were less dense and rather sparsely and homogeneously distributed throughout the subdivision (Fig. 3.2, B). From the PMv, retrogradely labeled neurons were found in the infralimbic cortex, the lateral septum, the BNST, the anterior hypothalamus, the medial preoptic area, the cortical amygdala, the VMH medial and lateral, the piriform cortex and all subdivisions of the MeA (data not shown). In the MeAp, we observed retrogradely labeled neurons that were homogeneously distributed throughout the ventral and dorsal regions of the MeA (Fig. 3.2, D). Overall, anterograde labeling experiments reveal a strong projection of the MeApd VGAT neurons to the VMHvl, the PMv and the BNST. In addition, retrograde labeling suggest that mainly neuron in the MeApv, as compared to MeApd, project to the VMHvl while the PMv receives inputs from both subdivisions of the MeAp to a similar degree.

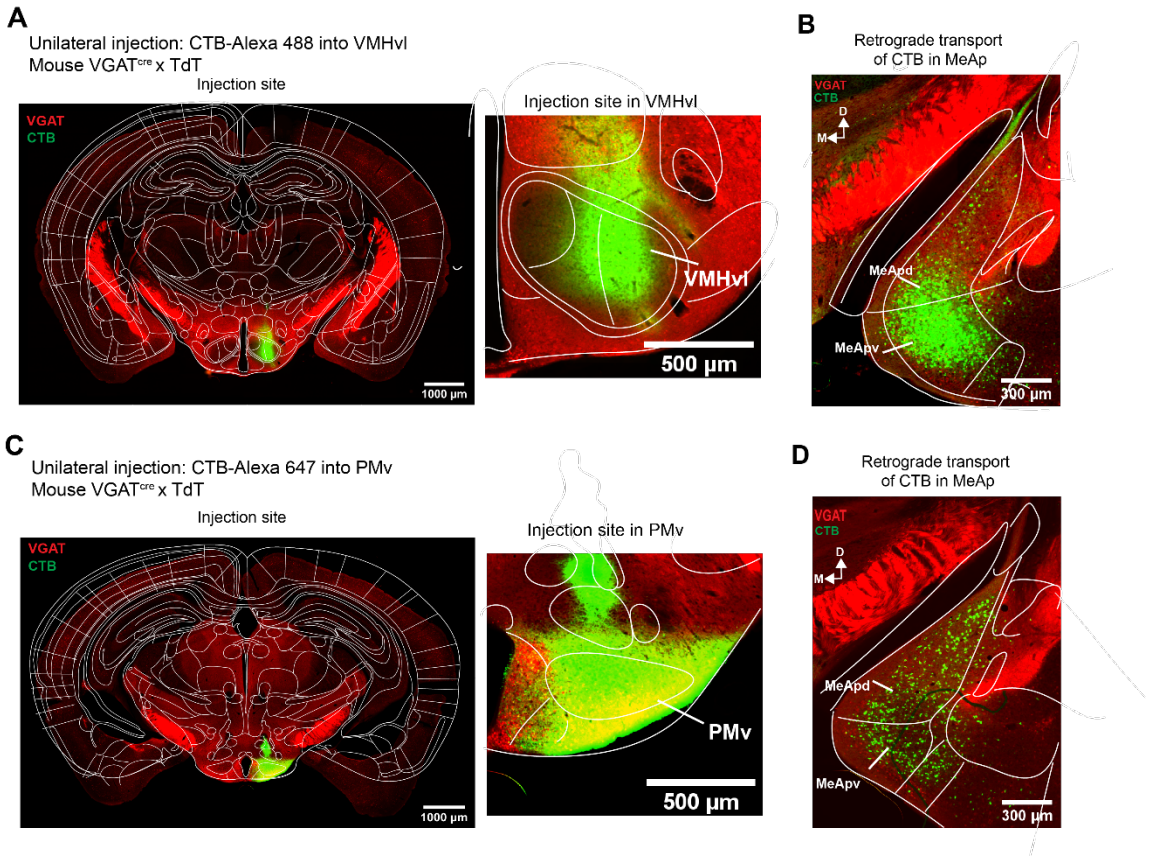

Figure 3.2 | Both dorsal and ventral posterior MeA divisions send axonal projections to the VMHvl and the PMv: a retrograde labelling approach using cholera toxin B. (A) *Left*, a slide scanner widefield fluorescent image of a coronal brain section, obtained from a VGAT^{Cre} × tdTomato mouse (tdTomato; red) injected into the left VMHvl with cholera toxin subunit B (CTB) conjugated with Alexa Fluor 488 (CTB-488; green). Scale bar: 1000 µm. *Right*, A fragment of the image on the left zooming in on the CTB injection site in the VMHvl. **(B)** A widefield fluorescent image of the posterior MeA from the experiment in (A). Note that a large fraction of the retrogradely labeled neuronal cell bodies are located in the ventral part of the MeA, MeApv. Arrows: M, medial; D, dorsal. **(C)** Similar as in (A), but the images taken from a coronal obtained from a VGAT^{Cre} × tdTomato mouse (tdTomato; red) injected into the left PMv with a CTB conjugated with Alexa Fluor 647 (CTB-647; green). Scale bar: 1000 µm. **(D)** A widefield fluorescent image of the posterior MeA from the experiment in (C). Note that the distribution of labelled cells is different from the retrograde labeling following the injection into VMHvl (A-B), with the labelled cells more evenly distributed across the ventral and dorsal subdivisions of the MeApd.

MeApd VGAT+ neurons inhibit VGLUT2+ neurons in ventromedial hypothalamus

Excitatory neurons and their subpopulations in the VMHvl have been identified to be active during aggression (Kim et al., 2019; Falkner et al., 2020; Remedios et al. 2017; Lee et al., 2014). To confirm the tracing results of Fig. 3.1 and 3.2 and to test whether these excitatory aggression effector neurons receive functional input from inhibitory neurons in the MeApd, we performed optogenetically-assisted circuit mapping. For this, the MeApd of $VGAT^{Cre}$ mice were injected bilaterally with AAV8:hSyn:DIO:ChETA-eYFP or AAV2:EF1α:DIO:ChR2-eYFP to drive the expression of the channelrhodopsin variants ChETA or ChR2 in MeApd GABA neurons. In addition, the VMHvl was injected with AAV8:$VGluT2^{1.8kb}$:eGFP to label excitatory neurons (Fig 3.3 A). Three to four weeks after the injections, animals were sacrificed and voltage-clamp recordings of the GFP fluorescent cells in the VMHvl were performed. Axons originating from the MeApd were stimulated by applying brief blue light pulses, which should activate the channelrhodopsin (Fig 3.3 B). Patch-clamp recordings were done using high chloride internal solution $[Cl]_i$=140 mM clamping the voltage of the neurons at -70 mV. In the animals expressing ChETA, blue light pulses (5 ms; 20 Hz, 10mW) reliably evoked inhibitory post synaptic currents (IPSCs) in the majority of the VMHvl GFP positive neurons (20 out of 25) (n= 25 recordings from N=6 mice, Fig 3.3 C, D, E). Neurons with optically evoked IPSCs of 5 pA or less were not included in the average and were assigned to non-responders (filled bar in Fig. 3.3 D, G). The average optically evoked IPSC amplitude was 139.3 pA with the individual values ranging from 9.8 pA to 986.3 pA (Fig 3.3 D, E). To verify that the postsynaptic currents were inhibitory, we added 10 µM GABAzine to the recording solution and found that the inward PSC disappeared, confirming that the recorded PSCs are indeed GABAergic inhibitory PSC (IPSC) (Fig. 3.2 C). In the animals expressing ChR2 as an opsin, optical stimulation of the MeApd axons in the VMHvl evoked IPSCs in 22 out of 24 GFP fluorescent neurons with an average amplitude of 138.9 pA (n=24 recordings from N=4 mice) (Fig 3.3 H). These neurons received IPSCs ranging from 6 pA to 536.6 pA (Fig 3.3 G, H) and were also blocked with 5 µm GABAzine (Fig. 3.3F; n=2). To conclude, by optogenetically stimulating MeApd GABA terminals in the VMHvl we found that excitatory neurons in the VMHvl receive inhibitory inputs from the MeApd.

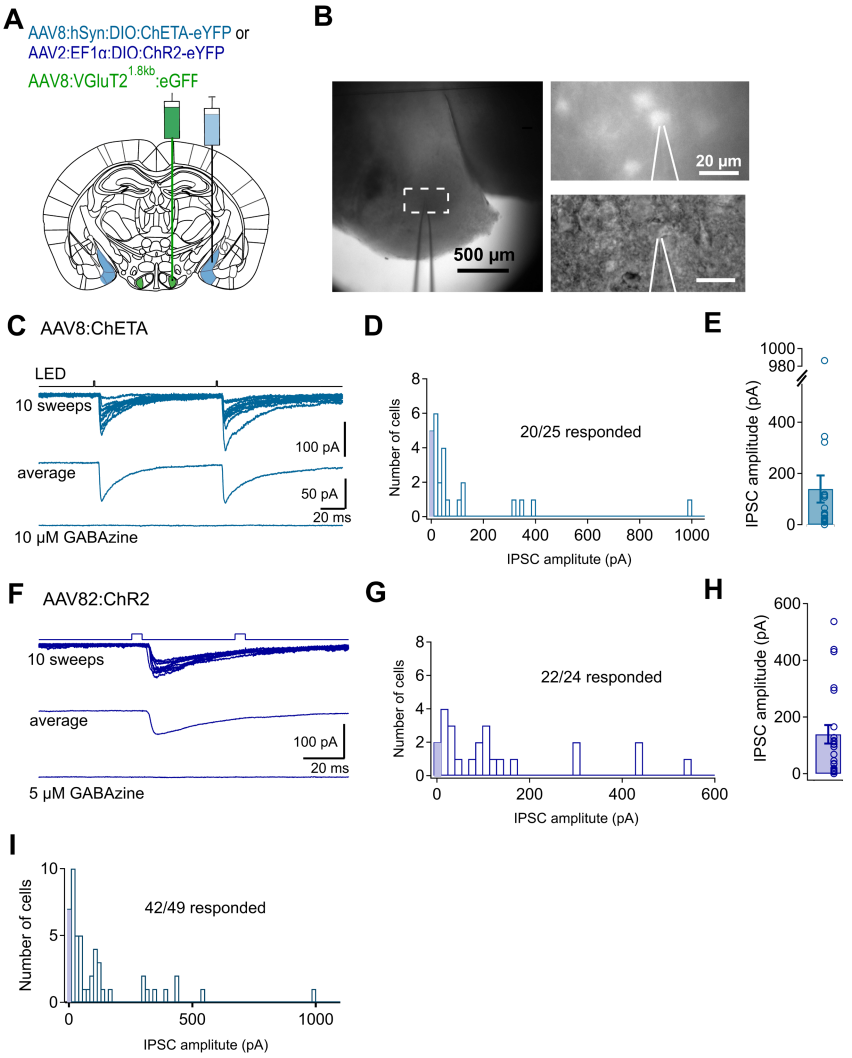

Figure 3.3 | MeApd-GABA neurons make inhibitory synapses onto glutamatergic neurons in the VMHvl. **(A)** Schematic of the experimental design: a Cre-dependent AAV8 viral vector expressing ChETA-eYFP or a Cre-dependent AAV2 vector expressing ChR2-eYFP was injected into the MeApd, *and* AAV8 vector expressing eGFP under the VGluT2 promoter was co-injected into the ipsilateral VMHvl of $VGAT^{Cre}$ mice. **(B)** *Left*, An image of acute brain slice containing an injected VMHvl (4x objective) showing the position of the recording patch pipette. *Right top*, fluorescent image of an eGFP expressing neuron in the VMHvl before whole-cell configuration was obtained (same pipette position as in the left; 60x objective). *Right bottom*, An infrared Dodt gradient contrast image of the same eGFP-positive neuron being recorded in the whole-cell configuration. **(C)** Whole-cell recording traces from an example VMHvl eGFP-positive neuron receiving the inhibitory synaptic input from MeApd axons expressing ChETA (see A; AAV8:ChETA-eYFP experiment). Short-duration (1 ms) pairs of blue-light pulses were applied at 100 ms intervals. Traces from top to bottom show: n=10 repeats of the light-gated currents (oIPSCs) recorded at -70 mV holding potential with high-Cl^- (140 mM) recording solution; average of n=10 individual repeats; average of n=10 repeats after bath application of 5 µM GABAzine. **(D)** A histogram of the average oIPSC amplitudes in response to the first light pulse across all recorded eGFP-positive neurons. Out of n=25 recorded cells, 20 were receiving the oIPSCs above the "zero" threshold of 7.5 pA. Non-connected cells were sorted into the filled "zero" bin of the histogram. **(E)** Same data as in (D), presented as an average bar (mean ± s.e.m of 54 pA) and as individual data points. (**F-H**) Similar data as in (C-E), but from the experiment using AAV2:ChR2-eYFP viral vector (see A). Note that here the light pulses of 5 ms length were used at 50 ms inter-pulse interval (F; as in in-vivo experiments). Despite these differences, a similar connectivity ratio (G) and average oIPSC amplitudes (H; mean ± s.e.m, 33.45pA) were found as compared to AAV8:ChETA-eYFP design (C-E). **(I)** A histogram of the average oIPSC amplitudes comprising values from (D) and (G). Total n=42 out of n=49 recorded eGFP cells received IPSC from MeApd-GABA neurons.

The lateral border of the VMHvl contains a higher density of inhibitory neurons compared to the core of the VMHvl and has been suggested to provide local inhibition to the VMH (Choi et al., 2005). Thus, we next investigated whether these inhibitory neurons of the VMHvl receive inhibition from the MeApd GABA neurons, because such inhibition might potentially cause a disinhibition of VMHvl principal neurons. To test this, we bilaterally injected the MeApd of $VGAT^{Cre}$×tdT with AAV8:hSyn:DIO:ChETA-eYFP (Fig 3.4 A, left) or the MeApd of $VGAT^{Cre}$ mice with AAV2:ef1a:DIO:ChETA-eYFP. In addition the VMHvl was injected with AAV8:EF1α:DIO:mCherry to label local inhibitory neurons (Fig 3.4 A, right). After 3-4 weeks following the injections, we performed voltage-clamp recordings of the tdT or mCherry fluorescent cells in the VMHvl, and applied blue light stimulation to evoke potential inhibitory inputs from the MeApd to VMHvl inhibitory neurons (Fig 3.4 B, E). We found that in both conditions, when ChETA was delivered using AAV2 or AAV8, 5ms light stimulation evoked IPSCs in a fraction of tdT+/mCherry+ neurons of the VMHvl (Fig 3.4 B, E). Optical stimulation elicited IPSCs in 5 out of 9 cells of average 28.7 pA in the AAV2-ChETA group (n=9 recordings from N=3 mice) (Fig 3.4 E, F) and in 6 out of 12 cells of average 83.2 pA in AAV8-ChETA group (n=12 recordings from N=2 mice) (Fig 3.4 C, D). Thus, about half of the recorded tdT+/mCherry+ neurons in the VMHvl received rather small inhibitory inputs from the MeApd GABA neurons. Interestingly, in some tdT or mCherry fluorescent cells in the VMHvl we observed suppression of spontaneous PSCs upon light stimulation, suggesting a potential dis-inhibition of these neurons (Fig 3.4 H).

Together, these data demonstrate that both excitatory and inhibitory neurons in the VMHvl receive inhibition from the GABAergic MeApd neurons. When we grouped IPSC data from Fig 3.3 E and H, we found that the optically evoked IPSC average amplitude on glutamatergic neurons was 139.1 pA in 42 out of 49 neurons that had measurable IPSC amplitude (higher that 5 pA) (Fig 3.3 I). On the other hand, on the inhibitory neurons in the VMHvl the total average (Fig. 3.4 D+F) amplitude was 55.95 pA in 11 out of 21 neurons that responded to light stimulation.The fraction of connected neurons (42/49 on excitatory vs 11/21 on inhibitory) was was significant (The Fisher exact test, p=0.0054). These results demonstrate that MeApd-GABA neurons largely inhibit excitatory neurons compared to inhibitory neurons in the VMHvl.

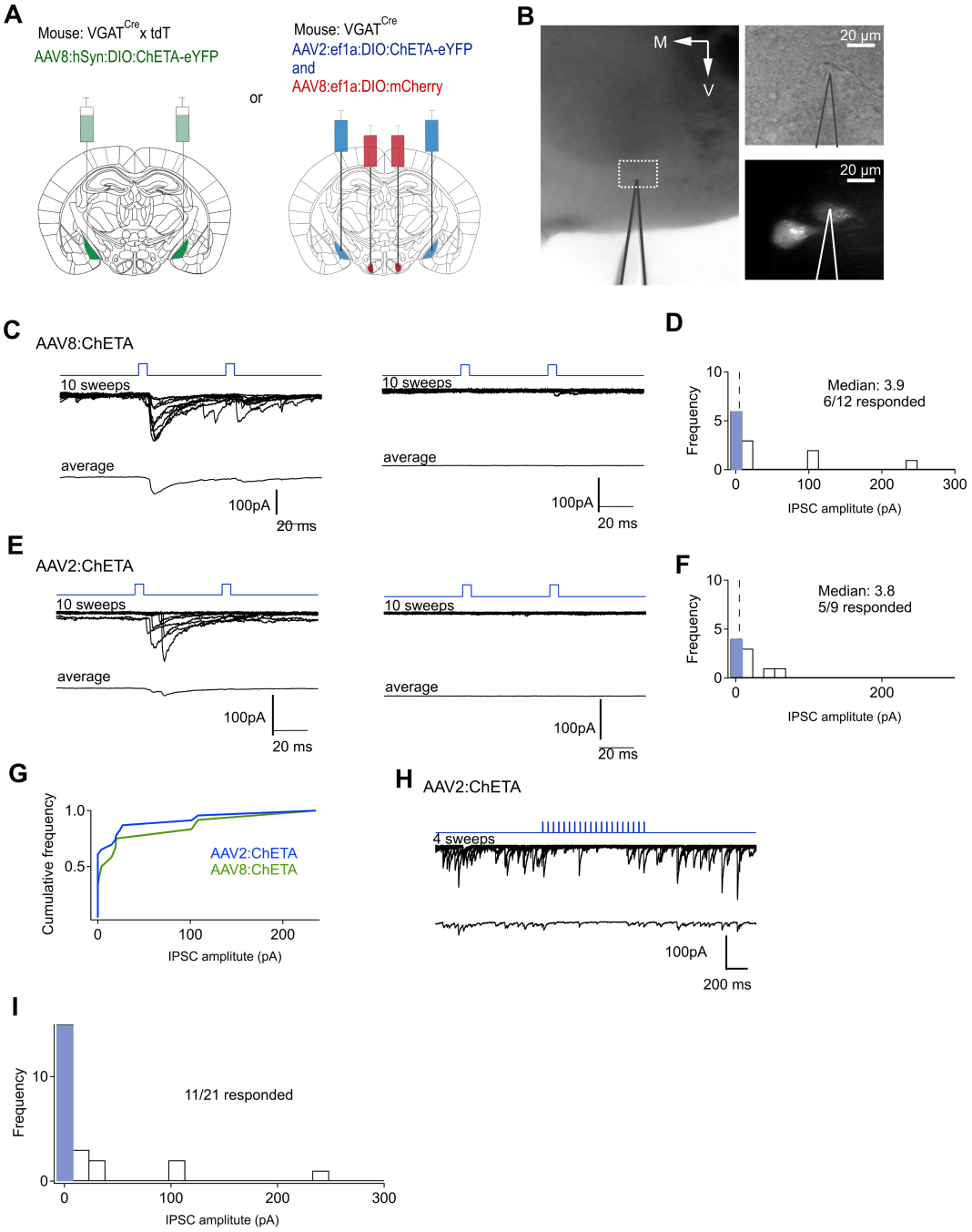

Figure 3.4 | Inhibitory inputs from the MeApd-GABA projecting neurons could be found also on inhibitory neurons in the VMHvl. (A) Schematics of two experimental designs used. *Left*, a Cre-dependent AAV8 vector expressing ChETA-eYFP was injected ito the MeApd of VGAT^{Cre} × tdT mice, bilaterally. *Right*, a Cre-dependent AAV2 vector expressing ChETA-eYFP was injected into the MeApd, *and* a Cre-dependent AAV8 vector expressing mCherry was injected into the VMHvl of VGAT^{Cre} mice, bilaterally. In both designs, GABAergic neurons of the VMHvl could be identified by their red fluorescence in acute brain slices. **(B)** *Left*, An image of acute brain slice containing a VMHvl (4x objective) made from the animal injected with AAV8:mCherry vector (see A, right) showing the position of the recording patch pipette. *Right* top, An infrared Dodt gradient contrast image of a mCherry-positive neuron being recorded in the whole-cell configuration. *Right bottom*, fluorescent image of the same neuron confirming mCherry expression (60x objective). **(C)** Whole-cell recordings from two example tdTomato-positive neurons recorded in VMHvl (see A, left for experimental design). One neuron did (left panel), and the other (right panel) did not receive detectable inhibitory inputs from the MeApd-GABA

projecting neurons. Traces from top to bottom show: top, light pulses (5 ms duration / 50 ms interval); middle, ten individual repeats of light-evoked synaptic currents (oIPSCs) recorded at -70 mV holding potential and 140 mM intracellular chloride concentration; bottom, average of n=10 individual oIPSCs. Note a large number of failures after the second light pulse. **(D)** A histogram of the average oIPSC amplitudes measured in response to the first light pulse across all recorded tdTomato positive neurons. Filled "zero" bars shows the cells with oIPSCs below detection threshold (50% of recorded neurons). (**E-F**) Similar data as in (C-D), but resulting from the experiments according to the second design (see A, right) using an AAV8:mCherry vector injection into the VMHvl. Out of n=9 recorded cells, in 5 recordings detectable oIPSCs were found. **(G)** Cumulative frequency distribution of the average oIPSC amplitudes observed in two types of experiments (see D, F). Note that the second design (E-F) revealed even smaller synaptic currents. **(H)** An example recording from a mCherry expressing VMHvl neuron (see A, right) in which short trains (1 s long, 20 Hz) of blue-light pulses (5 ms duration) were applied. Traces show n=4 individual responses to the light trains (top) and the average over these traces. Note that the spontaneous synaptic currents (presumably IPSCs) were visibly inhibited during the train of light pulses, indicating that either the MeApd-GABA axons inhibited spontaneously active surrounding neurons producing the AP-evoked spontaneous inputs onto the recorded cell, or they presynaptically inhibited the spontaneous (AP-independent) transmitter release from other incoming inputs. This effect needs further investigation using TTX and GABA-A/GABA-B blockers.

MeApd VGAT+ neurons inhibit VGLUT2+ neurons in the ventral premammillary nucleus

Previous studies have identified the premamillary nucleus as another hypothalamic area involved in aggression control in males and females (Stagkourakis et al., 2018; Motta et al, 2013). For example, stimulation of dopamine transporter (DAT) positive neurons that release glutamate leads to goal-oriented aggression in male mice (Stagkourakis et al., 2018). The PMv was also strongly labeled in our anterograde tracing studies indicating anatomically aconnection from MeApd-GABA neurons to PMv (Fig 3.1). Therefore, we next investigated whether Vglut2+ neurons of the PMv also receive functionl inhibitory synapses from the MeApd GABA neurons. To investigate this, we expressed ChETA in MeApd GABA+ neurons by bilaterally injecting the MeApd of $VGAT^{Cre}$ mice with AAV8:hSyn:DIO:ChETA-eYFP. In addition, we labelled the excitatory neurons in the PMv by bilateral injection of AAV8:VGluT21.8kb:eGFP, in order to target recordings to putative excitatory neurons (Fig 3.5 A). After at least 3 weeks following the injections, we performed voltage-clamp recordings of GFP fluorescent cells in the PMv (Fig 3.5 B). We found that 22 out of 28 cells had evoked IPSCs of average amplitude of 161 pA with the individual cell response varying from 17.3 pA to 461.4 pA (n=28 recordings from N=4 mice; Fig 3.5 C, D, E). To verify that the PSCs were inhibitory, we added 10 µM GABAzine to the recording solution and found that the inward PSCs were abolished, confirming that these currents were inhibitory (n=2 recordings; Fig. 3.5 C). Thus, these results show that the majority of excitatory neurons in the PMv receive

functional inhibitory inputs from the MeApd, suggesting a possible circuit connection that could modulate aggression.

Overall, *in vitro* optogenetic stimulation of MeApd GABA nerve terminals in two target hypothalamic nuclei confirmed our anatomical results presented in Figures 3.1 and 3.2. We showed that these MeApd neurons provide strong inhibition on the VMHvl in 42 out of 49 recordings, and on the PMv in 22 out of 28 recordings of glutamatergic neurons.

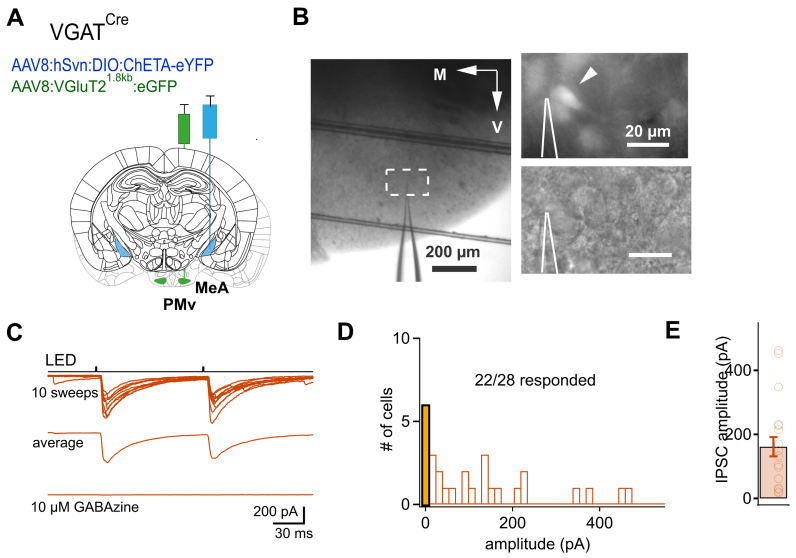

Figure 3.5 | MeApd-GABA projecting neurons make inhibitory synaptic contacts onto glutamatergic neurons in the PMv. (A) Schematic of the experimental design: a Cre-dependent AAV8 vector expressing ChETA-eYFP was injected into the MeApd, and an AAV8 vector expressing eGFP under the VGluT2 promoter was injected into the ipsilateral PMv of VGAT^{Cre} mice. **(B)** *Left*, an image of acute brain slice containing an injected PMv (4x objective), showing the position of the recording patch pipette. *Right top*, fluorescent image of an eGFP expressing neuron in the PMv before whole-cell configuration was established (same pipette position as in the left; 60x objective). *Right bottom*, an infrared Dodt gradient contrast image of the same eGFP-positive neuron being recorded in the whole-cell configuration. **(C)** Whole-cell recording traces from an example eGFP-positive PMv neuron receiving the inhibitory synaptic input from MeApd axons expressing ChETA-eYFP. Short-duration (1 ms) pairs of blue-light pulses were applied at 100 ms intervals. The traces show: top, n=10 repeats of oIPSCs (recorded at -70 mV holding potential with 140 mM concentration of Cl^- in recording solution); middle, the average trace of n=10 individual repeats; bottom, the average trace of other 10 repeats after bath application of 10 µM GABAzine. **(D)** A histogram of the average oIPSC amplitudes in response to the first light pulse across all recorded eGFP-positive neurons. Out of n=28 recorded cells, 22 received detectable oIPSCs above the "zero" threshold of 7.5 pA. Non-connected cells were sorted into the filled "zero" bin of the histogram. (**E**) Same data as in (D), presented as an average bar (mean ± s.e.m of 30.2 pA) and as individual data points.

Fiber placement for stimulation of GABAergic MeApd inputs to VMHvl cause mounting

We found above that excitatory neurons in the VMHvl and PMv receive functional inhibitory inputs from MeApd GABA neurons (Fig. 3.1, 3.3, 3.4, 3.5). Because these hypothalamic areas are key brain areas in aggression control (Lin et al., 2011; Stagkourakis et al., 2018), we next wanted to test whether the MeApd to VMHvl or PMv GABAergic connection has a functional role in modulating aggression. One way of testing the role of long-range projections in behavior is by placing an optic fiber over the output axons in the distant target area (Tye and Deisseroth, 2012). Therefore, I used this method to stimulate MeApd GABA axons and nerve terminals in the VMHvl by placing optic fibers above the VMHvl bilaterally, and injecting AAV8:hSyn:DIO:ChETA-eYFP in the MeApd of VGAT^{Cre} mice (N=3 mice). Four weeks after the surgery mice were habituated to the optic cable and to the handling of the experimenter for 4-5 days. This was followed by 2 sessions of a resident-intruder (RI) test where mice in their home cage were presented with an adult male BALB/cByJ mouse as an intruder. We used trains of blue light pulses (5 ms, 10 mW, 20 Hz, length of 60s). These were delivered at regular intervals (60s dark periods), to avoid a possible bias by experimenter-driven stimulation. During the entire behavioral session, we recorded various social behaviours of the resident mouse such as aggression, mounting, social investigation, following of the other mouse as well as passive- and asocial behaviour (Fig. 3.6 B). To our surprise, the resident mice were little aggressive and instead were mounting on the intruder mice throughout the duration of the resident intruder test (Fig. 3.6 B, C, D). In our previous behavioral studies in which we manipulated MeApd neuron somata, we very seldomly observed mounting behaviour (see Results, Chapter 2). A reason for such a difference in behavior could be that the fiber implantation over the VMHvl lesioned hypothalamic nucleus. To avoid this, we have decided to repeat the experiments by placing the fiber unilaterally above VMHvl and at the same time to inject AAV8:hSyn:DIO:ChETA-eYFP or AAV8:hSyn:DIO:GFP (in controls) into the MeApd in male VGAT^{Cre} mice (Fig. 3.6 A).

These mice have also exhibited increased mounting behaviour towards the intruder during the full course of the experiment independently of the light stimulation and whether they expressed ChETA, or GFP (in control mice) (Fig. 3.6 G;H). Averaging the behavioral scores from individual mice injected unilateraly or bilaterally showed that mounting behaviour was not dependent on the blue light (Fig. 3.6 H, In ChETA mice: p =0.78, N = 7; in control mice: p

=0.8, N = 2; two-tailed paired t-test). Thus, it seems that destruction of the hypothalamic tissue above the VMHvl induces artificial mounting.

When we quantified aggression in these experiments we observed that blue light had no effect on the time that the mouse spent attacking, from 0.045 s per 30 s of dark period (averaged over n = 11 dark periods), to 0.25 s per 30s of light period (n = 11; Fig. 3.6 D). Blue light had no effect on the time mice spent attacking in all animals of the ChETA group (Fig. 3.6 D, G; p =0.43, N = 5 mice, 2 mice not aggressive; two-tailed paired t-test) and in control mice expressing eGFP (N =2 mice, p =0.24; two-tailed paired t-test, Figure 3.6 F, G).

In these experiments we found that mice implanted above VMHvl prefered mounting rather than attacking the intruder. This artificially induced mounting was likely caused by lesioning hypothalamic nuclei when implanting an optic fiber above VMHvl.

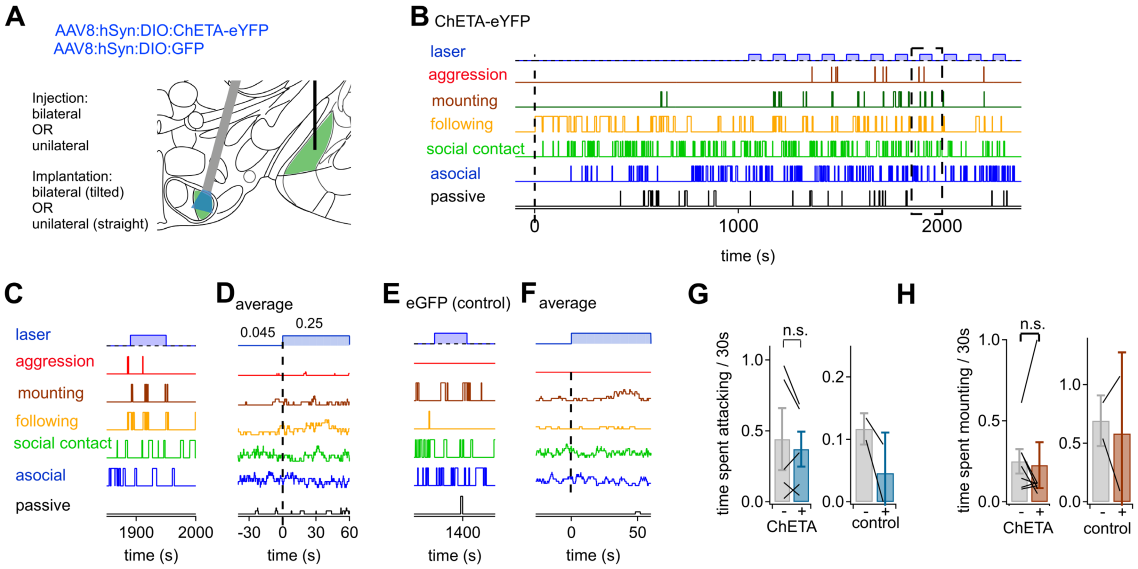

Figure 3.6 | In-vivo optogenetic stimulation of MeApd-GABA neurons' projecting axons above the VMHvl does not alter inter-male aggression, while experimental design leads to mounting behaviour. (A) Schematic of the experimental approach: a Cre-dependent AAV8 vector expressing ChETA-eYFP is injected into the MeApd, and optic fiber implantated bilaterally (tilted 12°) or ipsilaterally (straight) is made above the VMHvl. **(B)** Traces showing quantified behaviors of a resident mouse during a resident-intruder test (see Materials and Methods in Chapter 2). Note that here, in contrast to previous experiments (Chapter 2), mounting behavior was also quantified, because it was expressed only in these experiments involving optic fiber implantation above VMHvl. An intruder was introduced at t = 0. Trains of laser light pulses (5 ms, 20 Hz repetition rate, 10 mW intensity) were applied for 60s, interleaved by 60s dark periods. **(C)** An example light train episode marked by the dotted rectangle in (B). **(D)** Aligning the behavior traces to the onsets of light trains with subsequent averaging showed no change in aggression after the start of the light train. In this animal, the mounting was increased during the light train. **(E, F)** Behavioral data from a control mouse expressing eGFP, both before and during a single light train and corresponding average behavior traces for n = 11 light trains (F). In this control mouse, blue-light stimulation did not modulate aggressive behavior. **(G)** Quantification of the time spent attacking during the 30 s before (-), and 30 s into (+) the light stimulation in mice expressing ChETA (N = 5, 4 mice injected and implanted unilaterally, 1 bilaterally) or eGFP (N = 2, 2 mice injected and implanted bilaterally). For each mouse, the

individual values are averages across two tests performed on subsequent days. Note that there was no modulatory effect of light trains on aggression. **(H)** Quantification of the time spent mounting during the 30 s before (-), and 30 s into (+) the light stimulation in mice expressing ChETA (N = 7, 4 mice injected and implanted unilaterally, 3 bilaterally) or eGFP (N = 2, 2 mice injected and implanted bilaterally). For each mouse, the individual values are averages across two tests performed on subsequent days. Note that on average there was no modulatory effect of the light trains on mounting behavior except one animal used as an example in (B-D).

Stimulation of GABAergic MeApd inputs to PMv does not seem to modulate aggression

We next wanted to investigate whether the MeApd inhibition of PMv neurons, which we have observed in the ex-vivo optogenetic stimulation experiments (Fig. 3.5), modulates aggressive behavior of the resident male mouse *in vivo*. For this purpose, we ipsilaterally injected AAV8:hSyn:DIO:ChETA-eYFP or AAV8:hSyn:DIO:GFP (in controls) into the MeApd and placed an optic fiber above the ipsilateral PMv in the male VGAT^{Cre} mice (Fig. 3.7 A). Four weeks after injection and additional 4 days of habituation, we performed 2 sessions of a resident-intruder (RI) test identically as described above. Aligning and averaging the behavioral scores from individual mice showed that while in individual mice light increased or decreased aggression, there was no consistent effect across ChETA-expressing mice. Thus, on average mice spent attacking from 1.18 s per 30 s of dark period (over n = 10 dark periods), to 1.1 s per 30s of light period (over n = 10 light periods), showing no global change of aggression ($p = 0.83$, N = 7, Fig. 3.7 E). Importantly, during these experiments we have not observed any other unusual behaviors such as mounting which was very prominent in the experiments where the optic fiber was implanted above VMHvl (see above). Overall, this data suggests that unilateral stimulation of MeApd inhibitory inputs to PMv does not significantly affect aggressive behavior in resident mice.

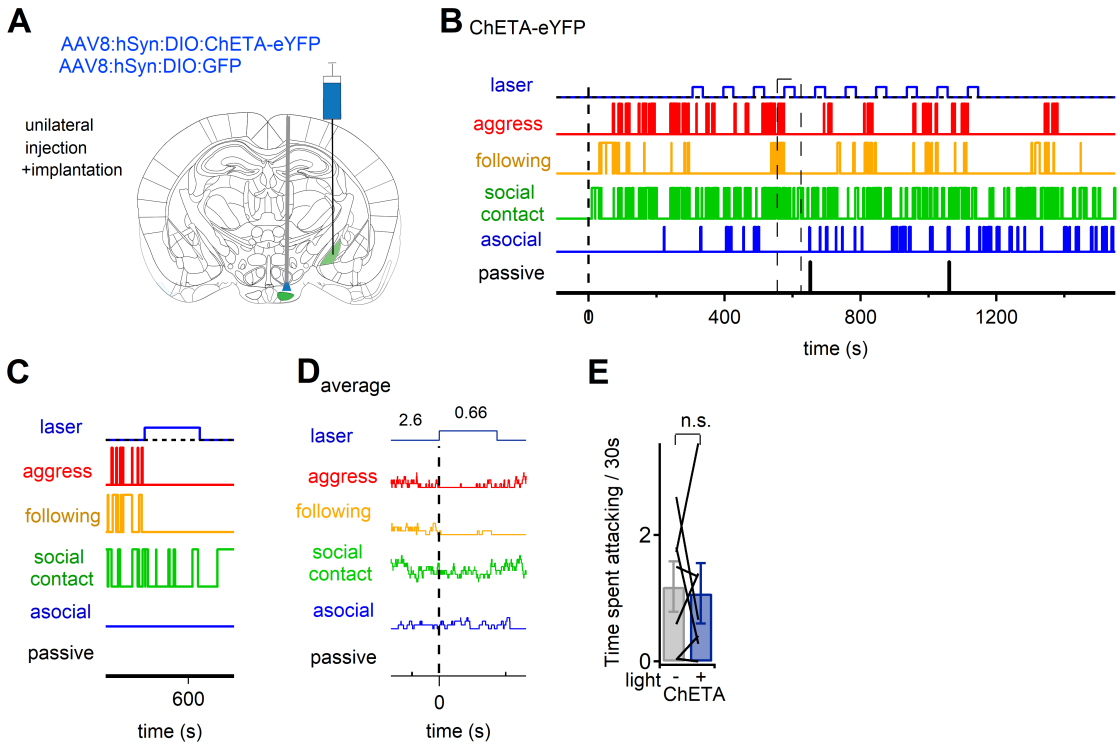

Figure 3.7 | In-vivo optogenetic stimulation of MeApd-GABA neurons' projecting axons above the PMv does not modulate inter-male aggression. (A) Schematic of the experimental approach: a Cre-dependent AAV8 vector expressing ChETA-eYFP is ipsilaterally injected into the MeApd, and straight optic fiber implantation is made above the ipsilateral PMv. **(B)** Traces showing quantified behaviors of a resident mouse during a resident-intruder test (no mounting behaviour was detected in these mice). An intruder was introduced at t = 0. Trains of laser light pulses (5 ms, 20 Hz repetition rate, 10 mW intensity) were applied for 30s, interleaved by 60s dark periods. **(C)** An example light train episode marked by the dotted rectangle in (B). **(D)** Aligning the behavior traces to the onsets of light trains with subsequent averaging showed an apparent reduction in aggression after the start of the light train in this example animal. **(E)** Quantification of the time spent attacking during the 30 s before (-), and 30 s into (+) the light stimulation in mice expressing ChETA-eYFP (N = 5). For each mouse, the individual values are averages across two tests performed on subsequent days. Note that despite a sensible reduction of aggression during the light periods in two mice, and an increase in another animal, on average there was no statistically significant effect of optogenetic stimulation of PMv projecting axons on aggressive behavior.

Stimulation of VMHvl-projecting MeApd GABA neurons reduced aggression in aggressive mice

To continue investigate the role of the MeApd to VMHvl circuit in aggression control, we have decided to change the approach and instead of implanting optic fibers above the VMHvl, which, as we found induces mounting and possibly could lesion one of the important "social" nuclei in the hypothalamus, we have combined retrograde AAV with Cre ON/Flip ON approach called "con/fon" below.

The rationale is to we target the VMHvl with an AAVretro, which will drive the expression of Flip in functionally connected upstream nuclei to theVMHvl, such as the MeA. Simultaneously, we target the MeApd by expressing a Cre and Flip dependent virus in the $VGAT^{Cre}$ mice. This approach should allow us to selectively label inhibitory cells of the MeApd that project to the VMHvl, and initial anatomical studies indeed showed labelling of GABAergic neurons in the MeApd by this approach (data not shown). Specifically, using $VGAT^{Cre}$ mice, we bilaterally injected the VMHvl with AAVretro:hSyn:mCherry-2A-FlpO and the MeApd with AAV2:hsyn:con/fon:ChETA-eYFP (or with the AAV2:hsyn:con/fon:eYFP, in control mice); and simultaneously implanted optic fibers above the MeApd (Fig. 3.8 A). Four weeks later, we performed resident intruder tests using 30 sec pulse trains repeated 10 times 5 ms pulses repeated at 20Hz. (Fig. 3.8 A). In this set of experiments, only 2 out of 8 mice injected with the ChETA-construct showed spontaneous aggressive behaviour. However, in the aggressive mice, blue light stimulation decreased the duration of attacks, as compared to the dark periods In an example animal, the time spent attacking decreased from an average of 0.99 s per 30 s of dark periods, to an average of 0.4 sec per 30 sec of light stimulation period (Figures 3.8 B-D; G). In two aggressive ChETA-expressing mice, blue-light stimulation decreased aggression, however, this change was not significant (Figure 3.8 G; N = 2 mice; p =0.41 two-tailed paired t-test). In control mice expressing eYFP under an AAV2 vector, stimulation with blue light did not change the levels of aggression (Figure 3.8 H; N = 5 mice; p = 0.4 two-tailed paired t-test). Importantly, 6 out of 8 ChETA-expressing miceshowed no spontaneous aggressive behaviour. In these mice light stimulation had no effect on aggression and aggression continued to be absent during the light period (Fig. 3.8 I). This suggests, importantly, that the MeApd GABA pathway is not a route that could explain a stimulatory role of the MeApd GABA neurons in aggression (see Hong et al., 2014, and Chapter 2).

Next, we have tried to increase the aggressiveness of the male subject mice by placing a female mouse into each of their home cage for 24 hours and then repeated the RI test. On this third day of experiments, we saw a slight increase of aggression compared to day 1 and day 2, and additionally, a third mouse that was not aggressive on the first two days became aggressive (Fig 3.8 J). However, the average time spent attacking before light was 0.5 sec per 30 sec, while during light it was 0.29 per 30 s of light stimulation period, still not significant (Fig. 3.8 J, N=3, p=0.41). Therefore, using the Cre ON/Fon On approach to stimulate VMHvl projecting MeApd GABA neurons, we observed a tendency of reduced aggression during the blue light

stimulation in 2 aggressive mice, however, this result was not significant and should be repeated with more aggressive mice in the future.

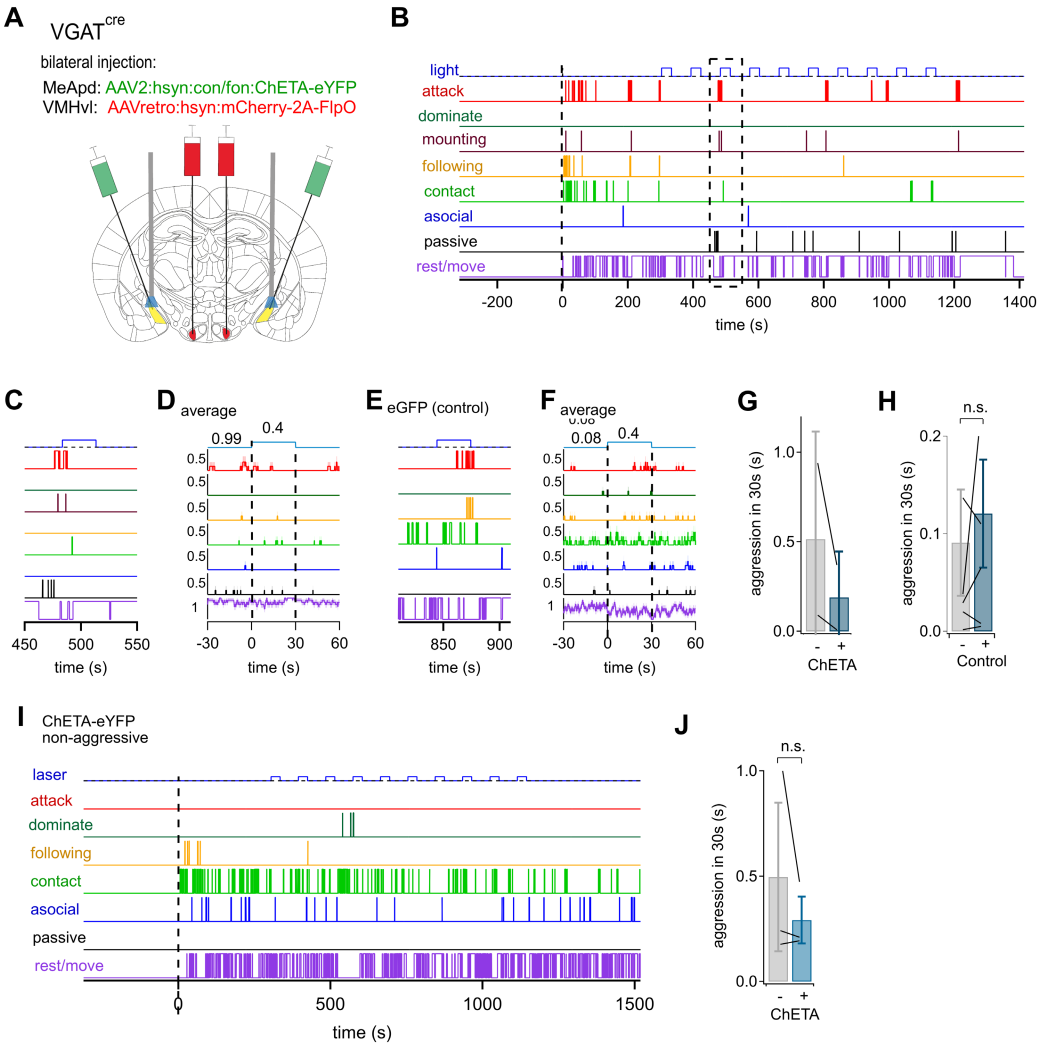

Figure 3.8 | In-vivo optogenetic stimulation of the retrogradely defined VMHvl projecting MeApd-GABA neurons suggestively leads to reduction of aggression. (A) Schematic of the experimental approach: an AAV2 vector for Cre- and Flp-recombinase dependent (Cre-ON/Flp-ON, or con/fon) expression of ChETA-eYFP was bilaterally injected into the MeApd, and an AAVretro vector co-expressing Flp recombinase and mCherry under neuron-specific hsyn promoter was bilaterally injected into the VMHvl. Optic fibers were bilaterally implanted above the MeApd injection sites. **(B)** Traces showing quantified behaviors of a resident mouse during a resident-intruder test (see Materials and Methods in Chapter 2). An intruder was introduced at t = 0. Trains of laser light pulses (5 ms, 20 Hz repetition rate, 10 mW intensity) were applied for 30s, interleaved by 60s dark periods. **(C)** An example light train episode marked by the dotted rectangle in (B). **(D)** Aligning the behavior traces to the onsets of light trains with subsequent averaging **(E, F)** Behavioral data from a control mouse expressing eGFP, both before and during a single light train (E) and corresponding average behavior traces for n = 10 light trains (F). **(G)** Quantification of the time spent attacking during the 30 s before (-), and 30 s into (+) the light stimulation in N=2 mice expressing ChETA-eYFP that expressed aggressive behaviour during experiment. **(H)** Quantification of the time spent attacking during the 30 s before (-), and 30 s into (+) the light stimulation in mice expressing eGFP (N = 5). The data in (G-H) was obtained by averaged across two first days of aggression testing. **(I)** An example mouse expressing ChETA-eYFP, which showed no aggression against the intruder (N= 6 mice that did

not express aggression on any of the experimental days, were excluded from the samples shown in G, J). **(J)** Quantification of the time spent attacking during the 30 s before (-), and 30 s into (+) the light stimulation on the additional (third) day in mice expressing ChETA-eYFP that showed aggression at least on one day. Note that one mouse that was not aggressive on the first two days became aggressive on the third day (N = 3).

VMHvl projecting MeApd GABA neurons are active during various social behavours

MeApd neurons have been shown to be involved in regulation of various social behaviors such as mating, social recognition memory, social novelty preference and aggression (Lin et al., 2011; Gur et al., 2014; Shemesh et al., 2016; Hong et al., 2014). Recent in vivo studies using extracellular recordings or optical imaging approaches have found that the MeA neurons differentially activate upon exposure to different social cues such as the scents of males, females, pups, or predators (Bergan et al., 2014; Li et al., 2017), and also during approach or avoidance behaviours (Miller et al., 2019). The activity of target area-defined cell populatios in the MeA has never been studied before, thus after using optogenetic tools to stimulate MeApd GABA inputs to the VMHvl, we became interested to investigate the activity of these neurons during the RI test.

To this end, we combined the Cre ON/Flip ON approach (Fenno et al., 2014; see also Fig. 3.8 above) in order to target GCaMP6m expression to VMHvl projecting MeApd GABA neurons, for *in vivo* calcium imaging. We unilaterally injected VGAT^{Cre} mice into the left VMHvl with AAVretro:hSyn:mCherry-2A-FlpO, and into the ipsilateral MeApd - with AAV2:EF1α:con/fon:GCaMP6m (Fig. 3.9 A). Then we have implanted a GRIN lens above the injected MeApd (Fig. 3.9 B) to image calcium dynamics in GABA neurons by the means of fluorescence of GCaMP6m sensor (Chen et al., 2013) as an indirect readout of neuronal spiking activity. Four weeks after surgery, preceded by one week of habituation to the microendoscope attachment, the mice underwent the RI test during which Ca^{2+} imaging of GABA population in the MeApd was performed. After the post-hoc analysis of mouse behavior (using DeepLabCut/Simba pipeline as described above) and extraction of fluorescent signals using ROIs automatically assigned by CaImAn algorithm (Giovannucci et al., 2019; Fig. 3.9 C), behavioral bouts and Z-scored fluorescent readouts were aligned with each other (Fig. 3.9 D). In an example mouse FV5266, Z-score traces of the Ca^{2+} signal in many responsive cells showed a strong rapid increase upon introduction of the intruder into the resident´s cage (Fig. 3.9 D, dotted line), indicating a stark rise in neuronal spiking activity when the intruder was added. We found that the MeApd GABA neurons projecting to the VMHvl were active during various subtypes of social behaviours such as aggression, following, and non-aggressive investigation (Fig. 3.9 D, E). The responsiveness of individual neurons temporally correlated

with the onsets or the offsets of different subtypes of behavioural bouts was statistically assessed using receiver operating characteristics analysis (ROC; see Methods). Thus, the imaged cell population were sorted by their respective response strength (RS) values, and the example cellular responses were time-aligned to the onsets of social behavior (investigation), following and aggression could be shown as color-coded raster plots (Fig. 3.9 E) in which the top part contains the cells whose activity is most strongly correlated, and the bottom part – the least correlated cells with the respective type of behaviour. Shortly after introducing the intruder, the neuronal activity increased just before the social contact and slowly decayed towards the end of social behavior in a sub-population of the imaged cells (Fig. 3.9 E, left). In this example mouse, there was also an increase of activity in some cells during following of the intruder (Fig. 3.9 E, middle). We have also noticed that a fraction of cells was active during the aggression, and some of them continued firing after the end of the attack (Fig. 3.9 E, right). When the binned cell activity in a 0.5s time window centered around the onset of the respective behavioural bout (i.e. the raw input to ROC analysis; see Methods) was plotted over time throughout the entire experiment, we observed that the activity of cells responding to social behavior notably decayed over time after introduction of the intruder (in this example animal, could be fitted with a mono-exponential function, $\tau \approx 80s$), and stayed close to baseline for the rest of the RI test (Fig. 3.9 E, green trace). In contrast, the activity of cells correlated with aggressive behavioural bouts fluctuated but in general remained at a high level around the aggression bout onsets across the experiment (Fig. 3.9 E, red trace). These observations were consistent across tested animals (N=4). Thus, we found that the VMHvl projecting MeApd GABA neurons were active during various social behaviors including attack, following and social investigation. The activity of neurons time-correlated with non-aggressive investigation peaked immediately after introduction of the intruder and decayed to the baseline, while the levels of activity associated with the bouts of aggressive behaviour were sustained throughout the duration of the experiment.

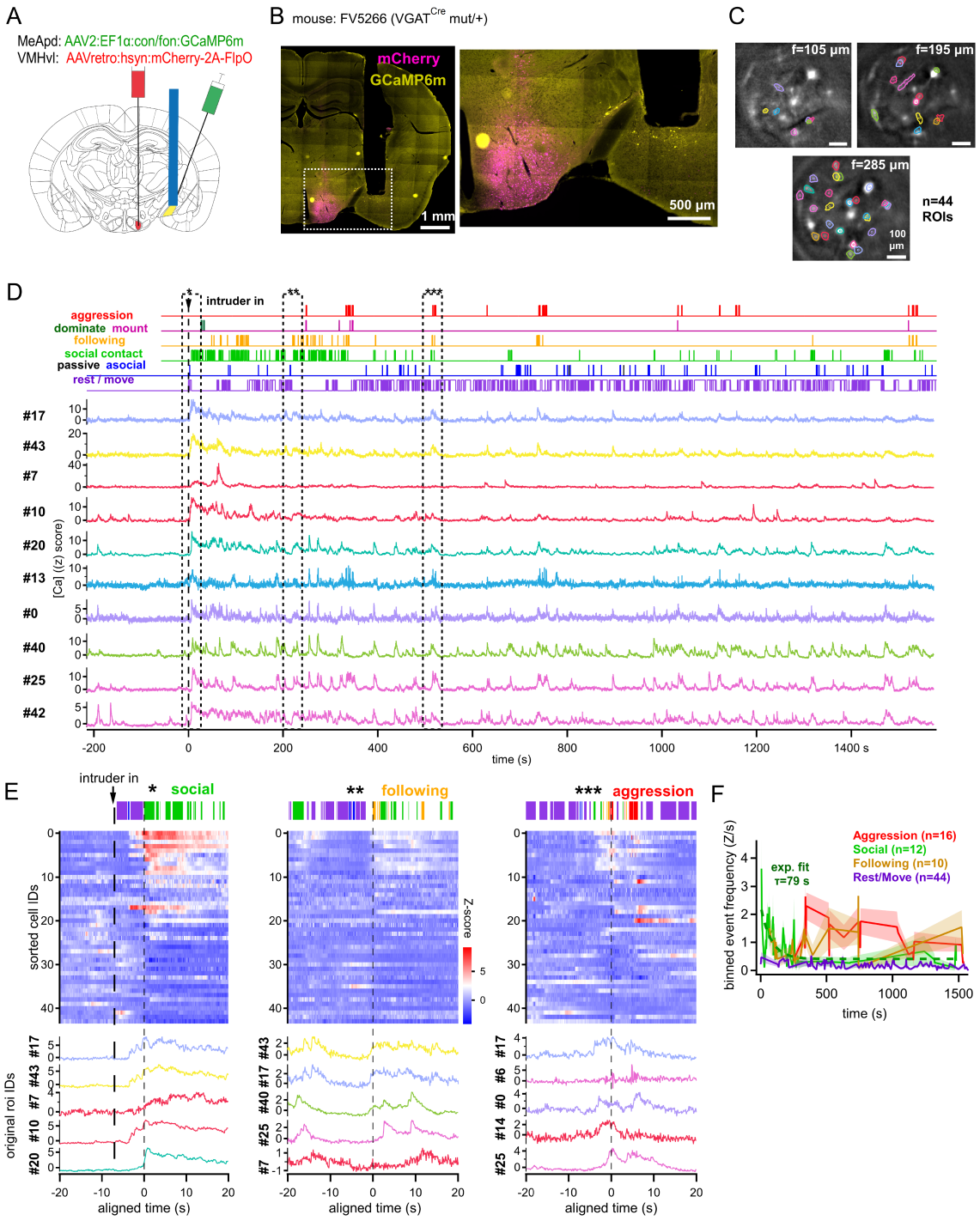

Figure 3.9 | VMHvl projecting MeApd GABA neurons are active during various social behaviors as revealed by the microendoscopic *in-vivo* Ca^{2+}-imaging. (A) A schematic of the experimental approach: an AAV2 vector expressing GCaMP6m in a Cre- and Flp-recombinase dependent manner (con/fon) was unilaterally injected into the MeApd, and an AAVretro vector co-expressing Flp recombinase and mCherry under hsyn promoter was injected ipsilaterally into the VMHvl of a $VGAT^{Cre}$ mouse. A GRIN lens (600 µm diameter) was implanted above the injected MeApd to image MeApd-GABA cells projecting to VMHvl using a nVista3.0 microendoscope (Inscopix). **(B)** *Left*, a post-hoc slide scanner widefield fluorescent image of an example coronal section (mouse FV5266; data in C-F) containing the injected MeApd and VMHvl, and a tract made by the GRIN lens. mCherry fluorescence is shown in magenta; native GCaMP6m signal was imaged with a GFP filter set (yellow) with a strong contribution of background signal. R*ight*, an image zooming in on a dashed rectangle on

the left; single GCaMP6m cells can be distinguished below the GRIN lens edge. **(C)** Average intensity projection images generated by the nVista3.0 microendoscope camera at three focal depth away from the GRIN lens edge, as indicated. The single-cell ROIs automatically assigned by the CaImAn algorithm after elimination of duplicates from neighboring focal planes were overlaid on the images; the color code used for the ROIs outlines is kept for the data traces in D-E. **(D)** *Top six traces*, traces showing quantified behaviors of a resident mouse during a resident-intruder test (see Materials and Methods, Chapter 2). An intruder was introduced at t = 0 (dashed line). *Bottom ten traces*, Z-scored output traces from the CaImAn algorithm, defined as top-10 responders to non-aggressive social interactions according to the ROC analysis. **(E)** Example cellular responses time-aligned to the onsets of a social behavior (investigation) bout (left), a following bout (middle) and an aggression bout (right) marked by the dotted rectangles with respective asterisks in (D). *Top*, a behavior bar with color-coded stripes corresponding to the respective single behavior bouts in (D, top). *Middle*, a raster plot encoding the activity (Z-score values) of all n=44 detected cells in this example animal aligned to the onset (t=0) of a given behaviour bout. Note that the cell order in the raster plots is different for the three panels: the position from the top to bottom row was defined by the cell's response strength (RS value) as estimated by the ROC analysis *across the whole experiment* for the response to non-aggressive social contact, to following, or to aggression, respectively. *Bottom*, time-aligned Z-score traces for the top-5 responding neurons (top 5 rows in the raster plot), with the cell IDs indicated. Note that some cells (e.g. #17, #43) are multimodal being in top-5 for all three behaviours, but some (like #6) are more selective (see also Fig. 3.11). **(F)** Population-averaged timecourses (mean±s.e.m.) of the binned activity (sum of the amplitudes of events detected by deconvolution over a 0.5s time window centered around the onset of the respective behaviour bout), plotted separately for aggression (red), social contact (green), following (orange) and asocial resting/moving (purple). Such values for individual neurons served as the input into ROC analysis. There was a notable decay over time for the social contact behavior (dashed green line is a mono-exponential fit), not seen for the other behaviours. The average traces were calculated across the sub-population reported as significant responders (numbers indicated), except resting/moving (all 44 cells included) which is a proxy to a baseline input featuring the smallest values across the experiment. (These experiments were performed and analyzed by Dr. Olexiy Kochubey)

We further looked at the activity of the aggression-responsive cells across 4 tested animals (Fig. 3.10 A, B), including the example animal presented in Fig 3.9 (red trace and the raster plots). For this, neuronal responses were averaged across aggression bouts after alignment to their onsets (Fig. 3.10 A, top trace) or to the offsets (Fig. 3.10 B, top trace) to construct average peri-stimulus time histograms (PSTH). Using the ROC analysis, the cells were sorted according to their responsiveness within the 0.5s time windows centered at the onsets or the offsets of aggression bouts (Fig. 3.10 A, B, respectively) such that significantly responding cells were above the white dashed line (raster plots). Note that the sub-populations of onset- and offset-responders are different, comprising n=16 and 30 neurons in this example (Fig. 3.10 A, B), from which some may overlap. The average activity across this sub-populations of responder cells (Fig. 3.10, A, traces below the raster plot) showed that these cells start to be active with a short delay after the attack initiation (Fig. 3.10, A). Note that the spike of activity in the mouse FV5220 (Fig. 3.10, A) could be related to the offset of an aggression bout that once took place at a short delay (0.2s) prior to the alignment point. Upon the offset of aggression, in 3 animals the aggression-responsive cells had a clear activity peak around the end of attack (Fig. 3.10, B). In another animal, this peak was not so evident (Fig. 3.10, B, bottom trace, FV5262). These

results show that a fraction of neurons start to increase their activity briefly after the attack initiation and have a pronounced peak around the end of aggression. This activity pattern is consistent with the idea that these inhibitory neurons might play a role in terminating attack behaviour.

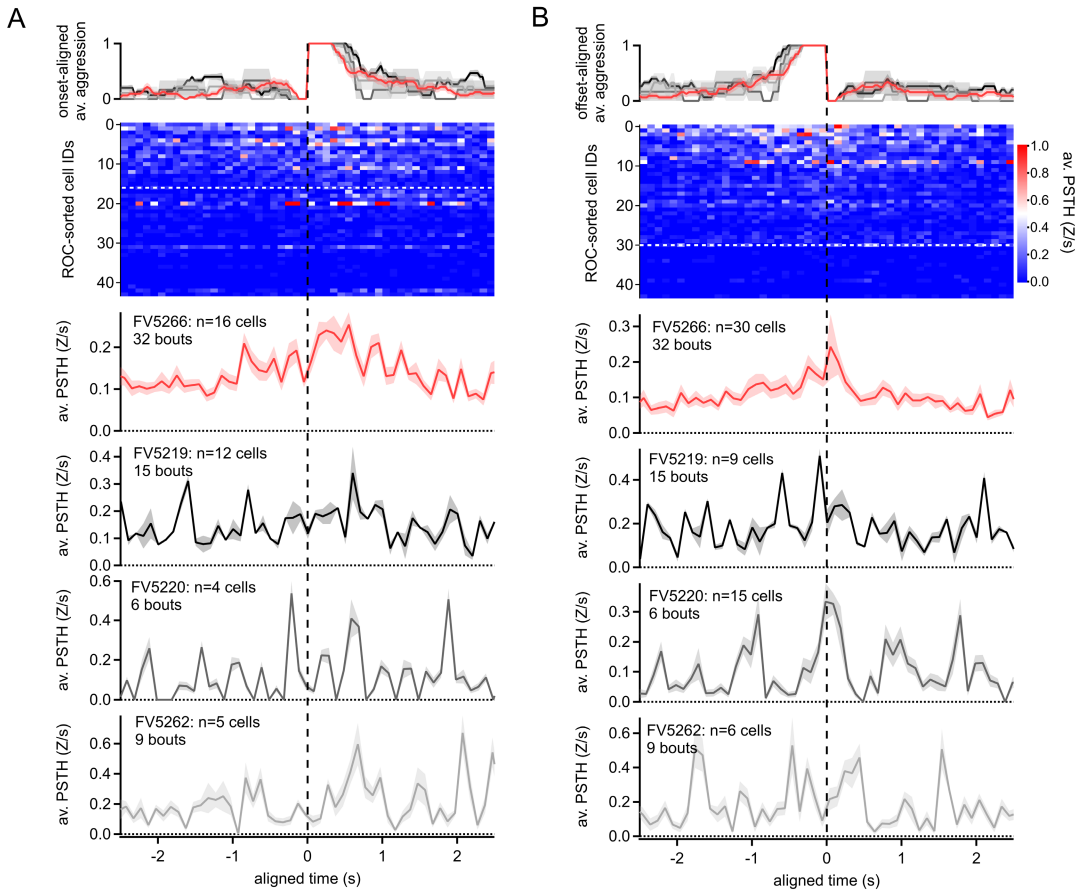

Figure 3.10 | A fraction of VMHvl projecting MeApd-GABA neurons activate during aggression. (A) Averaged activity of MeApd-GABA neurons after alignment to the onsets of individual aggression bouts in N=4 animals. *Top*, averaged aligned aggression bouts (mean±s.e.m.), color-coded for individual mice. Red trace corresponds to the example mouse FV5266 (see Fig. 3.9). *Middle*, a color-coded raster plot based on the recordings in FV5266 mouse, where each row represents the cell activity (amplitudes of the Ca^{2+}-events detected by deconvolution), aligned to the onsets of, and averaged across the 32 aggression bouts; note that this is analogous to a peri-stimulus timing histogram (PSTH) analysis. Dashed horizontal line marks the top 16 cells that were reported by ROC analysis as significant responders to the onset of aggressive bouts (±0.25s window). *Bottom*, red trace: average PSTH trace ± s.e.m. across top n=16 cells for the example animal FV5266. Grey-scale traces at the bottom: analogous analysis was performed for the other N=3 mice, with the numbers of aggression bouts and of the neurons significantly responding to the aggression onset indicated. **(B)** Similar analysis as in (A), but the responses were aligned to and averaged across the *offsets* of aggression bouts. Note that often more cells were identified by ROC analysis as significant responders to the offsets than to the onsets of aggression bouts in the same mice (except mouse FV5219), and that, interestingly, the average PSTH traces often showed a peak of activity towards the end of the aggressive bout. (These experiments were performed and analyzed by Dr. Olexiy Kochubey)

A large fraction of recorded MeApd neurons that project to the VMHvl (N=4 mice) responded to more than one social stimulus, and thus, we constructed triangle plots as in (Bergan et al., 2014; Li et. al., 2017) to visualize the response selectivity of these neurons to the onsets of behaviour bouts of different types (Fig. 3.11, A). Only the cells that were significantly responding to aggression, following or social investigation (as reported by the ROC analysis) were represented in these plots. In all tested animals, many cells were located in the central part of the triangle, meaning that they were responsive to aggression, following and social behavior (investigation) to a similar degree (Fig. 3.11, A). In addition, many cells were also located in between the aggression and the following behavior (along the right leg of the triangle) which shows their selectivity to these two behaviors (Fig. 3.11, A). Fewer cells were responsive only to one of the aggressive or following behaviors, thus located near the respective corners of the triangles (Fig. 3.11, A). Only a single cell showed selectivity for the social behavior alone (Fig. 3.11, A, mouse FV5219). Finally, a histogram of response selectivity indices was constructed on the pooled responder cell from all animals (n=73 neurons; Fig. 3.11, B). Given that the values closer to 1 mean higher selectivity to one of the behaviours, it is thus apparent that most of the cells are not selective to any of the three analyzed behaviors (aggression, following and social behaviour). Very few cells were selective for one of the behaviors and, based on their distribution inside the triangles (Fig. 3.11, A), these behaviors are aggression or following (Fig. 3.11, B).

Altogether, *in vivo* imaging revealed that the VMHvl projecting MeApd GABA neurons are active during different social behaviours, including social investigation, aggression and following. Aggression-responsive cells had an increased activity throughout attack episodes with a small peak towards the end of the attack. Furthermore, many recorded cells had no strong selectivity of their response to any of the analyzed behaviors but rather were non-selectively responsive to aggression, social behavior and following. These results also show that only a few MeApd GABA neurons are selectively activated by aggression as compared to other social behviours.

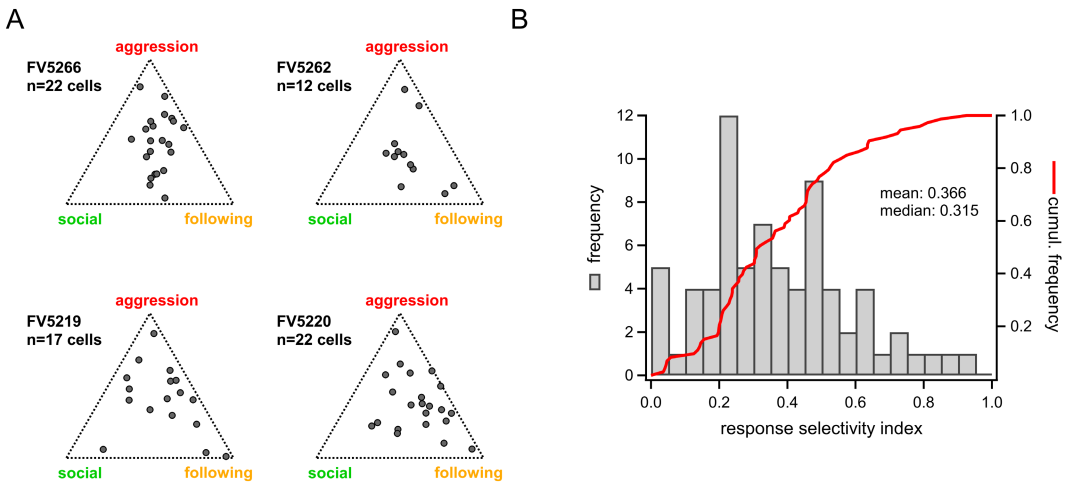

Figure 3.11 | VMHvl projecting MeApd-GABA neurons are largely multimodal in respect different types of social behaviour. (A) Triangle plots generated for each animal based on the normalized RS values for each neuron (a circle), assuming non-aggressive social contact (investigation), following and aggression as three orthogonal behavior axes (see (Hashikawa et al., 2017)). Only cells significantly responding to at least one of the behaviour types were considered for these plots. Note that a large fraction of cells falls into the central zone of the triangle, indicating that RS values for all three behaviours were close, thus these cells responding to multiple behaviours. Only several cells per animal fell close to the vertices of the triangles, being the most selective cells for respective behaviour. (**B**) Histogram of the response selectivity indices for individual neurons (n=73) pooled from N=4 mice, all represented separately in (A). Note that the distribution is skewed towards smaller values, "0" being completely non-selective, "1" – perfectly selective for certain behaviour type. (These experiments were performed and analyzed by Dr. Olexiy Kochubey)

Discussion

MeApd-GABA neurons send their axons to the hypothalamic nuclei involved in aggression control, including the VMHvl and the PMv (Choi et al., 2005; Keshavarzi et al., 2014; Stagkourakis et al., 2018, Fig. 3.1). Nevertheless, this connection has never been described functionally, and the exact behavioral significance of the VMHvl and the PMv projecting MeApd-GABA neurons has not been evaluated. In this study, we showed that MeApd-GABA neurons are synaptically connected with, and inhibit excitatory neurons in the VMHvl and the PMv. Furthermore, they provide a small inhibitory input on the inhibitory neurons surrounding the VMHvl. We further describe, using in-vivo Ca^{2+} imaging, that the majority of the VMHvl-projecting MeApd GABA neurons are non-selectively active during various social behaviours such as non-aggressive social investigation, following and attacking. This low selectivity could in part account for the absence of a clear behavioural effect upon direct optogenetic stimulation of the axons of MeApd-GABA neurons projecting to the VMHvl or PMv. Only a small fraction of MeApd-GABA projecting neurons is specifically active during aggression, and some neurons displayed more specific activation towards the end of aggression bouts. This temporal in-vivo activity pattern, together with functionally proven synaptic inputs into the VMHvl and PMv, is compatible with the contribution of a projecting sub-population of MeA-GABA neurons to inhibit aggressive behavior.

Previous studies have postulated that MeApd-GABA neurons promote aggression via disinhibition of the glutamatergic neurons in the VMHvl (Choi et al., 2005; Hong et al, 2014), however there has been no evidence for a disinhibitory circuit required for such a role. Our initial study (Baleisyte et al., 2021; see Chapter 2) showed that stimulation of MeApd-GABA neurons could increase or decrease aggression in the resident mice, depending on the channelrhodopsin variant used for the optogenetic stimulation. Thus, the results of our first paper challenged the widely accepted view that activity of MeApd-GABA neurons promotes aggression, and provided a significant evidence that these neurons, when activated, rather lead to a stop of aggression. The idea that MeApd neurons initiate aggression via local disinhibition of glutamatergic neurons in the VMHvl largely lacks experimental proof. A few studies have shown that the excitatory neurons and their sub-populations in the VMHvl are active during aggression (Falkner et al., 2020; Kim et al., 2019; Lee et al., 2014; Remedios et al., 2017; Yang et al., 2017). However, it has never been tested whether these excitatory VMHvl neurons receive local inhibition, neither that inhibitory neurons in the VMHvl receive functional inputs

from the MeApd. In contratry, we have demostrated here (Cahpter 3) that MeApd-GABA neurons have significatly higher connectivity rate and larger IPSC amplitudes measured in the excitatory postsynaptic VMHvl neurons, rather than in inhibitory ones. Further, while recording from VMHvl inhibitory neurons in slices, we also observed that in a fraction of cells (see Fig. 3.4 H), optogenetic stimulation of MeApd-GABA axonal terminals suppressed spontaneous synaptic currents in these neurons. At the moment we can not identify these spontaneous currents as EPSCs or IPSCs as the pharmacology was not done in these recordings. In case some of the recorded events were glutamatergic EPSCs, these synaptic inputs likely originate from the local glutamatergic VMHvl neurons, and the inhibitory effect of optogenetic stimulation would support the conclusion about efficient inhibition of VMHvl principal cells by the MeApd-GABA projectors. In case these spontaneous currents were IPSCs, the observed inhibition of spontaneous events would indicate, first, that GABA neurons of VMHvl are interconnected between each other, and, second, that MeApd-GABA inputs indeed inhibit this local inhibitory network around VMHvl (see Fig. 3.4 H). The latter explanation is in line with disinhibition as it has been postulated i (Choi et al., 2005, Hong et al., 2014). However, the net output of the self-interconnected inhibitory circuit is hard to predict as we have seen at the level of the MeApd (see Chapter 2). Furthermore, stepping away from the VMHvl, multiple studies have shown that the PMv excitatory neurons are active during aggression and control various components of the attack (Cavalcante et al., 2014; Chen et al., 2020; Lin et al., 2011; Motta et al., 2013; Stagkourakis et al., 2018). Our experiments revealed that the glutamatergic neurons in the PMv received strong inhibition from the MeApd-GABA neurons.Given the reciprocal excitatory conectivity between PMv and VMHvl glutamatergic cells (Stagkourakis et al., 2018), this suggests another likely mechanism of aggression suppression. Altogether, these results propose that MeApd-GABA neurons are more likely to inhibit aggression as a consequence of a strong inhibition of the VMHvl and of the PMv glutamatergic neurons.

In vivo optogenetic stimulation of MeApd-GABA axonal terminals above VMHvl, unfortunately, has not provided conclusive results as the implanted mice had strongly increased levels of mounting. We have never observed such a high levels of mounting when mice were implanted above the MeApd, which suggests that the implantantion above the VMHvl could have lesioned hypothalamic nuclei that are involved in inhibiting sexual mounting behaviour. On the other hand, the absence of conclusive effect could be due to the multimodal nature of the MeA-GABA projecting neurons in respect to the social behaviour of the mouse (see below). To circumvent the mounting artefact, we used a combination of a retroAAV virus (injected into

VMHvl) that drives expression of Flp recombinase, and an AAV2 that drives the expression of ChETA in the MeA of $VGAT^{Cre}$ mice in a Cre-ON/Flp-ON manner. Indeed, mounting in these mice was virtually absent.Unfortunately, in this series of experiments, only very few mice were aggressive on the baseline. In the two mice that were aggressive, optogenetic stimulation reduced the time spent attacking. At the same time, none of the experimental mice (n=7) had an increase of aggression during the optogenetic stimulation. This shows that direct stimulation of the MeApd-GABA to VMHvl pathway does not lead to an increase of aggression, and therefore not account for the stimulation of aggression observed by Hong et al. (2014). Furthermore, preliminary optrode recordings of the VMHvl neurons while optogenetically stimulating the MeApd-GABA projecting axons locally in the VMHvl, reduced AP firing frequency in a fraction of the recorded neurons (Olexiy Kochubey, personal communication). Therefore, these data support our *in-vitro* findings and suggest that MeApd-GABA neurons contribute to reducing aggression by inhibiting principal neurons in the VMHvl. However, to confirm the initial *in-vivo* results on optogenetic stimulation of VMHvl projecting MeA-GABA neurons, more tests with more aggressive mice have to be conducted in the future.

Next, we performed Ca^{2+}-imaging of the VMHvl projecting MeApd-GABA neurons during the RI test in the resident mouse. The data has revealed that many of these MeApd-GABA neurons start to be active upon the introduction of the intruder into the resident`s cage, probably due to activation of direct vomeronasal input into the MeApd during the bouts on non-aggressive social contact (investigation). Later in the course of the experiment, the activity of neurons associated with social investigation episodes decreased (with a near-exponential time course; Fig. 3.9 F). At the same time, these and other neurons got activated during other behaviours such as following and aggression. Some neurons showed increased activity during aggression bouts, while a subset of MeApd-GABA neurons projecting to the VMHvl showed a peak of activation selectively around the offset of aggression bouts. The activity of these latter neurons did not precede the onset of aggression, rather they start to be active after the attack initiation and are probably contributing to supress or stop the aggression. Furthermore, we have not observed aggression-selective neurons that would be solely active at the onset of aggression. Regarding the selectivity of neuronal activity to the sub-types of social behaviour displayed by the animals, to our surprise, very few neurons were strictly selective only for aggression; rather in majority the same neurons were active during several types of behaviour. Multimodality of the MeApd neurons has been shown before by Li et al. (2017), who they showed that the neuronal MeApd ensembles which are responsive to females, males, pups or

predatorsoverlap, and that the population of the responsive neurons shifts upon experience and the internal state of an animal (Li et al., 2017). This observed multimodality in our and in the previous study obviously indicates that optogenetic stimulation experiments directed at modulating social behaviors, at least in the MeApd, are very hard to interpret, especially if a wide non-selective cell population is concerned. For example, many cells strongly fire upon introduction of the intruder, when animals usually don`t attack during the initial bouts of non-aggressive investigation. It means that their activity as measured in-vivo in not sufficient to initiate attack as would be expected from the study by Hong et al. (2014). Contrary, this would be consistent with our results using ChETA (Chapter 2) showing that exogenous activation of cells inhibits attacks. In the view of the Ca^{2+}-imaging data, it could possibly mean the recruitment of the cells or activation of firing regimes that correspond to non-aggressive social interaction. The native in-vivo activity of cells upon social investigation decreases with time, indicating that the cell activity might changes its meaning with changing the animal state. Alternatively, upstream sensory inputs in the AOB that provide direct excitation to the MeA are decreased leading to a reduced excitatory drive in the MeA. Also, it seems that the execution of the aggression is not straightforward but rather is a result of the integration of multiple sensory inputs and is relative to other behaviours encoded by the same neurons. Therefore, future studies should aim on targeting very specific cell populations (defined genetically and/or by connectivity), and on paying significant attention to when and how these cells should be activated in optogenetic trials, in order to be able to assign the meaningful behavioural role to these cell groups.

Taken together, here our work provides an important evidence on how MeA-GABA neurons functionally connect to the VMHvl and the PMv neurons. Here we challenged a previous assumption that MeApd-GABA neurons regulate aggression via disinhibition of the VMHvl and experimentally showed that a robust direct inhibitory input on the MeApd to the excitatory neurons and weaker disinhibition occur in this circuit. We have also demonstrated by in-vivo imaging that the activity of some MeApd-GABA neurons is compatible with their role in inhibition of aggression, however the same data provided a note of caution for interpretation of direct optogenetic stimulation experiments due to complex and mostly non-selective activity patterns of these neurons associated with different behaviour types. Overall, our study provides a mechanistic evidence of how MeApd-GABA neurons could supress aggression and show that this can occur via inhibition of glutamatergic neurons in the VMHvl and/or PMv.

Chapter 4: General Discussion

In my PhD thesis, I sought to understand how the MeApd-GABA neurons control aggressive behaviour in mice used as an experimental model, by identifying the behavioural significance of this neuronal population and of their output synaptic connections. In the first part of the thesis, behavioural testing revealed that optogenetic stimulation of the MeApd-GABA neurons leads to suppression of the territorial inter-male aggression (Baleisyte et al., 2021). This finding has challenged the interpretation of previous experimental results described by Hong et al. (2014) showing, in contrary, that optogenetic stimulation of the same population of neurons activates aggression. A methodological difference lied in the use of different channelrhodopsin variants between theirs and our studies. In a search for the mechanistic explanation for this discrepancy, I broadened the knowledge on the inhibitory neurons in the MeApd by describing their intrinsic firing properties, their local connectivity, and the particularities of using different channelrhodopsin variants in these cells. These new data, however, were not sufficient for drawing an exhaustive picture of a circuit mechanism by which the MeApd-GABA neurons control aggression. To deepen our understanding, in the second part of my thesis I wished to focus on the function of synaptic outputs of the MeApd-GABA neurons in their downstream hypothalamic target nuclei well accepted to be necessary for the aggression control. I have found that MeApd-GABA neurons strongly connect with the VMHvl and the PMv by making inhibitory synapses on the principal cells and interneurons in those nuclei. *In vivo* stimulation of this inhibitory MeApd-GABA→VMHvl pathway, targeted with the help of combinatorial expression approach, had a tendency to suppress aggression in some animals, while it has never led to stimulation of aggression. Finally, we demonstrated behavioural multimodality of the VMHvl projecting MeApd-GABA neurons as we have found that they activated during various social behaviours, including aggression. In the following sections, I will go deeper into discussing our findings about the MeA and will relate our results with the published knowledge in the field.

Heterogeneity of the MeApd neurons and their role in aggression control

Early studies described the MeApd as a striatal structure based on its very dense expression of GABAergic neurons (Swanson and Petrovich, 1998). While the comparison to a striatal-like structure has been challenged by recent studies, together with the central amygdala, the MeApd remains the most GABAergic nucleus in the amygdalar complex (Bupesh et al., 2011; Keshavarzi et al., 2014; Swanson and Petrovich, 1998). Multiple studies revealed a high genetic diversity of neurons in the MeApd (see Chapter 1, Fig. 1.4) (Keshavarzi et al., 2014; Miller et al., 2019; Padilla et al., 2016; Unger et al., 2015; Wu et al., 2017). It is important to note that many neuronal subtypes in the MeA that express a certain genetic marker can be either GABAergic or glutamatergic (Fig. 1.4), and there are also indications of the MeA neurons with the mixed transmitter types (Wu et al., 2017), to be yet functionally confirmed. This obviously complicates the experimental design and interpretation of the results when studying the involvement of genetically identified neurons in control of social behaviours. Therefore, we have decided to start studying the role of the MeApd-GABA neurons first by manipulating the whole population of inhibitory neurons using the $VGAT^{Cre}$ mouse line.

<u>One point mutation away: so close and yet so far?</u>

Optogenetic *in vivo* stimulation of the MeApd-GABA neurons using $ChETA^{E123T,H134R}$ variant of ChR2 (Gunaydin et al., 2010) led to a suppression of aggression in the resident mice during the resident-intruder test (Fig. 2.1, Chapter 2). To our surprise, these results were directly opposite to the previously published results by Hong et al. (2014), where the authors have found that stimulation of the MeApd-GABA neurons using a slower $ChR2^{H134R}$ variant promoted aggression. Therefore, we have decided to compare the two studies in detail.

First, we compared the mice that were used in our study (Baleisyte et al., 2021) and in the study by Hong et al. (2014). Resident $VGAT^{cre}$ mutant mice in both studies were identical, initially described in Vong et al. (2011). However, a slight difference might lie in the backcrossing and housing as we have maintained our mice on C57Bl6/J background at 12-h light-dark cycle while Hong et al. (2014) on C57BL/6N background and on a reversed 12-h light-dark cycle. Intruder BALB/c mice used in both studies were purchased from Charles Rivers Laboratory. We have also verified if housing mice socially after the surgery would change the experimental outcome using the ChETA variant for optogenetic stimulation, which it did not (data not

shown). Next, we confirmed that our virus injections and optic fiber implantations indeed targeted mostly the MeApd (Fig. 2.2, Chapter 2). While Hong et al. (2014) in their study have not provided information about the titer of the virus, the injected volume in the MeApd was the same in their and our studies. The visual comparison of the post-hoc images from both studies shows similar injection locus. However, to better asses the compatibility between two studies one would have to count infected cells and transduced area of the MeApd in both studies, similarly as we have done in Figure 2.2.

In both studies light stimulation was delivered in pulses at 20 Hz frequency. In our study the light was delivered automatically in trains of 30 sec long with 30-60 sec dark periods, whereas in the experiments by Hong et al. (2014) the light was turned on manually for 15 sec trains "based on resident mouse behavior" (Hong et al., 2014). Another important difference is the length of the light pulse which was 5 ms in our and 20 ms in their study. Longer light pulses may favour higher plateau potential, and thus, stronger depolarization block. Interestingly, Hong et al. (2014) reported that stimulation of the MeApd-GABA neurons at lower light intensity using ChR2 triggered mounting behaviour. In our hands, using ChETA, lowering the stimulation intensity expectedly stopped inhibiting aggression, but has never triggered mounting (Suppl., Fig. 2.1, Chapter 2). The only unrelated condition under which we saw mounting the intruder by the resident mouse, was implantation of the optic fibers above the VMHvl (see Chapter 3). It has been shown that decreasing light stimulation intensity could lead to failures in triggering APs in the cells expressing ChR2 (Berndt et al., 2011); concurrently, lower light intensity is expected to recruit less neurons, which may shift the balance between the local and long-range inhibition by the MeA-GABA neurons. However, neither of these scenarios have been experimentally verified *in vivo*, and other more recent studies in the MeA (Miller et al., 2019; Padilla et al., 2016; Unger et al., 2015) have not reported an effect of mounting. Thus, currently it is not clear how mounting behaviour can be evoked by the optogenetic stimulation of the MeA neurons.

Finally, we have identified unambiguously that the channelrhodopsin variant was the decisive factor for the opposite behavioural results between our study and the study by Hong et al. (2014). Larger current amplitudes with a slower decay time induced by the ChR2, as compared with ChETA (Fig. 2.5; in agreement with the previous works by Berndt et al., 2011; Gunaydin et al., 2010; Mattis et al., 2012), resulted in a prolonged plateau depolarization of neuronal membrane upon 20 Hz train of light pulses when using ChR2. In case of longer trains (>3-5 sec), this leads to a decrease in the light-evoked AP amplitudes and failures to follow the

stimulation (Fig. 2.5, Chapter 2), a side effect significantly more pronounced with ChR2 than with ChETA. Note that under our *in vivo* and *in vitro* conditions (light pulses of 5 ms duration) we are likely underestimating the effect of depolarization block leading to AP train failure due to the Na^+-channel inactivation, that possibly took place in the study by Hong et al. (2014) who used 20 ms long light pulses at the same frequency and intensity. The consequences of the prolonged plateau depolarization and reduced AP amplitudes on the neuronal activity and on the local and long-range synaptic outputs remain unclear. However, it is possible that less physiological conditions of AP stimulation using ChR2 (as compared to ChETA) could lead to a net misbalance between local and long-range inhibitory outputs, and under certain condition may cause unpredictable regimes of the MeApd network activity which does not correspond to desired regular 20 Hz firing upon the delivered train of light pulses. This makes direct interpretation of optogenetic stimulation experiments using ChR2 unjustified, given the clear side effects of this tool in a particular network such as MeApd-GABA neurons. One way out could be the optogenetic inhibition experiments that were performed by Hong et al. (2014): they activated halorhodopsin with for 3 sec long yellow laser pulses initiated during the aggression bouts, which led to immediate interruption of aggression (Hong et al., 2014). We also attempted optogenetic silencing experiments using eNpHR3.0 halorhodopsin with the regular light intervals (to avoid the possible experimental bias when an experimenter is required to press a button to turn on the laser whenever aggression starts, given the naturally short bouts of aggressive behavior). However, we did not observe any significant effect of optogenetic silencing of MeApd-GABA neurons on aggression (data not shown).

What are the possible network mechanisms underlying different effects of ChR2 and ChETA?

One possible mechanism leading to diverging results of optogenetic experiments could be an interaction between the channelrhodopsin variant and the intrinsic excitability (firing properties) of different subpopulations of the MeApd-GABA neurons. For example, one subtype can rapidly inactivate and stop following the optogenetic stimulation train, while the other subtypes may be resistant or hyperactivate, firing extra APs. From the previous studies we know that the MeA contains a very diverse population of inhibitory neurons (Bian, 2013; Keshavarzi et al., 2014), however, these studies rather focused on MeApv and did not specifically test electrophysiological properties of the MeApd-GABA neurons. We found a

high diversity in the intrinsic firing properties of MeApd-GABA neurons and tentatively subdivided them into 6 AP-firing types (Suppl. Fig. 2.5, Chapter 2). While there was a trend for the neurons from the groups 1 and 2 to fail AP-following, however, due to low number of recordings we found that there was no significant difference in AP-following between the ChR2 and ChETA across the 6 different AP-firing types (Suppl. Fig. 2.5, Chapter 2). These results suggest that the cell type heterogeneity may not be an immediate cause for the opposing behavioral results.

MeApd-GABA neurons are interconnected, forming a local inhibitory network. Differential recruitment of the local inhibition by ChR2 or ChETA may be another possible mechanism for different behavioural outcomes, if the net inhibitory strength imposed by one or the other variant leads to a stronger or weaker net inhibition of the MeApd network. We found that *in vitro* optogenetics stimulation of the MeApd-GABA neurons using ChETA or ChR2 evoked IPSCs of a similar amplitude (Fig. 2.5, Chapter 2), however, the decay time of the IPSCs in the ChR2 group, and thus the synaptic charge transfer, was significantly higher than in ChETA group (Fig. 2.5, Chapter 2). These provides a compelling evidence that ChR2 leads to a stronger local inhibition within the MeApd, which can result in less firing, and therefore, in less transmission of Aps to long-range output targets such as the VMHvl and PMv (see Chapter 3 and discussion below), causing disinhibition of aggressive behaviour. Using ChETA, the effect of local inhibition during the optogenetic stimulation train is weaker, allowing for efficient long-range inhibition of hypothalamic targets that finally leads to inhibition of aggression.

Taken together, the results that we have gathered when manipulating the MeApd locally *in vivo* revealed that the choice of the channelrhodopsin variant might be crucial for the behavioral outcome. In brain areas with such a high heterogeneity and inter-connectivity as the MeApd, the kinetic properties of the used opsins might strongly influence the behavioral outcome. The final details of the mechanism underlying these differences, still have to be investigated in future studies.

<u>The role of MeAp neurons in aggression: independent evidences</u>

Other recent studies have also found intriguing effects on aggression using different transgenic mouse lines to target and manipulate various subpopulations of MeAp neurons, among which

a significant fraction were GABA neurons (see Fig. 1.4, Chapter 1). One study found that male mice with either bilateral ablation or chemogenetic inhibition of aromatase-expressing neurons (Aro+; mostly GABAergic) took significantly longer time to initiate attack against the intruder, while the attacks still took place (Unger et al., 2015). On the other hand, chemogenetic activation of Aro+ MeApd neurons did not modulate aggression in any way, altogether suggesting that Aro+ neurons might be responsible for processing social information relevant for attack, but not for directly triggering or enabling attacks. It would be interesting to know the outcome of optogenetic stimulation of these Aro+ neurons and their connectivity (local, projection or both) which was not reported.

Another study demonstrated that chemogenetic activation of the MeAp-GABA Npy1R+ neurons increased aggression (Padilla et al., 2016). Npy1R+ neurons send long-range projections to the pBNST where they cause IPSCs (Padilla et al., 2016). Nevertheless, little is known about the distribution of these neurons within the MeA. The post-hoc images provided by Padilla et al. (2016) indicated that these neurons are located more in the ventral part, MeApv, and the cannulas were implanted at the most posterior border of the MeAp. These observations suggest that Npy1R+ neurons might comprise a population only weakly overlapping with the MeApd-GABA neurons studied in this thesis. Furthermore, it is important to note that for the RI testing Padilla et al. (2016) used sexually experienced males (different from virgin males used here), and the effect of excitatory DREADD on cell firing in vivo is hard to control, and moreover, impossible to compare with the AP firing in response to optogenetic stimulation.

A more recent study by Miller et al. (2019) provided compelling evidence that dopamine receptor Type 1 (D1R) neurons of the MeAp also regulate aggression. A majority of the D1R+ neurons are located in the MeApv, and 40% of these are GABA neurons (Miller et al., 2019). A majority of the GABA D1R+ neurons project to the BNSTp, and optogenetic stimulation of this MeApv-D1R→BNST pathway leads to an increased aggression during RI assay (Miller et al., 2019). These results thus consolidate the earlier study by Padilla et al. (2016), that has used $NpyR1^{Cre}$ mice. Interestingly, 40% of D1R+ neurons in the MeApv overlap with Npy1R+ neurons, thus it is very likely that D1R+ and Npy1R+ neurons that stimulate aggression via inhibition of the BNSTp, are the same population of neurons (Miller et al., 2019; Padilla et al., 2016).

Thus, recent studies in the MeAp have demonstrated that the GABA cells in the ventral part of the nucleus, MeApv, stimulate aggression by inhibiting the BNSTp (Miller et al., 2019; Padilla

et al., 2016). Nevertheless, none of the studies investigated through which downstream nuclei the GABA neurons of the dorsal part, MeApd, control aggression.

MeApd-GABA neurons regulates aggression via inhibition of the VMHvl and the PMv

We have shown that MeApd-GABA neurons strongly project to BNST, VMHvl, PMv (Fig. 3.1, Chapter 3) and decided to investigate the putative inhibitory pathways to the hypothalamic nuclei in more detail, since the VMHvl and the PMv were strongly implicated in generation of aggressive behaviour: VMHvl (Falkner et al., 2020; Kim et al., 2019; Lee et al., 2014; Remedios et al., 2017; Yang et al., 2017), PMv (Chen et al., 2020; Stagkourakis et al., 2018). Whole-cell recordings in the VMHvl and PMv with optogenetic circuit mapping showed that principal neurons in these nuclei received inhibitory synapses from the MeApd-GABA neurons at a high connectivity rate (Fig. 3.3, 3.5, Chapter 3). This led to the hypothesis that this pathway may be responsible for inhibition of aggression observed with ChETA-mediated optogenetic stimulation of the MeApd (Chapter 2). With some disappointment, however, we found that *in vivo* stimulation of the MeApd-GABA axons in the PMv did not have a significant effect (Fig. 3.7), and that implantation of optic fibers above the VMHvl led to mounting behaviour (Fig. 3.6). The latter effect has never been reported in the literature despite the fact that similar surgeries have often been performed (Falkner et al., 2020; Lee et al., 2014). In the experiment where VMHvl-projecting MeApd-GABA neurons were optogenetically stimulated at their soma level, many mice were not aggressive, but in those mice that were aggressive, stimulation showed a trend to reduce aggression (Fig. 3.8, Chapter 3). Overall, manipulation of the MeApd-GABA to VMHvl pathway using two different approaches had never induced aggression, while in a small number of aggressive mice it rather suppressed aggression. Such experiments aiming on activation of the MeApd-GABA→VMHvl and →PMv pathways, have not yet been reported to our knowledge. At the same time, the MeApd-GABA→VMHvl pathway was postulated to stimulate aggression via disinhibition of VMHlv (Choi et al., 2005; Hong et al., 2014) without direct experimental proof. One possibility for disinhibitory pathway could be a loop via BNST (Fig. 4.1), but a separate dedicated study would be needed to delineate that pathway because of the complex BNST content and connectivity. As for the possible local VMHvl disinhibitory loop (Choi et al., 2005), we indeed for the first time found an evidence for inhibitory input from the MeApd-GABA neurons onto the local VMHvl-GABA interneurons (Fig. 3.4, Chapter 3). It will however require more work to prove that this disinhibitory pathway is strong enough

to be functional in order to trigger aggression when the MeApd-GABA neurons are active. None of our behavioural experiments (Chapters 2, 3), except those using ChR2 (Chapter 2), support this idea.

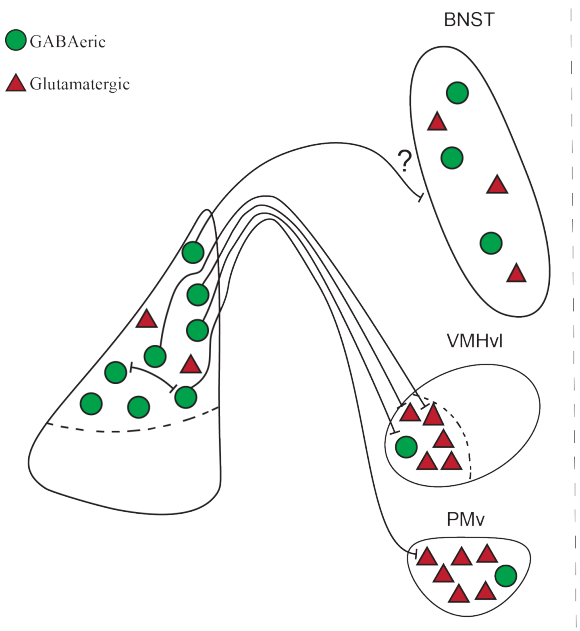

Figure 4.1 | Schematic summary of the MeApd connections to the downstream attack areas studied in this thesis. The MeApd-GABA neurons inhibit glutamatergic and GABAergic neurons in the VMHvl and glutamatergic neurons in the PMv. Note the connection to from MeApd-GABA neurons to the BNST remains to be further investigated.

In the last portion of the thesis (Chapter 3), we performed a correlative study using *in vivo* Ca2+-imaging of the VMHvl-projecting MeApd-GABA neurons during the RI test by matching the cell activity with the temporal occurrence of different social behaviors. MeApd-GABA neurons demonstrated pronounced multimodality (Fig. 3.9, 3.11, Chapter 3), in line with multimodal sensory-evoked responses in the MeA (Bergan et al., 2014; Li et al., 2017). It is quite interesting, because many cells fire strongly during the non-aggressive social investigation shortly after intruder is introduced (Fig. 3.9, Chapter 3), which is inconsistent with the idea that strong activation of these cells should unconditionally trigger aggression (Hong et al., 2014). Moreover, some MeApd-GABA neurons projecting to the VMHvl showed increased activity during aggression bouts, with a subset of these neurons having activation peak selectively around the offset of aggression bouts (Fig. 3.10, Chapter 3); such a peak around the onset of aggression bouts was not or less pronounced. This observation supports our hypothesis that the sub-population of MeApd-GABA neurons projecting the VMHvl may cause the inhibition of aggression.

Overall, we believe that our results support the hypothesis that inhibition of the principal neurons in the VMHvl and the PMv by the MeApd-GABA neurons act towards suppression of aggression. However, our *in vivo* stimulation experiments are not significant and still lack higher mouse numbers with sufficient baseline aggression. We also do not know how this inhibitory input changes the firing of the VMHvl and the PMv glutamatergic neurons *in vivo*; thus, our *in vitro* optogenetic mapping experiments from the Chapter 3 (Fig. 3.3-3.5) should be repeated *in vivo*. Finally, alternative pathways for attack inhibition via BNST may also exist but this still needs to be proven experimentally.

The MeA plays a highly complex role in regulation of the inter-male aggression. Recent studies have just started addressing in more specific details how the MeA modulates attacks by the long-range connections (Miller et al., 2019; Nordman et al., 2020; Padilla et al., 2016; Unger et al., 2015). Our current view is that the MeApd directly inhibits the VMHvl and thus negatively regulates aggression (Chapter 2 and Chapter 3, Baleisyte et al., 2021). A different effect of channelrhodopsin variants on the local inhibitory strength with thin the MeApd may lie at the core of the behavioral discrepancy observed using different optogenetic tools. In the future studies, one should continue investigating the mechanisms of how MeApd-GABA neurons inhibit aggression in the target nuclei. Also, the local connectivity within the MeA is still strongly understudied and its role in aggression control is currently unclear. The local inhibitory network of the MeA-GABA neurons, especially in the posterior part, has to be investigated in the future studies.

Acknowledgements

During the years of my PhD studies, I was fortunate to learn from many outstanding people. I have received support and encouragement which benefited me in many ways as a young scientist.

First and foremost, I would like to thank my thesis supervisor and co-supervisor, Prof. Ralf Schneggenburger and Dr. Olexiy Kochubey for their guidance. I will always be thankful to my supervisor Prof. Ralf Schneggenburger for his continuous counselling, dedication to science throughout the years and for supporting the MeA project. I am also extremely grateful to my co-supervisor Olexiy Kochubey for his enormous amount of help, knowledge and patience that he shared with me.

I would like to thank my mentor prof. Carmen Sandi, who was always available for me. I felt very lucky to have a mentor that tried to understand my scientific story and shared her experience and support with me.

I would also like to thank my Jury committee to have the time to evaluate my thesis: Prof. Carl Petersen, Prof. Johhannes Graff, Prof. Alan Carleton and Prof. Sam Golden.

Most of my time here in Lausanne I spent with my colleagues at the Laboratory of Synaptic Mechanisms. Thank you for sharing the journey with me during the last years: Shriya, Michael, Bei-Xuan, Denys, Aya, Enida, Elin, Brice, Wei and Chris. I have learned a lot from you! Special thanks to Heather for introducing lobsters to me.

When I came to Lausanne 7 years ago, I could have never guessed how my life will turn out to be here. This journey was very educational, unpredictable and has definitely shaped me a lot. Foremost, I would like to thank you all the incredible people that I have met here and with whom I have shared dinners and cultural nights, who came to support me at my concerts, who have inspired and cheered me up uncountable times. Thank you Radu, Silvia, Eric, Vaida, Allie, Gulia, Soumya, Kamile, Firat, Josefine, Gaelle and Lucie. And of course, the people on the third floor corridor that I passed by and always shared a chat: Vahid and Anastasia!

I would like to thank my family for inspiring me to strive for meaning in life. For not putting boundaries and expectations but instead encouraging to be free and independent. By showing that the biggest values in life are knowledge, people, experience and creativity.

CURRICULUM VITAE

Aiste Baleisyte

born 22.05.1991 in Kaunas, Lithuania

Address | Chemin du Levant 139
1005 Lausanne, Switzerland
Telephone | +41788220481
E-mail | aistebaleisyte@gmail.com

Languages | Lithuanian: native proficiency
English: full professional proficiency
French: intermediate
Russian: basic knowledge

Education |

August 2015 – present - **Ecole Polytechnique Fédérale de Lausanne (EPFL)**, Switzerland
PhD student, Laboratory of Synaptic Mechanisms,
Advisors: Prof. Ralf Schneggenburger, Dr. Olexiy Kochubey

09/2013 - 07/2015 - **University of Strasbourg**, France
Joint Master in Neuroscience (Between University of Basel, University of Strasbourg and University of Freiburg)

09/2010 - 06/2013 - **Jacobs University Bremen**, Germany
BSc degree in Biochemistry and Cell Biology

09/2007 – 06/2010 - **Kaunas University of Technology Gymnasium**, Lithuania
Completed secondary education

Practical Experience |

June 2011 - present **Laboratory of Synaptic Mechanisms (LSYM), EPFL, Switzerland**
PhD thesis research: *"Electrophysiological properties of oxytocin - activated neurons in the medial amygdala in vitro."*

09/2014 - 08/2015 **Laboratory of Synaptic Mechanisms (LSYM), EPFL, Switzerland**
Master's thesis research: *"Electrophysiological properties of oxytocin - activated neurons in the medial amygdala in vitro."*

02/2014 - 03/2014 **Development and Stem Cell Laboratory, Team of Dr. Pascal Dolle, Institut de génétique et de biologie moléculaire et cellulaire (IGBMC) - Strasbourg, France**
Analyses of retinoic acid control of gene expression in the brain.

02/2013 - 06/2013 **Molecular Genetics Laboratory, Jacobs University – Bremen, Germany**
Bachelor thesis research: "Investigation of the patterns of fis gene communications in Escherichia coli during the bacterial growth cycle". Final thesis grade: 1.0 out of 1.0.

03/2011 – 12/2012 **Biophysics Laboratory, Jacobs University – Bremen, Germany**
Research assistant in Biophysics Research Group.

06/2012 – 08/2012 **Nanion Technologies GmbH – Munich, Germany**

06/2011 – 08/2011 **Cavendish Laboratory, Cambridge University – Cambridge, United Kingdom**
Summer Internship in Dr. Ulrich Keyser's research group. Project: 'Norfloxacin Transport Across Membranes in DPhPC and Escherichia coli Lipid Formed Liposomes'.

Conference abstracts and talks

- Poster at the 3rd Conference on the Neurobiology of Mental Health, February 26-28, 2020, Geneva (Switzerland): “Role of specific medial amygdala inhibitory neurons in aggression control” Baleisyte A., Schneggenburger R, Kochubey O.

- Short oral presentation at the ‘Annual Meeting of the NeuroLeman Network and Doctoral Schools, Diablerets (Switzerland), May 3-4, 2019: “Role of specific medial amygdala inhibitory neurons in aggression control”. Best presentation award.

- Poster at the GRC: Modulation of Neural Circuits and Behavior, May 26-31, 2019: “Role of specific medial amygdala inhibitory neurons in aggression control” Baleisyte A., Schneggenburger R, Kochubey O.

- Poster at the SFN, November 3-7, 2018, San Diego (USA): “Role of specific medial amygdala inhibitory neurons in aggression control” Baleisyte A., Schneggenburger R, Kochubey O.

- Poster at the FENS, July 7-11, 2018, Berlin (Germany): “Role of specific medial amygdala inhibitory neurons in aggression control” Baleisyte A., Schneggenburger R, Kochubey O.

- Short oral presentation at the ‘Giessbach meeting: Cellular and Molecular Neurobiology of Mental Disease (Switzerland), May 24-26, 2018: “Role of specific medial amygdala inhibitory neurons in aggression control”.

- Poster at the 2nd Conference on the Neurobiology of Mental Health, January 24-26, 2018, Geneva (Switzerland): “Role of specific medial amygdala inhibitory neurons in aggression control” Baleisyte A., Schneggenburger R, Kochubey O.

Teaching experience

Teaching Assistant, Undergraduate level course: *" Physiologie par systemes I"*, EPFL (2016-2019)

Teaching Assistant, Undergraduate level course: *"Scientific Literature Analysis in Neuroscience"*, EPFL (2018-2019)

Teaching Assistant, Undergraduate level course: *" Neuroscience III: Behavioral and Cognitive Neuroscience"*, EPFL (2017-2018)

Publications

Baleisyte A, Schneggenburger R, Kochubey O (preprint). Optogenetic stimulation of medial amygdala GABA neurons with kinetically different channelrhodopsin variants yield opposite behavioral outcomes. bioRxiv 2021.06.30.450543.

Perino A, Velázquez-Villegas LA, Bresciani N, Sun Y, Huang Q, Fénelon VS, Castellanos-Jankiewicz A, Zizzari P, Bruschetta G, Jin S, **Baleisyte A**, Gioiello A, Pellicciari R, Ivanisevic J, Schneider BL, Diano S, Cota D and Schoonjans K (2021). Central anorexigenic actions of bile acids are mediated by TGR5. Nat Metab; 3:595–603.

References

Adams, D.B. (2006). Brain mechanisms of aggressive behavior: an updated review. Neurosci Biobehav Rev *30*, 304–318.

Aleyasin, H., Flanigan, M.E., and Russo, S.J. (2018). Neurocircuitry of aggression and aggression seeking behavior: nose poking into brain circuitry controlling aggression. Curr Opin Neurobiol *49*, 184–191.

Alheid, G.F., and Heimer, L. (1988). New perspectives in basal forebrain organization of special relevance for neuropsychiatric disorders: The striatopallidal, amygdaloid, and corticopetal components of substantia innominata. Neuroscience *27*, 1–39.

Altenberg, K.L.H. (1950). Konrad Lorenz 1950 The comparative method in studying innate behavior patterns Symposia of the Society for Experimental Biology 4 (Physiological Mechanisms in Animal Behavior): 221-254. 49.

Anderson, C.A. (2001). HUMAN AGGRESSION. HUMAN AGGRESSION 28.

Aravanis, A.M., Wang, L.P., Zhang, F., Meltzer, L.A., Mogri, M.Z., Schneider, M.B., and Deisseroth, K. (2007). An optical neural interface: in vivo control of rodent motor cortex with integrated fiberoptic and optogenetic technology. J Neural Eng *4*, S143-56.

Averill, J.R. (1983). Studies on Anger and Aggression. American Psychologist 16.

Baleisyte, A., Schneggenburger, R., and Kochubey, O. (2021). Optogenetic stimulation of medial amygdala GABA neurons with kinetically different channelrhodopsin variants yield opposite behavioral outcomes. bioRxiv.

Ballester, J., Goldstein, T., Goldstein, B., Obreja, M., Axelson, D., Monk, K., Hickey, M., Iyengar, S., Farchione, T., Kupfer, D.J., et al. (2012). Is bipolar disorder specifically associated with aggression? Bipolar Disord *14*, 283–290.

Bayless, D.W., Yang, T., Mason, M.M., Susanto, A.A.T., Lobdell, A., and Shah, N.M. (2019). Limbic Neurons Shape Sex Recognition and Social Behavior in Sexually Naive Males. Cell *176*, 1190-1205.e20.

Bergan, J.F., Ben-Shaul, Y., and Dulac, C. (2014). Sex-specific processing of social cues in the medial amygdala. Elife *3*, e02743.

Berndt, A., Schoenenberger, P., Mattis, J., Tye, K.M., Deisseroth, K., Hegemann, P., and Oertner, T.G. (2011). High-efficiency channelrhodopsins for fast neuronal stimulation at low light levels. Proc Natl Acad Sci U S A *108*, 7595–7600.

Bian, X. (2013). Physiological and morphological characterization of GABAergic neurons in the medial amygdala. Brain Res *1509*, 8–19.

Bian, X., Yanagawa, Y., Chen, W.R., and Luo, M. (2008). Cortical-like functional organization of the pheromone-processing circuits in the medial amygdala. J Neurophysiol *99*, 77–86.

Blanchard, D.C., and Takahashi, S.N. (1988). No change in intermale aggression after amygdala lesions which reduce freezing. Physiology & Behavior *42*, 613–616.

Boyden, E.S., Zhang, F., Bamberg, E., Nagel, G., and Deisseroth, K. (2005). Millisecond-timescale, genetically targeted optical control of neural activity. Nat Neurosci *8*, 1263–1268.

Brady, K.T., Myrick, H., and McElroy, S. (1998). The relationship between substance use disorders, impulse control disorders, and pathological aggression. Am J Addict *7*, 221–230.

Brigandt, I. (2005). "The Instinct Concept of the Early Konrad Lorenz." J Hist Biol *38*, 571–608.

Bupesh, M., Legaz, I., Abellán, A., and Medina, L. (2011). Multiple telencephalic and extratelencephalic embryonic domains contribute neurons to the medial extended amygdala. J. Comp. Neurol. *519*, 1505–1525.

Busch, D.E., and Barfield, R.J. (1974). A failure of amygdaloid lesions to alter agonistic behavior in the laboratory rat. Physiology & Behavior *12*, 887–892.

Bushman, B.J. (1997). Effects of alcohol on human aggression. Validity of proposed explanations. Recent Dev Alcohol *13*, 227–243.

Cadiz-Moretti, B., Otero-Garcia, M., Martinez-Garcia, F., and Lanuza, E. (2016). Afferent projections to the different medial amygdala subdivisions: a retrograde tracing study in the mouse. Brain Struct Funct *221*, 1033–1065.

von Campenhausen, H., and Mori, K. (2000). Convergence of segregated pheromonal pathways from the accessory olfactory bulb to the cortex in the mouse. Eur J Neurosci *12*, 33–46.

Canteras, N.S., Simerly, R.B., and Swanson, L.W. (1992). Projections of the ventral premammillary nucleus. J. Comp. Neurol. *324*, 195–212.

Canteras, N.S., Simerly, R.B., and Swanson, L.W. (1995). Organization of projections from the medial nucleus of the amygdala: a PHAL study in the rat. J. Comp. Neurol. *360*, 213–245.

Cardona, A., Saalfeld, S., Preibisch, S., Schmid, B., Cheng, A., Pulokas, J., Tomancak, P., and Hartenstein, V. (2010). An integrated micro- and macroarchitectural analysis of the Drosophila brain by computer-assisted serial section electron microscopy. PLoS Biol *8*.

Carney, R.S., Mangin, J.M., Hayes, L., Mansfield, K., Sousa, V.H., Fishell, G., Machold, R.P., Ahn, S., Gallo, V., and Corbin, J.G. (2010). Sonic hedgehog expressing and responding cells generate neuronal diversity in the medial amygdala. Neural Dev *5*, 14.

Catlett, R.H. (1961). An evaluation of methods for measuring fighting behaviour with special reference to Mus musculus. Animal Behaviour *9*, 8–10.

Cavalcante, J.C., Bittencourt, J.C., and Elias, C.F. (2014). Distribution of the neuronal inputs to the ventral premammillary nucleus of male and female rats. Brain Research *1582*, 77–90.

Chamero, P., Marton, T.F., Logan, D.W., Flanagan, K., Cruz, J.R., Saghatelian, A., Cravatt, B.F., and Stowers, L. (2007). Identification of protein pheromones that promote aggressive behaviour. Nature *450*, 899–902.

Chen, P., and Hong, W. (2018). Neural Circuit Mechanisms of Social Behavior. Neuron *98*, 16–30.

Chen, A.-X., Yan, J.-J., Zhang, W., Wang, L., Yu, Z.-X., Ding, X.-J., Wang, D.-Y., Zhang, M., Zhang, Y.-L., Song, N., et al. (2020). Specific Hypothalamic Neurons Required for Sensing Conspecific Male Cues Relevant to Inter-male Aggression. Neuron *108*, 763-774.e6.

Chen, P.B., Hu, R.K., Wu, Y.E., Pan, L., Huang, S., Micevych, P.E., and Hong, W. (2019). Sexually Dimorphic Control of Parenting Behavior by the Medial Amygdala. Cell *176*, 1206-1221.e18.

Choi, G.B., Dong, H.W., Murphy, A.J., Valenzuela, D.M., Yancopoulos, G.D., Swanson, L.W., and Anderson, D.J. (2005). Lhx6 delineates a pathway mediating innate reproductive behaviors from the amygdala to the hypothalamus. Neuron *46*, 647–660.

Davis, M., Walker, D.L., Miles, L., and Grillon, C. (2010). Phasic vs Sustained Fear in Rats and Humans: Role of the Extended Amygdala in Fear vs Anxiety. Neuropsychopharmacol *35*, 105–135.

Deisseroth, K. (2015). Optogenetics: 10 years of microbial opsins in neuroscience. Nat. Neurosci. *18*, 1213–1225.

Dong, H.W., Petrovich, G.D., and Swanson, L.W. (2001). Topography of projections from amygdala to bed nuclei of the stria terminalis. Brain Res Brain Res Rev *38*, 192–246.

Dulac, C., and Torello, A.T. (2003). Molecular detection of pheromone signals in mammals: from genes to behaviour. Nat Rev Neurosci *4*, 551–562.

Edelstein, A.D., Tsuchida, M.A., Amodaj, N., Pinkard, H., Vale, R.D., and Stuurman, N. (2014). Advanced methods of microscope control using μManager software. J Biol Methods *1*, 10.

Egger, M.D., and Flynn, J.P. (1963). EFFECTS OF ELECTRICAL STIMULATION OF THE AMYGDALA ON HYPOTHALAMICALLY ELICITED ATTACK BEHAVIOR IN CATS. Journal of Neurophysiology *26*, 705–720.

Emery, N.J., Capitanio, J.P., Mason, W.A., Machado, C.J., and Mendoza, S.P. The Effects of Bilateral Lesions of the Amygdala on Dyadic Social Interactions in Rhesus Monkeys (Macaca mulatto). 30.

Falkner, A.L., Dollar, P., Perona, P., Anderson, D.J., and Lin, D. (2014). Decoding Ventromedial Hypothalamic Neural Activity during Male Mouse Aggression. Journal of Neuroscience *34*, 5971–5984.

Falkner, A.L., Grosenick, L., Davidson, T.J., Deisseroth, K., and Lin, D. (2016). Hypothalamic control of male aggression-seeking behavior. Nature Neuroscience *19*, 596–604.

Falkner, A.L., Wei, D., Song, A., Watsek, L.W., Chen, I., Chen, P., Feng, J.E., and Lin, D. (2020). Hierarchical Representations of Aggression in a Hypothalamic-Midbrain Circuit. Neuron *106*, 637-648.e6.

Fenno, L.E., Mattis, J., Ramakrishnan, C., Hyun, M., Lee, S.Y., He, M., Tucciarone, J., Selimbeyoglu, A., Berndt, A., Grosenick, L., et al. (2014). Targeting cells with single vectors using multiple-feature Boolean logic. Nat Methods *11*, 763–772.

Ferenczi, E.A., Tan, X., and Huang, C.L.-H. (2019). Principles of Optogenetic Methods and Their Application to Cardiac Experimental Systems. Front. Physiol. *10*, 1096.

Franklin, K.B.J., and Paxinos, G. (2013). Paxinos and Franklin's The mouse brain in stereotaxic coordinates (Amsterdam: Academic Press, an imprint of Elsevier).

Fu, L.-Y., and van den Pol, A.N. (2008). Agouti-Related Peptide and MC3/4 Receptor Agonists Both Inhibit Excitatory Hypothalamic Ventromedial Nucleus Neurons. Journal of Neuroscience *28*, 5433–5449.

George C. Williams (1992). Natural Selection: Domains, Levels, and Challenges (Oxford University Press).

Gong, S., Doughty, M., Harbaugh, C.R., Cummins, A., Hatten, M.E., Heintz, N., and Gerfen, C.R. (2007). Targeting Cre Recombinase to Specific Neuron Populations with Bacterial Artificial Chromosome Constructs. Journal of Neuroscience *27*, 9817–9823.

Gregg, T.R., and Siegel, A. (2001). Brain structures and neurotansmitters regulating aggression in cats: implications for human aggression. Progress in Neuro-Psychopharmacology and Biological Psychiatry *25*, 91–140.

Gunaydin, L.A., Yizhar, O., Berndt, A., Sohal, V.S., Deisseroth, K., and Hegemann, P. (2010). Ultrafast optogenetic control. Nat Neurosci *13*, 387–392.

Halász, J., Liposits, Z., Meelis, W., Kruk, M.R., and Haller, J. (2002). Hypothalamic attack area-mediated activation of the forebrain in aggression. Neuroreport *13*, 1267–1270.

Hall, C.S. (1937). Emotional behavior in the rat. IV. The relationship between emotionality and stereotyping of behavior. Journal of Comparative Psychology *24*, 369–375.

Haller, J. (2018). The role of central and medial amygdala in normal and abnormal aggression: A review of classical approaches. Neurosci Biobehav Rev *85*, 34–43.

Han, Y., Shaikh, M.B., and Siegel, A. (1996). Medial amygdaloid suppression of predatory attack behavior in the cat: I. Role of a substance P pathway from the medial amygdala to the medial hypothalamus. Brain Research *716*, 59–71.

Hashikawa, K., Hashikawa, Y., Falkner, A., and Lin, D. (2016). The neural circuits of mating and fighting in male mice. Current Opinion in Neurobiology *38*, 27–37.

Hashikawa, K., Hashikawa, Y., Tremblay, R., Zhang, J., Feng, J.E., Sabol, A., Piper, W.T., Lee, H., Rudy, B., and Lin, D. (2017). Esr1+ cells in the ventromedial hypothalamus control female aggression. Nature Neuroscience.

Herman, A.M., Huang, L., Murphey, D.K., Garcia, I., and Arenkiel, B.R. (2014). Cell type-specific and time-dependent light exposure contribute to silencing in neurons expressing Channelrhodopsin-2. Elife *3*, e01481.

Hirata, T., Li, P., Lanuza, G.M., Cocas, L.A., Huntsman, M.M., and Corbin, J.G. (2009). Identification of distinct telencephalic progenitor pools for neuronal diversity in the amygdala. Nat Neurosci *12*, 141–149.

Hodgkin, A.L., and Huxley, A.F. (1952). The dual effect of membrane potential on sodium conductance in the giant axon of Loligo. J Physiol *116*, 497–506.

Hong, W., Kim, D.W., and Anderson, D.J. (2014). Antagonistic control of social versus repetitive self-grooming behaviors by separable amygdala neuronal subsets. Cell *158*, 1348–1361.

Hu, R.K., Zuo, Y., Ly, T., Wang, J., Meera, P., Wu, Y.E., and Hong, W. (2021). An amygdala-to-hypothalamus circuit for social reward. Nat Neurosci.

Karigo, T., Kennedy, A., Yang, B., Liu, M., Tai, D., Wahle, I.A., and Anderson, D.J. (2020). Distinct hypothalamic control of same- and opposite-sex mounting behaviour in mice. Nature.

Karl von Frisch (1967). The dance language and orientation of bees. (Cambridge, Mass., Belknap Press of Harvard University Press).

Kemble, E.D., Blanchard, D.C., Blanchard, R.J., and Takushi, R. (1984). Taming in wild rats following medial amygdaloid lesions. Physiology & Behavior *32*, 131–134.

Keshavarzi, S., Sullivan, R.K., Ianno, D.J., and Sah, P. (2014). Functional properties and projections of neurons in the medial amygdala. J Neurosci *34*, 8699–8715.

Keshavarzi, S., Power, J.M., Albers, E.H., Sullivan, R.K., and Sah, P. (2015). Dendritic Organization of Olfactory Inputs to Medial Amygdala Neurons. J Neurosci *35*, 13020–13028.

Kim, D.-W., Yao, Z., Graybuck, L.T., Kim, T.K., Nguyen, T.N., Smith, K.A., Fong, O., Yi, L., Koulena, N., Pierson, N., et al. (2019). Multimodal Analysis of Cell Types in a Hypothalamic Node Controlling Social Behavior. Cell *179*, 713-728.e17.

Kim, H., Kim, M., Im, S.-K., and Fang, S. (2018). Mouse Cre-LoxP system: general principles to determine tissue-specific roles of target genes. *34*, 13.

Kipp, M. (2001). Anvil - A Generic Annotation Tool for Multimodal Dialogue. In EUROSPEECH-2001, (Aalborg, Denmark: ISCA Archive), pp. 1367–1370.

Klapoetke, N.C., Murata, Y., Kim, S.S., Pulver, S.R., Birdsey-Benson, A., Cho, Y.K., Morimoto, T.K., Chuong, A.S., Carpenter, E.J., Tian, Z., et al. (2014). Independent optical excitation of distinct neural populations. Nature Methods *11*, 338–346.

Knobloch, H.S., Charlet, A., Hoffmann, L.C., Eliava, M., Khrulev, S., Cetin, A.H., Osten, P., Schwarz, M.K., Seeburg, P.H., Stoop, R., et al. (2012). Evoked axonal oxytocin release in the central amygdala attenuates fear response. Neuron *73*, 553–566.

Koolhaas, J.M., Coppens, C.M., de Boer, S.F., Buwalda, B., Meerlo, P., and Timmermans, P.J.A. (2013). The Resident-intruder Paradigm: A Standardized Test for Aggression, Violence and Social Stress. JoVE 4367.

Krause, W.C., and Ingraham, H.A. (2017). Origins and Functions of the Ventrolateral VMH: A Complex Neuronal Cluster Orchestrating Sex Differences in Metabolism and Behavior. In Sex and Gender Factors Affecting Metabolic Homeostasis, Diabetes and Obesity, F. Mauvais-Jarvis, ed. (Cham: Springer International Publishing), pp. 199–213.

Krettek, J.E., and Price, J.L. (1978). A description of the amygdaloid complex in the rat and cat with observations on intra-amygdaloid axonal connections. J. Comp. Neurol. *178*, 255–279.

Kruk, M.R. (1991). Ethology and pharmacology of hypothalamic aggression in the rat. Neuroscience & Biobehavioral Reviews *15*, 527–538.

Lammers, J.H., Kruk, M.R., Meelis, W., and van der Poel, A.M. (1988). Hypothalamic substrates for brain stimulation-induced attack, teeth-chattering and social grooming in the rat. Brain Res *449*, 311–327.

Lebow, M.A., and Chen, A. (2016). Overshadowed by the amygdala: the bed nucleus of the stria terminalis emerges as key to psychiatric disorders. Mol Psychiatry *21*, 450–463.

Lee, H., Kim, D.W., Remedios, R., Anthony, T.E., Chang, A., Madisen, L., Zeng, H., and Anderson, D.J. (2014). Scalable control of mounting and attack by Esr1+ neurons in the ventromedial hypothalamus. Nature *509*, 627–632.

Lehman, M.N., Winans, S.S., and Powers, J.B. (1980). Medial nucleus of the amygdala mediates chemosensory control of male hamster sexual behavior. Science *210*, 557–560.

Li, N., Chen, S., Guo, Z.V., Chen, H., Huo, Y., Inagaki, H.K., Chen, G., Davis, C., Hansel, D., Guo, C., et al. (2019). Spatiotemporal constraints on optogenetic inactivation in cortical circuits. ELife *8*, e48622.

Li, Y., Mathis, A., Grewe, B.F., Osterhout, J.A., Ahanonu, B., Schnitzer, M.J., Murthy, V.N., and Dulac, C. (2017). Neuronal Representation of Social Information in the Medial Amygdala of Awake Behaving Mice. Cell.

Lin, D., Boyle, M.P., Dollar, P., Lee, H., Lein, E.S., Perona, P., and Anderson, D.J. (2011). Functional identification of an aggression locus in the mouse hypothalamus. Nature *470*, 221–226.

Lin, J.Y., Lin, M.Z., Steinbach, P., and Tsien, R.Y. (2009). Characterization of engineered channelrhodopsin variants with improved properties and kinetics. Biophys J *96*, 1803–1814.

Lischinsky, J.E., and Lin, D. (2020). Neural mechanisms of aggression across species. Nat Neurosci *23*, 1317–1328.

Lischinsky, J.E., Sokolowski, K., Li, P., Esumi, S., Kamal, Y., Goodrich, M., Oboti, L., Hammond, T.R., Krishnamoorthy, M., Feldman, D., et al. (2017). Embryonic transcription factor expression in mice predicts medial amygdala neuronal identity and sex-specific responses to innate behavioral cues. ELife *6*.

Lledo, P.-M., Gheusi, G., and Vincent, J.-D. (2005). Information Processing in the Mammalian Olfactory System. Physiological Reviews *85*, 281–317.

Lo, L., Yao, S., Kim, D.-W., Cetin, A., Harris, J., Zeng, H., Anderson, D.J., and Weissbourd, B. (2019). Connectional architecture of a mouse hypothalamic circuit node controlling social behavior. Proc Natl Acad Sci USA *116*, 7503–7512.

Lorenz, K. (2005). On aggression (London: Taylor & Francis e-Library).

Luan, H., and White, B.H. (2007). Combinatorial methods for refined neuronal gene targeting. Current Opinion in Neurobiology *17*, 572–580.

Madisen, L., Zwingman, T.A., Sunkin, S.M., Oh, S.W., Zariwala, H.A., Gu, H., Ng, L.L., Palmiter, R.D., Hawrylycz, M.J., Jones, A.R., et al. (2010). A robust and high-throughput Cre reporting and characterization system for the whole mouse brain. Nat Neurosci *13*, 133–140.

Masugi-Tokita, M., Flor, P.J., and Kawata, M. (2016). Metabotropic Glutamate Receptor Subtype 7 in the Bed Nucleus of the Stria Terminalis is Essential for Intermale Aggression. Neuropsychopharmacol *41*, 726–735.

Mathis, A., Mamidanna, P., Cury, K.M., Abe, T., Murthy, V.N., Mathis, M.W., and Bethge, M. (2018). DeepLabCut: markerless pose estimation of user-defined body parts with deep learning. Nat Neurosci *21*, 1281–1289.

Matos, H.Y., Hernandez-Pineda, D., Charpentier, C.M., Rusk, A., Corbin, J.G., and Jones, K.S. (2020). Sex Differences in Biophysical Signatures across Molecularly Defined Medial Amygdala Neuronal Subpopulations. ENeuro *7*, ENEURO.0035-20.2020.

Mattis, J., Tye, K.M., Ferenczi, E.A., Ramakrishnan, C., O'Shea, D.J., Prakash, R., Gunaydin, L.A., Hyun, M., Fenno, L.E., Gradinaru, V., et al. (2012). Principles for applying optogenetic tools derived from direct comparative analysis of microbial opsins. Nat Methods *9*, 159–172.

McDonald, A.J., and Augustine, J.R. (1993). Localization of GABA-like immunoreactivity in the monkey amygdala. Neuroscience *52*, 281–294.

McHugh, P.R., and Treisman, G. (2007). PTSD: A problematic diagnostic category. Journal of Anxiety Disorders *21*, 211–222.

Miczek, K.A., Brykczynski, T., and Grossman, S.P. (1974). Differential effects of lesions in the amygdala, periamygdaloid cortex, and stria terminalis on aggressive behaviors in rats. J Comp Physiol Psychol *87*, 760–771.

Miczek KA and Meyer-Lindenberg A. (2014). Neuroscience of Aggression (Berlin, Heidelberg: Springer Berlin Heidelberg).

Miller, S.M., Marcotulli, D., Shen, A., and Zweifel, L.S. (2019). Divergent medial amygdala projections regulate approach–avoidance conflict behavior. Nature Neuroscience.

Mohedano-Moriano, A., Pro-Sistiaga, P., Úbeda-Bañón, I., Crespo, C., Insausti, R., and Martinez-Marcos, A. (2007). Segregated pathways to the vomeronasal amygdala: differential projections from the anterior and posterior divisions of the accessory olfactory bulb. European Journal of Neuroscience *25*, 2065–2080.

Motta, S.C., Guimaraes, C.C., Furigo, I.C., Sukikara, M.H., Baldo, M.V.C., Lonstein, J.S., and Canteras, N.S. (2013). Ventral premammillary nucleus as a critical sensory relay to the maternal aggression network. Proceedings of the National Academy of Sciences *110*, 14438–14443.

Nagel, G., Ollig, D., Fuhrmann, M., Kateriya, S., Musti, A.M., Bamberg, E., and Hegemann, P. (2002). Channelrhodopsin-1: a light-gated proton channel in green algae. Science *296*, 2395–2398.

Nagel, G., Szellas, T., Huhn, W., Kateriya, S., Adeishvili, N., Berthold, P., Ollig, D., Hegemann, P., and Bamberg, E. (2003). Channelrhodopsin-2, a directly light-gated cation-selective membrane channel. Proceedings of the National Academy of Sciences *100*, 13940–13945.

Nagel, G., Brauner, M., Liewald, J.F., Adeishvili, N., Bamberg, E., and Gottschalk, A. (2005). Light Activation of Channelrhodopsin-2 in Excitable Cells of Caenorhabditis elegans Triggers Rapid Behavioral Responses. Current Biology *15*, 2279–2284.

Nilsson, S.R., Goodwin, N.L., Choong, J.J., Hwang, S., Wright, H.R., Norville, Z.C., Tong, X., Lin, D., Bentzley, B.S., Eshel, N., et al. (2020). Simple Behavioral Analysis (SimBA) – an open source toolkit for computer classification of complex social behaviors in experimental animals (Animal Behavior and Cognition).

Nordman, J.C., and Li, Z. (2020). The Dorsal Raphe Regulates the Duration of Attack through the Medial Orbitofrontal Cortex and Medial Amygdala. ENeuro *7*, ENEURO.0331-20.2020.

Nordman, J.C., Ma, X., Gu, Q., Potegal, M., Li, H., Kravitz, A.V., and Li, Z. (2020). Potentiation of Divergent Medial Amygdala Pathways Drives Experience-Dependent Aggression Escalation. J. Neurosci. *40*, 4858–4880.

Oakes, M.E., and Coover, G.D. (1997). Effects of small amygdala lesions on fear, but not aggression, in the rat. Physiology & Behavior *61*, 45–55.

Padilla, S.L., Qiu, J., Soden, M.E., Sanz, E., Nestor, C.C., Barker, F.D., Quintana, A., Zweifel, L.S., Ronnekleiv, O.K., Kelly, M.J., et al. (2016). Agouti-related peptide neural circuits mediate adaptive behaviors in the starved state. Nat Neurosci *19*, 734–741.

Panksepp, J. (1971). Aggression elicited by electrical stimulation of the hypothalamus in albino rats. Physiology & Behavior *6*, 321–329.

Parmigiani, S., Francesco Ferrari, P., and Palanza, P. (1998). An evolutionary approach to behavioral pharmacology: using drugs to understand proximate and ultimate mechanisms of different forms of aggression in mice. Neuroscience & Biobehavioral Reviews *23*, 143–153.

Putkonen (1966). Attack elicited by forebrain and hypothalamic stimulation in the chicken. Experientia 22:405.

Ralph Adolphs, and David J. Anderson (2018). The Neuroscience of emotion (Princeton University Press).

Remedios, R., Kennedy, A., Zelikowsky, M., Grewe, B.F., Schnitzer, M.J., and Anderson, D.J. (2017). Social behaviour shapes hypothalamic neural ensemble representations of conspecific sex. Nature *550*, 388–392.

Sachidhanandam, S., Sreenivasan, V., Kyriakatos, A., Kremer, Y., and Petersen, C.C.H. (2013). Membrane potential correlates of sensory perception in mouse barrel cortex. Nat Neurosci *16*, 1671–1677.

Sah, P., Faber, E.S.L., Lopez De Armentia, M., and Power, J. (2003). The Amygdaloid Complex: Anatomy and Physiology. Physiological Reviews *83*, 803–834.

Saper, C.B., and Lowell, B.B. (2014). The hypothalamus. Current Biology *24*, R1111–R1116.

Scalia, F., and Winans, S.S. (1975). The differential projections of the olfactory bulb and accessory olfactory bulb in mammals. J. Comp. Neurol. *161*, 31–55.

Schindelin, J., Arganda-Carreras, I., Frise, E., Kaynig, V., Longair, M., Pietzsch, T., Preibisch, S., Rueden, C., Saalfeld, S., Schmid, B., et al. (2012). Fiji: an open-source platform for biological-image analysis. Nat Methods *9*, 676–682.

Schnütgen, F., Doerflinger, N., Calleja, C., Wendling, O., Chambon, P., and Ghyselinck, N.B. (2003). A directional strategy for monitoring Cre-mediated recombination at the cellular level in the mouse. Nat Biotechnol *21*, 562–565.

Scott, J.P., and Fredericson, E. (1951). The Causes of Fighting in Mice and Rats. Physiological Zoology *24*, 273–309.

Siegel, A., Roeling, T.A., Gregg, T.R., and Kruk, M.R. (1999). Neuropharmacology of brain-stimulation-evoked aggression. Neurosci Biobehav Rev *23*, 359–389.

Siever, L.J. (2008). Neurobiology of Aggression and Violence. Am J Psychiatry 14.

Sineshchekov, O.A., Jung, K.-H., and Spudich, J.L. (2002). Two rhodopsins mediate phototaxis to low- and high-intensity light in Chlamydomonas reinhardtii. Proc Natl Acad Sci U S A *99*, 8689–8694.

Sparta, D.R., Stamatakis, A.M., Phillips, J.L., Hovelso, N., van Zessen, R., and Stuber, G.D. (2012). Construction of implantable optical fibers for long-term optogenetic manipulation of neural circuits. Nat Protoc *7*, 12–23.

Stagkourakis, S., Spigolon, G., Williams, P., Protzmann, J., Fisone, G., and Broberger, C. (2018). A neural network for intermale aggression to establish social hierarchy. Nature Neuroscience *21*, 834–842.

Stoddard-Apter, S.L., and MacDonnell, M.F. (1980). Septal and amygdalar efferents to the hypothalamus which facilitate hypothalamically elicited intraspecific aggression and associated hissing in the cat. An autoradiographic study. Brain Research *193*, 19–32.

Stowers, L., Holy, T.E., Meister, M., Dulac, C., and Koentges, G. (2002). Loss of sex discrimination and male-male aggression in mice deficient for TRP2. Science *295*, 1493–1500.

Swanson, L.W. (2000). Cerebral hemisphere regulation of motivated behavior. Brain Res. *886*, 113–164.

Swanson, L.W., and Petrovich, G.D. (1998). What is the amygdala? Trends Neurosci. *21*, 323–331.

Swanson, J.W., Swartz, M.S., Van Dorn, R.A., Elbogen, E.B., Wagner, H.R., Rosenheck, R.A., Stroup, T.S., McEvoy, J.P., and Lieberman, J.A. (2006). A national study of violent behavior in persons with schizophrenia. Arch. Gen. Psychiatry *63*, 490–499.

Takahashi, A., and Miczek, K.A. (2013). Neurogenetics of Aggressive Behavior: Studies in Rodents. In Neuroscience of Aggression, K.A. Miczek, and A. Meyer-Lindenberg, eds. (Berlin, Heidelberg: Springer Berlin Heidelberg), pp. 3–44.

Tang, W., Kochubey, O., Kintscher, M., and Schneggenburger, R. (2020). A VTA to Basal Amygdala Dopamine Projection Contributes to Signal Salient Somatosensory Events during Fear Learning. J. Neurosci. *40*, 3969–3980.

Tierney, A.J., Godleski, M.S., and Massanari, J.R. (2000). COMPARATIVE ANALYSIS OF AGONISTIC BEHAVIOR IN FOUR CRAYFISH SPECIES. JOURNAL OF CRUSTACEAN BIOLOGY *20*, 13.

Tinbergen, N. (1951). The study of instinct. (New York, NY, US: Clarendon Press/Oxford University Press).

Ting, J.T., Daigle, T.L., Chen, Q., and Feng, G. (2014). Acute brain slice methods for adult and aging animals: application of targeted patch clamp analysis and optogenetics. Methods Mol Biol *1183*, 221–242.

Twining, R.C., Vantrease, J.E., Love, S., Padival, M., and Rosenkranz, J.A. (2017). An intra-amygdala circuit specifically regulates social fear learning. Nat Neurosci *20*, 459–469.

Tye, K.M., and Deisseroth, K. (2012). Optogenetic investigation of neural circuits underlying brain disease in animal models. Nat Rev Neurosci *13*, 251–266.

Unger, E.K., Burke, K.J., Jr., Yang, C.F., Bender, K.J., Fuller, P.M., and Shah, N.M. (2015). Medial amygdalar aromatase neurons regulate aggression in both sexes. Cell Rep *10*, 453–462.

Vochteloo, J.D., and Koolhaas, J.M. (1987). Medial amygdala lesions in male rats reduce aggressive behavior: interference with experience. Physiology & Behavior *41*, 99–102.

Volavka, J., Laska, E., Baker, S., Meisner, M., Czobor, P., and Krivelevich, I. (1997). History of violent behaviour and schizophrenia in different cultures. Analyses based on the WHO study on Determinants of Outcome of Severe Mental Disorders. Br J Psychiatry *171*, 9–14.

Vong, L., Ye, C., Yang, Z., Choi, B., Chua, S., Jr., and Lowell, B.B. (2011). Leptin action on GABAergic neurons prevents obesity and reduces inhibitory tone to POMC neurons. Neuron *71*, 142–154.

Wang, Y., He, Z., Zhao, C., and Li, L. (2013). Medial amygdala lesions modify aggressive behavior and immediate early gene expression in oxytocin and vasopressin neurons during intermale exposure. Behav. Brain Res. *245*, 42–49.

Wu, Y.E., Pan, L., Zuo, Y., Li, X., and Hong, W. (2017). Detecting Activated Cell Populations Using Single-Cell RNA-Seq. Neuron *96*, 313-329.e6.

Yang, T., Yang, C.F., Chizari, M.D., Maheswaranathan, N., Burke, K.J., Borius, M., Inoue, S., Chiang, M.C., Bender, K.J., Ganguli, S., et al. (2017). Social Control of Hypothalamus-Mediated Male Aggression. Neuron *95*, 955-970.e4.

Yizhar, O. (2012). Optogenetic insights into social behavior function. Biol Psychiatry *71*, 1075–1080.

de la Zerda, S.H., Netser, S., Magalnik, H., Briller, M., Marzan, D., Glatt, S., and Wagner, S. (2020). Social recognition in rats and mice requires integration of olfactory, somatosensory and auditory cues. BioRxiv 2020.05.05.078139.

Zhang, F., Aravanis, A.M., Adamantidis, A., de Lecea, L., and Deisseroth, K. (2007). Circuit-breakers: optical technologies for probing neural signals and systems. Nat Rev Neurosci *8*, 577–581.

Shani Haskal de la Zerda, Shai Netser, Hen Magalnik, Mayan Briller, Dan Marzan Sigal Glatt and Shlomo Wagner (2020). Social recognition in rats and mice requires integration of olfactory, somatosensory and auditory cues. bioRxiv